NTNU – Trondheim
Norwegian University of
Science and Technology

Wind Powered Marine Vehicle

A Concept Study

Emil Vestum

Marine Technology
Submission date: June 2015
Supervisor: Asgeir Johan Sørensen, IMT
Co-supervisor: Robert Biegler, PSY

Norwegian University of Science and Technology
Department of Marine Technology

NTNU – Trondheim
Norwegian University of
Science and Technology

Master Thesis

Wind Powered Marine Vehicle

A Concept Study

Emil A. S. Vestum

June 10, 2015

Supervisor: Professor Asgeir J. Sørensen
Co-supervisor: Associate professor Robert Biegler

NTNU Trondheim
Norwegian University of Science and Technology
Department of Marine Technology

MASTER THESIS IN MARINE CYBERNETICS

SPRING 2015

FOR

STUD. TECH. Emil Aleksander Stensrud Vestum

Wind Powered Marine Vehicle

Work description

Remotely operated or autonomous vehicles can carry out many measuring and monitoring tasks more cheaply than crewed vehicles, but due to their smaller sizes, they may lack endurance. One solution is to extract energy from the environment. Wind-powered vessels can extract a lot of energy quite efficiently, but mostly suffer from slow speed. A limiting factor is that the normal arrangement of foils in the air and the water generates a turning moment, which must be countered by a righting moment that is related to size. Resistance to wave-induced capsize depends on rotational inertia, also dependent on size. Small and cheap vehicles of conventional design are vulnerable. We will also consider hybrid concepts were the vehicle is able to harvest and store energy providing propulsion in low wind conditions.

This limitation is removed if force vectors from air and water foils can be aligned without a turning moment. Hagedoorn (1971, 1994) and Smith (1989) proposed that either a paraglider or an airship could serve as sail, and a paravane as the foil in the water. The high vantage point of the aerial element would further be useful for monitoring, for spotting other vessels, whether for collision avoidance or for spotting vessels fishing in marine sanctuaries, and for returning a radar echo that stays well clear of the clutter generated by a seaway. The speed of the vessel is not limited by stability, but only by how reliably the paravane remains hooked into the water, by structural integrity, and eventually by cavitation.

Scope of work

- Review relevant literature on aerodynamic loads on kites
- Review relevant literature on control systems associated with kites and surface/underwater vehicles
- Evaluate feasibility of different concepts considering operational conditions and limitations, cost, functions (payload capacity, endurance, speed, control modes) and select a concept of study of dynamics and control related problems
- Develop a mathematical model of selected concept, studying aerodynamics
- Propose feasible control objectives for concept for propulsion, and propose solution strategies
- Carry out simulations using the mathematical model to identify important loads
- Compare the mathematical model by simulations to real data
- Propose a control system setup (sensors, control surfaces)
- Propose set up for experimental testing, and realization of a pilot project
- Carry out field work and gather empiric data

NTNU Trondheim
Norwegian University of Science and Technology
Department of Marine Technology

The report language is English and it is going to be edited as a research report including literature survey, description of mathematical models, description of control algorithms, simulation results, model test results, discussion and a conclusion including a proposal for further work. Source code and digital content should be provided online by DAIM, with code listing enclosed in appendix. It is supposed that Department of Marine Technology, NTNU, can use the results freely in its research work, unless otherwise agreed upon, by referring to the student's work. The thesis should be submitted by June 10th 2015

Co-supervisor: Associate Professor Robert Biegler

Professor Asgeir J. Sørensen
Supervisor

June 10th 2015
Trondheim
Norway

Sammendrag

I konvensjonell design av seilbåter er krengemomentet fra rigide koblinger mellom foiler i luft og vann en begrensing på maksimal hastighet. Ved å eliminere skroget vil drag som resultat av våt overflate reduseres betydelig og øke den potensiale makshastigheten for seilefartøyet. Dagens ROV-er er begrenset av sin avhengighet til et forelderskip gjennom tilkoblingen i kommunikasjons- og kraftlederen. AUV-er er begrenset av kapasitet for lagring av energi ombord. Vind er en lett tilgjengelig energikilde til sjøs, noe som har blitt utnyttet av seilere i lang tid. Ved å utnytte denne energien kan et marint fartøy øke operasjonsområdet sammenliknet med konvensjonelle fartøy. Dette kan gjøres gjennom å utvikle et system av foiler beregnet for seiling, ved siden av et energihøstingsystem som kan sørge for ytelse under vindstille perioder. Høyden over vannet i banen til en drage kan utnyttes til kommunikasjon over lengre avstander, samt effektiv høsting av energi. Aerofoiler designet for høy ytelse har ustabil dynamikk og introduserer ulike utfordringer for utvikling av kontrollsystem. Ved å neglisjere høyere ordens aerodynamikk kan en forenklet modell utvikles. Kombinert med empirisk data kan dette benyttes til å studere forskjellige metoder for design av kontrollsystem for et vindkraftdrevet marint fartøy der en drage blir brukt til framdrift. En paravane kan reflektere kreftene fra en drage i vannet med minimal drag, og dermed åpne for et fartøy som kan seile i høy hastighet. Et slikt fartøy kan være med på å utvide eller kombinere eksisterende arbeidsområder for dagens ROV-er og AUV-er.

En PID-kontroller vil ikke klare å kontrollere en drage når støy er introdusert i vindmodellen. Forskjellige optimeringstilnærminger, som MPC og thrustallokeringsteori bør vurderes i fremtidig desing av kontrollsystem for drager. Thrustallokeringstilnærming kan være ikke-eksisterende til tider, spesielt i kritiske øyeblikk i dragens respons. Løsningen for en lineariseringstilnærming med tilbakekobling er ikke triviell, ettersom kontrollinputen er koblet for en parawing. Feil akkumuleres hurtig. Når approksimasjoner er benyttet, vil kontroll på feildynamikken etter lineariseringen bli unøyaktig.

Abstract

Remotely operated or autonomous vehicles can carry out many measuring and monitoring tasks more cheaply than crewed vehicles, but due to their smaller sizes, they may lack endurance. One solution is to extract energy from the environment. Wind-powered vessels can extract a lot of energy quite efficiently, but mostly suffer from slow speed. A limiting factor is that the normal arrangement of foils in the air and the water generates a turning moment, which must be countered by a righting moment that is related to size. Resistance to wave-induced capsize depends on rotational inertia, also dependent on size. Small and cheap vehicles of conventional design are vulnerable.

This limitation is removed if force vectors from air and water foils can be aligned without a turning moment. [1] and [2] proposed that either a paraglider or an airship could serve as sail, and a paravane as the foil in the water. The high vantage point of the aerial element would further be useful for monitoring, for spotting other vessels, whether for collision avoidance or for spotting vessels fishing in marine sanctuaries, and for returning a radar echo that stays well clear of the clutter generated by a seaway. The speed of the vessel is not limited by stability, but only by how reliably the paravane remains hooked into the water, by structural integrity, and eventually by cavitation.

The aerodynamics of kites are highly non-linear in nature and move in a quarter spherical plane. These notions are exploited by experienced kite surfers in order to maximize thrust in the direction of travel. A control system with the same properties applied on a kite of appropriate size and aspect ratio can provide a significant propulsive force in an autonomous marine application. In combination with other energy harvesting system the operational workspace can be expanded compared to ROV's and AUV's of today.

Summary

In conventional sailboat design, the heeling momentum introduced by the rigid connection of foils in air and water is a limitation on the maximum velocity. By removing the hull all together, wetted surface induced drag can be removed and increase the theoretical maximum velocity of a sailboat. Today ROV's are limited by their attachment to a parent ship through the umbilical. AUV's have operational limits due to energy storage capacity. Wind is a readably available energy source and is exploited in traditional sailing. By exploiting the wind energy a marine vehicle can increase the operational space compared to conventional vehicles. This can be done by incorporating foils for sailing and an energy harvesting system to increase no wind performance. The high vantage point of kites can improve communication and energy harvesting capabilities. Efficient aerofoils have unstable flight dynamics and high frequency response, and introduce several challenges for a control system. By neglecting higher order dynamics, a simplified model in combination with experimental data can be used to investigate different approaches in control system design regarding a wind powered marine vehicle application where a kite is utilized for propulsion. A paravane can reflect the kite forces in the water with minimum drag and opts for a high speed sailing vehicle that can expand or combine the existing workspace covered by ROV's and AUV's today.

A PID-controller will not be able to control a kite when a random walk process is introduced on the ambient wind. Different optimization approaches, such as MPC using NLP algorithms and thrust allocation theory, should be considered in future work regarding design of a control system for kites. However, the solution in a thrust allocation approach may not always exist, and specially at critical points in the system response. A feedback linearization approach may not be trivial to apply, as the control inputs are coupled for a parawing kite. Errors accumulate quickly, and when approximations are involved, control on the error dynamics based on the residual from the linearization may be insufficient.

Preface

This master thesis was written during the spring of 2015 as part of the master program at the department of Marine Technology at the Norwegian University of Science and Technology (NTNU), Trondheim, Norway. The thesis is edited as a technical report.

About the author

The author has always had a strong relationship to the sea and sailing. Growing up, the summers where spent somehow on water with the family. At the age of 10, the family bought their first sail boat, a Jeanneu 42 and fell in love with the art of sailing. Soon a lack of speed and thrills in this slow sailing mono hull was found. The emerging internet made following the dream of speed sailing grow, and the amazing world of multi-hulls was discovered. A Hobie Cat 16 Le Race became a first high speed sailing vessel, which is still in custody and sailed every summer to great amusement. But still, the search for speed in sailing was not satisfied. The world of foiling vessels was discovered through L'Hydroptère's world record attempts for fastest sailboat over 500 yards and one mile. Later on the evolution of foiling cats in Americas Cup was followed with interest. The next natural step was to desire to own and sail a foiling craft. When Robert Biegler's thesis proposal emerged, the choice of master thesis was without doubt.

Acknowledgements

The author would like to thank the following people for their contributions to this project thesis:

Asgeir J. Sørensen (Professor at the department of Marine Technology at the Norwegian University of Science and Technology (NTNU), Trondheim, Norway) for supervising the thesis and being a source of inspiration.

Robert Biegler (Associate Professor at the department of Psychology, NTNU) for sharing his knowledge and experience regarding the field of innovative sailboat design and being a source of inspiration.

Roger Skjetne (Professor at the Department of Marine Technology, NTNU) for supervising strategies regarding control plant design.

Torgeir Wahl (Senior Engineer at the department of Marine Technology, NTNU) for sharing his knowledge and discussing different approaches regarding actuation in a real world realization of a pilot project.

Astrid H. Brodtkorb and Svenn Are Værnø Tutturen (PhD candidates at the department of Marine Technology, NTNU) for supervising modelling of dynamics as well as design of process and control plant model.

Eirik Bøckmann and Jarle Kramer (PhD candidates at the department of Marine Technology, NTNU) for discussing the mathematical models of foils and fluid dynamics.

Bastian Solbakken (M.Sc. student at the department of Energy and Environmental Engineering, NTNU) has been a kite surfing instructor on both snow and water since 2010, and has been sharing his experience and explaining and demonstrating basic dynamics and control of kites.

Acronyms and symbols

Table of acronyms

ROV	Remotely Operated Vehicle
AUV	Autonomous Unmanned Vehicle
MPC	Model Predictive Control
NLP	Non Linear Programming
AYRS	Amateur Yacht Research Society
US	United States (of America)
LTA	Lighter Than Air
UV	Ultra Violet
NED	North East Down
NACA	National Advisory Committee for Aeronautics
PID	Proportional Integral Derivative
AIS	Automatic Identification System
NA	Not Announced

Table of symbols

Symbol	Description	Unit
F	Net force	[N]
T	Thrust force	[N]
$\mathbf{L}$	Lift force vector	[N]
$\mathbf{D}$	Drag force vector	[N]
$\mathbf{D}_t$	Tether drag force vector	[N]
$\mathbf{M}_g$	Gravitation vector	[N]
$\mathbf{F}_t$	Tow force vector	[N]
F_L	Lift force	[N]
F_D	Drag force	[N]
F_r	Radial force	[N]
F_z	Vertical force component	[N]
F_θ	Elevation angle force component	[N]
F_ϕ	Azimuth angle force component	[N]
F_c	Tether constraint force	[N]
D_θ	Elevation angle drag force component	[N]
D_ϕ	Azimuth angle drag force component	[N]
D_r	Radial drag force component	[N]
L_θ	Elevation angle lift force component	[N]
L_ϕ	Azimuth angle lift force component	[N]
L_r	Radial lift force component	[N]
$D_{t,\theta}$	Elevation angle tether drag force component	[N]
$D_{t,\phi}$	Azimuth angle tether drag force component	[N]
$D_{t,r}$	Radial tether drag force component	[N]
M_θ	Elevation angle gravitation component	[N]
M_ϕ	Azimuth angle gravitation component	[N]
M_r	Radial gravitation component	[N]
α_s	Total drag angle	[deg]
χ_h	Hydrodynamic drag angle	[deg]
χ_a	Aerodynamic drag angle	[deg]
V_b	Theoretical sailing velocity	[ms^{-1}]
ϕ	Angle between heading and true wind	[deg]
L/D	Lift-to-drag ratio	[-]
C_L	Lift coefficient	[-]
C_D	Drag coefficient	[-]
$C_\perp$	Normal reaction coefficient	[-]
E	Lift-to-drag-ratio	[-]
g	Acceleration of gravity	[ms^{-2}]
U	Fluid flow velocity	[ms^{-1}]
S	Surface area	[m^2]

Symbol	Description	Unit
ρ	Fluid density	[kgm^{-3}]
ρ_a	Density of air	[kgm^{-3}]
A_k	Surface area of kite	[m^2]
l	length	[m]
r	radius	[m]
l_t	Length of tether	[m]
l_k	Length of kite	[m]
l_c	Length of control bar	[m]
l_{rc}	Reel out length of control bar in yaw	[m]
d_t	Tether diameter	[m]
m	System mass	[kg]
m_k	Mass of kite	[kg]
m_c	Mass of control bar	[kg]
V	Volume	[m^3]
θ	Elevation angle	[rad]
ϕ	Azimuth angle	[rad]
φ_c	Kite control angle in pitch	[rad]
ψ_c	Kite control angle in yaw	[rad]
x	System state vector	[NA]
u	Control input	[rad]
h	Path constraint function	[NA]
r	Periodic boundary conditions	[NA]
$\mathbf{p}$	Position vector	[m]
$\mathbf{e}_r$	Radial unit vector	[-]
$\mathbf{e}_\theta$	Elevation angle unit vector	[-]
$\mathbf{e}_\phi$	Azimuth agnle unit vector	[-]
$\mathbf{e}_{We}$	Relative wind velocity unit vector	[-]
$\mathbf{e}_l$	Kite longitudinal axis unit vector	[-]
$\mathbf{e}_t$	Kite transverse axis unit vector	[-]
$\mathbf{e}_\psi$	Kite vertical axis unit vector	[-]
$\mathbf{W}$	Ambient wind velocity vector	[ms^{-1}]
$\mathbf{W}_e$	Relative wind velocity vector	[ms^{-1}]
$\mathbf{W}_e^p$	Projected relative wind velocity vector	[ms^{-1}]

Symbol	Description	Unit
ϵ	System state vector	[rad]
ω	System state vector	[rads^{-1}
J	Rotation matrix	[-]
R_{φ_c}	Control input rotation matrix	[-]
R_{ψ_c}	Control input rotation matrix	[-]
R_1	Control input rotation matrix	[-]
R_2	Control input rotation matrix	[-]
D	Non-linear damping matrix	[kgs^{-1}]
g	Gravitation vector	[kgs^{-2}]
g_r	Radial gravitation	[kgms^{-2}]
M	Mass matrix	[kg]
V	Non-linear damping matrix	[-]
χ	Unit vector projection matrix	[-]
χ_r	Unit vector projection matrix	[-]
Γ	Unit vector projection matrix	[-]
ξ_i	Unit vector projection	[-]
ξ_{ri}	Unit vector projection	[-]
f	Aerodynamic force vector	[N]
τ_t	Tether drag force vector	[kgs^{-2}]
τ_c	Control input vector	[kgs^{-2}]
v	Substitute vector	[N]
A	Linearized state equation state matrix	[NA]
B	Linearized state equation control input matrix	[NA]
$\mathcal{C}$	Controllability matrix	[NA]
C_{TB}	Controllability check matrix	[-]
λ_i	Roots of matrix	[NA]
c_i	Linear mapping constant	[-]
K_P	Proportional gain	[-]
K_I	Integral gain	[-]
K_D	Derivative gain	[-]
τ_θ	Control force on elevation angle	[N]
τ_ϕ	Control force on azimuth angle	[N]

Contents

Chapter 1

Introduction

Throughout history sailing has been central in the development of civilizations, from explorations and adventure to trade and warfare. Norwegian Thor Heyerdahl proved that the early human mastered the art of sailing before inventing the wheel nor the saddle, through his Kon-Tiki missions. Christopher Columbus discovered America by accident trying to find a westerly trade route to India.

According to [3] the energy demand will increase by 35 % in from 2014 to 2040, which could have more than doubled without advancements in efficiency. Oil will remain the preferred fuel for transportation purposes, and natural gas is emerging as growing choice of fuel. The growing population combined with an increase in burning of fossil fuels, with emissions following, raises a challenge to public health and environment. Estimations suggests the world oil reserve will last for another 53 years [4] and thus the need for alternative energy sources is imminent. Wind power is readily available and has been exploited in transportation by humans in at least the last two millennia.

> *To one who has turned lifeless materials into a thing alive and forced it to do his bidding against the resisting forces of nature, in silence, without fuel, and without defiling air or water, there can never be anything more wonderful than the sailboat. To one who has not had the experience, no telling of it can touch him. The sailboat never offends the senses of fish, fowl or man; to make it move faster is to make it yet more a thing of freedom and beauty.*
>
> - [2]

1.1 Motivation

ROV's and AUV's are performing a variety of tasks today. Mapping and monitoring of marine resources and environment for governance and decision making, and oil and gas in deep water conditions are examples of such tasks. As technology advances the operation complexity is allowed to increase. ROV's are typically deployed and operated from floating platforms, such as ships and have a depth range of $0-6000$ $[m]$ according to [5]. ROV's have the ability to report high resolution data for a targeted area, and an umbilical attachment provides unlimited electrical power and high bandwidth communication. They have a limited spatial range, usually less than 1 $[km]$ and a coverage area less than 100 $[m^2]$. Surface vehicles will have the ability to expand the workspace by wireless communication. Operations of an ROV attached by an umbilical are expensive due to the day rates of parent ships and operators, technicians and supervisors. The operation window is limited by weather, seeway and currents resulting in reduced availability. Increased autonomy and fault-tolerant control is a challenge and an area of research.

AUV's are mostly used in mapping and monitoring in marine applications today, and have a relative high survey area coverage over time compared to an ROV. The spatial resolution data is relatively high considering detailed seafloor and water column mapping. An AUV is less dependent on a parent ship during operations, which enables cost savings. Advancements in technology and science opens for the potential to take advantage of autonomy in operation planning and handling of unexpected events, resulting in smarter and more efficient operations. In an event of a critical system failure, there is a risk of total loss of data and vehicle, and the workspace is limited by the on board power supply. The possibility of collision with marine traffic and flotsam are possible operational limits as well. Some challenges and areas of research in developing AUV's are identified to be collision avoidance, real-time data processing, planning, inertial navigation systems, power supply, communication, payload capacity and operations in shallow water and Arctic areas. According to [5] AUV's can improve autonomy and implement the use of automatic docking stations in the future. Development of hybrid vehicles able to switch between AUV and ROV mode may become a possibility.

Traditional western sailing vessels are based on a displacement hull design and their maximum velocity is thus limited by the length of the waterline, making them slow. Even though the sailing sport has evolved and successfully beat speed records, they are only making incremental advances according to [2]. There should be a theoretical possibility to sail multiple times

faster than the ambient wind, based on lift-to-drag-ratio considerations, and a step-function advance in speed could be made. Iceboats sail up to perhaps four times the ambient wind speed, without brinkmanship.

The implementation of an on-board energy harvesting system could potentially expand the operation workspace for future autonomous marine vehicles. Wind power is readily available, and could be exploited in such applications. The idea of a high speed sailing autonomous marine surface vehicle can be market inspiring and part of the future in marine robotics.

1.1.1 Challenges of conventional sailboats

A conventional sailboat has a configuration of rigid connected hydrofoils and aerofoils where a hull acts as a float and the connecting link between the forces exerted by air and water. Seen in figure 1.1 a sketch of a close-hauled sailboat demonstrates the resulting forces experienced by the system. When the boat is sailed properly, the force resultant from aero and hydrofoils provides a forward momentum, and the boat accelerates until the drag on the hull equals the forward momentum and the boats maximum speed is reached. The illustration indicates a turning momentum from the sails that has to be countered by the keel. The main force contribution in this system is in the transverse direction and the associated momentum in roll. The righting moment has to be based on a suspended weight in such a configuration. Thus the force relations can be established and a the maximum load capacity and associated velocity can be identified. The heeling moment in such a configuration is traditionally exerted either by the crew shifting its weight, or by a high density bulb on the keel. The increased weight introduced by a bulb configuration results in an increase in the volume of the hull, in order to maintain the sailboats ability to remain afloat. An increased hull volume increases the wetted surface induced drag, associated with a decrease in maximal velocity.

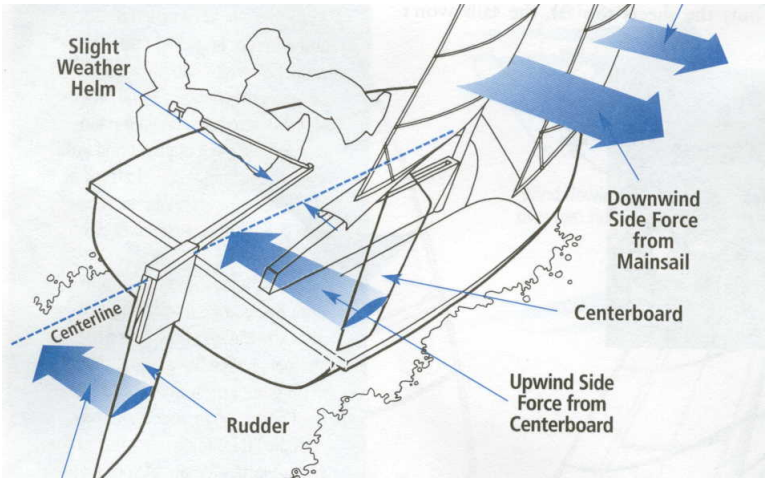

Figure 1.1: Conventional sailboat, image taken from www.boatdesign.net

1.2 Previous work

Several people have been intrigued with the idea of improving the performance of sailboats. The study of limitations on conventional sailboat design has been a main focus of their work. They have come to different designs, decreasing and ultimately removing the limitations introduced in section 1.1.1.

Bernhard Smith (1910-2010) was an American rocket scientist and sailboat designer. His work includes the first launch of a liquid-propellant rocket in America and research in naval surface weaponry. His book *Sailoons and Fliptackets* covers his ideas of the ultimate high speed sailboat, which completely defies traditional design, according to [2]. Some of his ideas on improving sailboat design was to offset the foils in water and air laterally and inclining them to line up the resulting forces, in order to decrease and ultimately remove heeling moment. His designs need a lot of structure to connect the foils rigidly, because the foils need to be separated by a relatively long distance. The Sailrocket project serves as a good example of these challenges.

Didier Costes independently invented the "Chien de Mer", or a hapa, and is known as a developer of the hapa and complementary kite rigs for heelfree sailing. Kites solve the structural problem seen in Smiths ideas, because they only need light weight tensile connections in order to separate the foils to line up the forces, and removing the heeling moment. The Cglider project of Cylvian Claudel is currently doing progress in developing Costes ideas and successfully experimented with a mass-less hydrofoil and kite setup.

If the boat is light weight compared to the resulting vertical forces exerted by a kite, the system risks getting pulled out of the water and become airborne. For an autonomous system, this might result in a system failure. Hagedoorn turned that vice into a virtue by removing the hull and letting the hydrofoil counteract the vertical force, in order to remain submerged. Professor J.G. Hagedoorns paper of 1971 was remarkable due to the fact that his idea eliminated the hull completely. His analysis started by reviewing the conventional sailboat configuration and proceeded by removing the keel from the hull and replacing it on an outrigger to windward, making it much more efficient in its traditional role, as well as increasing stability by countering the heeling moment from the sail. In the next step he removed the rigid coupling from the main hull to the outrigger foil all together, and replaced it by the hapa connected to the main hull by cables. The hapa can most easily be understood as a underwater kite. By eliminating the hull the resulting drag can be greatly reduced and stability can be improved. Paul Ashford has applied the hapa concept on a cruising boat, and his concept of dynamic incident control is said to be crucial for the development of high speed hapas.

According to [6], Robert Biegler performed experiments with the Wipika kite and an inflatable catamaran. Reportedly, the Wipika kite has more stable flight dynamics compared to that of a kite designed for kite surfing.

The Amateur Yacht Research Society (AYRS) is a UK registered Educational Charity dedicated to improve yachting. Its members range from professional yacht designers to eccentrics with ideas that they cannot make work. They claim to have produced the ideas for the modern sailing multihulls, self-steering gear, sailboards, sailing hydrofoils, the World Speed Sailing Record system etc. according to [7].

SkySail is a german based company that has developed a kite propulsion system for the shipping industry. The system involves a launch and recovery phase, as well as a dynamic flight control. The dynamic flight control system is maximizing the energy output by exploiting the local acceleration and increase apparent wind over the kite by flying in eight-number shaped paths, according to [8].

Figure 1.2: SkySails: Image rights SkySails GmbH

The pumping kite power system in [9] utilises the same principle as SkySail in maximizing energy output. On the contrary this system the kite is unrolling a cable hooked to a electric energy converter. When the cable spool is fully unrolled, the kite is set to the neutral position where lift is minimized, and the cable spool is re-rolled. This system has been tested in heights above $900[m]$ of unrolled cable. Experimental results reported a cycle efficiency of 62.20% and a average power output of $3726.40[W]$ using a $10[m^2]$ Hydra-kite.

Saildrone is a US based team of engineers and technicians who have developed a fully autonomous sailing drone. The sailing vessel incorporates a rigid wing sail and the hull is of a trimaran design with stabilizing outriggers. The wing is controlled by a tail and reports ultra-efficient aero and hydro dynamics according to [10].

Figure 1.3: Saildrone: Image rights [10]

- Length: 19 ft
- Width: 7 ft
- Height: 20 ft
- Draft 6 ft
- Average speed: 3-5 knots
- Maximum speed: 14 knots
- Payload capacity: 200 lbs
- Payload power supply: 5-10 W
- Deployment duration: 6-8 monts

Dipl. Phys. Moritz Mathias Diehl's PhD. thesis in real-time optimization for large scale nonlinear processes covers basic dynamics for roll-angle controlled kites and applied model predictive control (MPC) where steady state aerodynamics are assumed. His PhD thesis is cited in several projects, such as [8] and [11].

1.3 Main contributions

The main contributions of this thesis is a concept study of dynamics and control strategies of a multi panel soft fabric parawing kite. A literature study of existing concepts relevant in the study of the concept of a wind powered marine vehicle, where applications of harvesting of wind power for propulsion is central has been performed. A field study where experimental testing where identifying challenges regarding control system design and development of a conceptual wind powered marine vehicle was carried out.

1.3.1 The literature search process

The literature search was conducted by using the Oria search engine found at `www.oria.no`. When the Oria search engine is accessed from NTNU's intranet the user is able to perform specialized searches in the NTNU library resources spanning books, articles, journals, music, films, electronic resources and more. The information gathering process was interesting work and an important part regarding this thesis.

1.4 Organization of the thesis

First, the thesis establish its motivation and investigates relevant previous work. Then it proceeds in building a concept evaluation foundation for the evaluation of the following presentation of different existing concepts and ideas regarding the development of a wind powered marine vehicle. Thereafter a conceptual mathematical model of a parawing kite is established in order to carry out simulations. The simulations of the conceptual system is presented and then discussed. A field study regarding the chosen concept of study was carried out and described. Based on the findings within this thesis, it concludes with a suggestion for further work.

Chapter 2

Concept evaluation foundation

This section aims to build a foundation for evaluation of different concepts, that are relevant to the goals of this thesis. The criteria set are based on conversations with Sørensen and Biegler as there are no directly relevant data from an existing market, because the concept of a wind powered marine vehicle as defined within this thesis, does not exist elsewhere than in a conceptual space. Knowledge of existing ROV's and AUV's is combined to some extent based on [5]. The idea of the operational space of the wind powered marine vehicle is to span the workspace of both ROV's and AUV's presented. The reader should take note that the weightings in the score charts are personal preferences to the author.

2.1 Common concept criteria

In this section some common concept criteria are listed in a table providing definitions and a scoring chart for evaluations in a generalised manner.

Nr	Name	Definition	Scoring
1	Environmental effects	The ability to avoid and prevent flotsam and lightning damage, disturbance of life at sea	10
2	Launch and recovery	The ability to store, transport, launch and recover the vessel	15
3	Cost	The cost of research and development and operational costs have to meet the limitations of the market	10
4	Marine traffic monitoring	The ability to avoid collisions, spot crime and accidents	10
5	Robustness	The ability to endure extreme environmental and operational loads and structural redundancy (number of moving parts)	20
6	Endurance	The ability to harvest energy, no-wind and heavy weather performance	20
6a	Energy harvesting	The ability to store and generate power for propulsion and operation	15
6b	Heavy weather performance	The ability to predict, avoid and survive extreme conditions of seaway and wind	5
7	Level of autonomy	The ability to operate without input from commander	5
8	Path planning and path following	The ability to plan and follow paths to successfully reach operation and endurance goals	10
	Total		**100**

Table 2.1: Generalized score chart

2.2 Survey mode

Survey mode is hereby defined to be operations where the goal of the vessel is to span a predefined area and perform monitoring tasks. Examples of such survey tasks can be monitoring of marine traffic, sea life, crime spotting or oceanographic data collection. The span of the predefined area can be realized by path planning and path following algorithms, input from operator or a combination of both. Listed are some specified criteria for later scoring of concepts to help the evaluation process. No stationary operations are assumed in this section.

Nr	Name	Definition	Scoring
9	Path Realization	The ability to reach all points of planned path, or predefined area. The ability to sail hauled (incoming wind speed angle $< 90°$ will be a key property.	25
10	Vessel speed	Stable, predictable and market inspiring speed at design wind velocities	25
10a	Lift to drag ratio	Effectiveness of air foil	15
10b	Extra propulsion	The use of stored energy for propulsion in no-wind conditions	10
11	Communication	The ability to report sampled data (and communicate with operator)	25
12	Diving capabilities	The ability to maintain forward momentum under sub sea operations	25
	Total		100

Table 2.2: Score chart for survey mode concepts

2.3 Paylod (transport) mode

Payload mode is hereby defined to be operations where the vessel transport a design payload or cargo from one point of interest to another. An example can be autonomous transport of payload to a point of interest and transition

to **work mode**, or classic cargo transportation. Listed are some specified criteria for scoring of concepts to help the evaluation process. No stationary operations are assumed in this section.

13	Speed	The ability to transport design payload or cargo at market inspiring speed	30
14	Reliability	The ability to reach target point of interest within defined time limits. Key points will be effectiveness of path planning and path following algorithms and the ability to reach all points in planned path.	30
15	Robustness	Intact payload or cargo upon arrival at point of interest	20
16	Payload Capability	Total payload capacity	20
	Total		100

Table 2.3: Score chart for paylod mode concepts

2.4 Work mode

Work mode is hereby defined to be operations where the vessel remains stationary at a point of interest. Listed are some specified criteria for scoring of concepts to help the evaluation process. Stationary operations only is assumed in this section.

17	Station keeping	The ability to remain stationary at point of interest, for instance by dynamical positioning	50
18	Endurance	The ability to harvest energy when stationary to reach operation goals	30
19	Diving capabilities	The ability to conduct sub sea operations while remaining stationary	20
	Total		100

Table 2.4: Score chart for work mode concepts

Chapter 3

Concepts

This section aims to present and provide a way of quantitative evaluation of concepts found in a literature study, as well as by conversations and email correspondence with Robert Biegler, and other ideas who ultimately may be a part of a pilot project, and to reach the thesis goals. Scoring charts for different operation modes are established in order to score the different concepts in a way that suits the goals of this thesis.

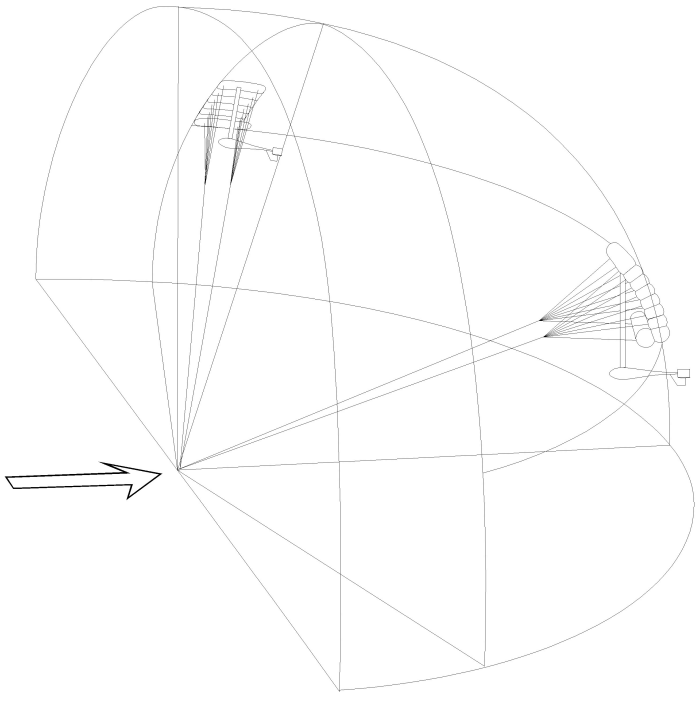

Figure 3.1: Flight window of a kite: Image courtesy of Robert Biegler

3.1 Concepts for wind power exploitation

This section aims to study and evaluate some different applications of wind power exploitation for propulsion and operational power consumption, based on existing documentation.

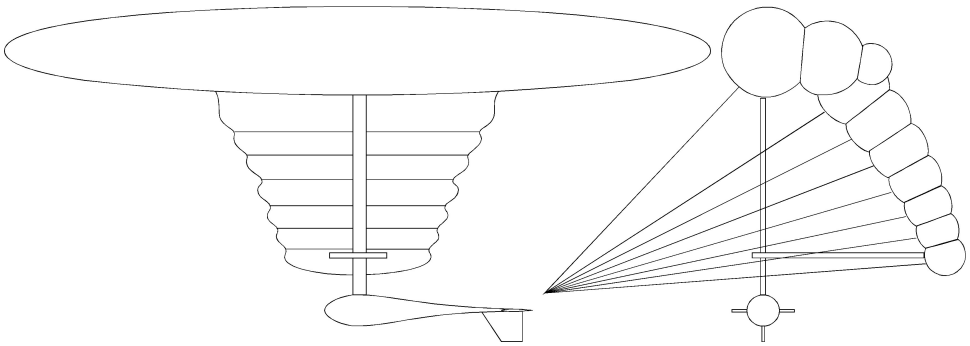

Figure 3.2: figure
Flying trapeze: Image courtesy of Robert Biegler

3.1.1 Blimps

Blimps are hereby defined to be inflated lighter-than-air (LTA) structures with control surfaces, such as air ships, aerostats and Zeppelins. Different designs can be seen in figure 3.5. Their strongest asset is their buoyancy based lift capabilities, which make them suited for air suspended payload or cargo operations, such as monitoring tasks and energy harvesting. Even with a low drag hull design, blimps will have a low lift-to-drag ratio compared to foils only structures, and may not be suited for sailing other than traction based sailing. One idea is to mount a ventral wing underneath the blimp, acting as an air keel to improve sailing properties. Their robustness in heavy weather, due to the large area facing incoming wind, is dependent on materials and structural integrity. As proposed in [2] a design incorporating a blimp with control surfaces attached to a paravane could park near shore or at a hub in strong winds, and later continue the mission. According to [12], The HeliKite as seen in figure 3.3, is capable of surviving heavy weather while remaining stationary to its point of attachment. Control and dynamics theory is available and well known. Depending on the structure of the blimp, it may take up little space when stored, due to its inflation properties. Environmental effects to be considered for blimps are leakage of inflation fluid to the environment. Helium is a commonly used inflation gas, and is a non-renewable resource, according to The Independent Newspaper, until a workable fusion reactor is made. Today, all helium comes from radioactive decay or a biproduct of hydrocarbon gas extraction. A blimp design may require a large hull and control surfaces to obtain sufficient buoyancy and control actuation to counter the resulting aerodynamic forces. If the hull is made of a non-conductive material, it may not be subject to lightning damage, and avoiding such an event should be considered in the concept development. Table 3.1 shows a score chart of a blimp as a part of a wind powered marine vehicle concept.

Nr	Scoring
1	7
2	15
3	10
4	10
5	10
6	15
7	4
8	2
Sum	**73**
9	10
10	15
11	7
12	25
Sum	**57**
13	30
14	15
15	15
16	20
Sum	**80**
17	50
18	30
19	20
Sum	**100**

Table 3.1: Blimp score chart

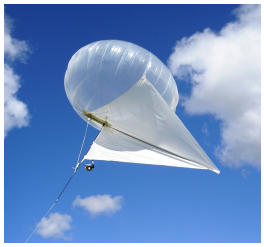

Figure 3.3: HeliKite: taken from [12]

3.1.2 Traditional kites

Traditional kites are hereby defined to be non-rigid fabric structured air foils. Kites can be be categorized as to have either permanently defined leading and trailing edges or not. Kites do not traditionally have any control surfaces but are controlled by tethers. In order to change roll angle, or yaw angle, the kite is twisted by pulling either control tethers, or both simultaneously to control pitch angle, depending on the design. They can further be quantitatively categorized by lift to drag ratios at 5 and below. Kites are traditionally used for leisure purposes, such as kite surfing. Due to their relative low cost and complexity in production and operation they are getting involved in propulsion purposes, such as the SkySails system in [8] and energy harvesting as in [13]. Kites are rigorously tested and practical experience is readily available through the kite surfing community in Trondheim. There exist documentation on kite control system proposals and dynamics. The advantage of a traditional kite applied to a realisation of a pilot project would be the ability to buy a kite off shelf for testing of hydrofoils and their local system behaviour and dynamics, as well as incorporated in a complete system. A modification by helium inflation could further improve no wind performance by adding buoyancy, such that the kite will not crash and potentially cause a system failure. Traditionally, kites have operational limits due to generated power related to wind speed, where the relative wind at the kite can increase by a factor of the square of its lift to drag ratio, according to [14]. Tacking would be an impossible manoeuvre for a mass less design, as a coincidence of the kite reaching a point where the resulting lift force will be vertical, and the hydrofoils having zero velocity resulting in zero lift force to counter the kite forces, the vehicle would become airborne and potentially cause a system failure.

Nr	Scoring
1	8
2	12
3	10
4	8
5	20
6	18
7	4
8	10
Sum	**90**
9	25
10	22
11	20
12	25
Sum	**92**
13	27
14	28
15	15
16	5
Sum	**75**
17	10
18	15
19	10
Sum	**35**

Table 3.2: Kite score chart

Figure 3.4: $10[m^2]$ kite. Image taken from [15]

Depending on the materials of the kite structure, lightning damage could be avoided. In the case of a system failure where the kite structure is destroyed, the materials of the kite would be dispersed in the sea and could potentially harm sea life. The fabric color of a kite should be taken into consideration regarding the possible disturbance of sea life. A kite with pitch and roll control could be able to survive extreme weather by adjusting the angle of attack to incoming wind in order to minimize lift. Kite surfers regularly park their kite in a neutral position, where aerodynamic and gravity loads balance each other.
The survival properties will depend on lift-to-drag-ratio regarding extreme loads. The relatively unstable flight dynamics of a kite, [8], could potentially complicate air suspended survey operations, which will ultimately depend on chosen flight pattern and control system. By incorporating an energy harvesting system the endurance could be improved regarding no wind performance. The maximal heading angle to ambient wind is dependent on lift-to-drag-ratio. Wind surfers are regularly seen to be able to sail upwind ($< 90°$) to incoming wind. Regarding a system incorporating a mass-less hydrofoil design, station keeping would be a demanding task, and may be impossible, due to the inherent unstable flight dynamics of a kite. As seen in leisure kite surfing, the opportunity of high speed sailing is inspiring regarding a concept of a wind powered marine vehicle. The kite concept score in table 3.2 is according to tables 2.1 through 2.4.

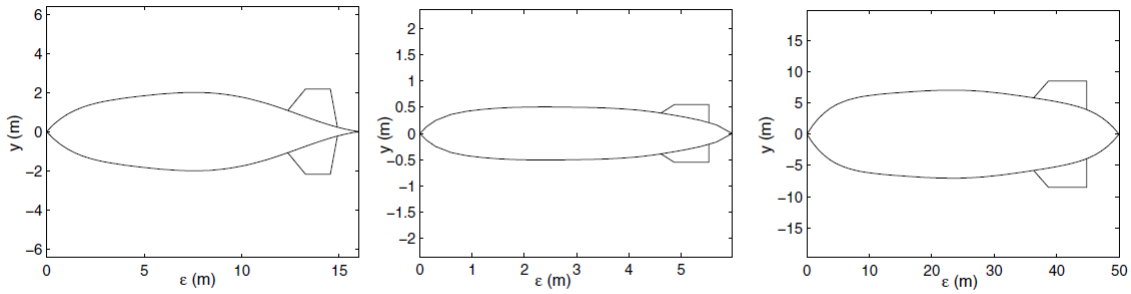

Fig. 12 Profiles of the airships in simulation examples.

Figure 3.5: Different blimp designs: Taken from [**?**]

3.1.3 Inflatable wing based on the concept of tensairity

According to [16] an aerofoil based on the concept of tensairity reports lift to drag ratios of 5 to 10 with only a 16% increase in mass compared to a soft fabric kite of similar design. The concept greatly improves the structure's stiffness and thus maximal load capacity. Due to the two panel design as seen in aeroplane wings, the possibility of incorporating LTA-properties by inflating the wing can improve its no wind performance. The concept can imitate well known and documented foil designs and possibly implement control surfaces if needed. The realization of a pilot project where this concept is incorporated will demand research and development and suggests a somewhat higher cost than the use of a traditional kite, due to the need for advanced materials. The same way as traditional kites, a tensairity kite will face the risk of resulting in an airborne system while tacking due to vertical resulting lift and zero fluid flow over the hydrofoils. The score chart seen in table 3.3 provides a generic evaluating of the concept in relation to the goals of this thesis.

Nr	Scoring
1	8
2	10
3	7
4	5
5	18
6	18
7	4
8	10
Sum	**80**
9	25
10	25
11	20
12	25
Sum	**95**
13	30
14	30
15	15
16	5
Sum	**80**
17	8
18	15
19	10
Sum	**33**

Table 3.3: Tensairity kite score chart

Figure 3.6: Tensairity kite: Image taken from [16]

3.1.4 Flying squaresail and trapeze kite

The flying squaresail and trapeze kite is essentially a square soft fabric kite with inflatable panels, designed for LTA-properties by Robert Biegler, as an attempt to design kits that would maintain a constant altitude. As seen in figure 3.2 , the squaresail design has a nacelle attached in the origin of the system, for steering purposes. The nacelle is connected with rigid bars to the side edges of the kite. The main idea of the design is a kite flying at constant altitude to avoid the possibility of take off during change of tacks in a massless hydrofoil configuration, as well as improving no wind performance. By incorporating LTA-properties, this configuration should be able to carry a relatively larger payload than a traditional kite, as well as maintaining a good lift-to-drag-ratio for sailing, compared to a blimp configuration. The increased payload capacity could be exploited by a energy harvesting system, such as a wind turbine. By bridling the kite swept back, in order to let the kite park in the neutral position by zero control actuation. The neutral position defined to be the position in the kites flight window where the gravity and aerodynamic forces are balanced, and the system is at rest. But in the neutral position, the fence of bridles at the top will act as a low aspect ratio wing, with its angle of attack controlled by the bridle. This principle could keep the wing above the water with reduced pull, for parking and improve station keeping capabilities. The flying trapeze is intended to provide swept back edges that may give the kite a stable altitude when it is maximally depowered. The concept will need research and development, which suggests increase in cost. Depending on the materials in use, an evaluation of environmental impact should be done before realizing this concept. The use of soft fabric panels suggests that the kite would take up minimal space when stored. Launch and recovery should be fairly straight forward given the stable altitude flight dynamics and LTA-properties in light wind conditions. Launching in strong winds could be problematic. Modelling of aeroelasticity is computational expensive.

Nr	**Scoring**
1	8
2	10
3	7
4	5
5	18
6	18
7	4
8	10
Sum	**80**
9	25
10	25
11	20
12	25
Sum	**95**
13	30
14	30
15	15
16	5
Sum	**80**
17	8
18	15
19	10
Sum	**33**

Table 3.4: Flying square sail and trapeze kite score chart

3.1.5 Hybrids and other concepts

The *Square Box kite* described in [17] is worth mentioning, as it reportedly removes the problem of vertical lift during tacks. Lingual difficulties suggest translation aid in a further study of this concept. Hybrids of mentioned concepts should be considered. There exist some concepts worth mentioning, such as a blimp-kite-hybrid called HeliKite, the helium filled wind turbine, wing with center blimp. Other concepts from [17] worth mentioning are the speed wing, quarter sphere traction kite, the Cody kite, cone or cylinder kite, the Wipika and a delta wing kite known as a hang-glider.

3.1.6 Energy harvesting

As proposed, an energy harvesting system may be necessary. One idea can be to suspend a propeller under the air foil that can generate and store electrical power during flight and generate propulsion in reverse in no wind conditions. The higher vantage point suggests stronger winds, and thus more potential of generated power. One important aspect of incorporating such a system is the increase in drag and weight on the air foil system. Thus, minimization of drag and weight should be an important aspect of design, further suggesting an increase in cost due to development and advanced materials. Such a system can potentially decrease the systems overall redundancy. Another idea can be to mount a energy harvesting system on the hydrofoil system to reduce drag and weight on the aerofoil system, with a decrease in possible energy harvesting due to the relative lower apparent wind velocity near the sea surface compared to the aerofoil, according to [14]. The energy storing system would consist of batteries, and the weight to energy storing capacity would be a important design aspect. A configuration where the harvesting system is air suspended and the energy storage system is water suspended, an umbilical will have to be attached in order to secure the power transition. The umbilical may be subject to damage and could further decrease the systems overall redundancy.

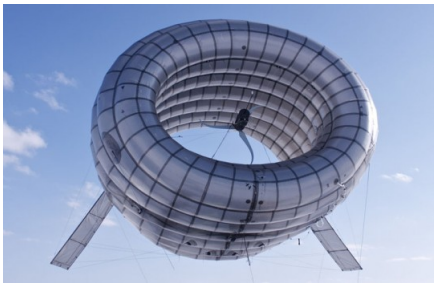

Figure 3.7: Altaeros airborne wind turbine. Image taken from [18]

3.2 Concepts of hydrodynamics

This section aims to present and evaluate some concepts of hydrodynamics, based on a literature study and by conversations and email correspondence with Robert Biegler, as well as other ideas. The main goal of the hydrodynamic system is to reflect the forces from the wind power exploitation system to maximize forward momentum. Reduction of drag and weight are important aspects regarding the maximum velocity and maximum heading angle to the ambient wind. Ventilation and cavitation are important aspects of wear and tear for hydrofoils, and will affect stability. Extreme loads and structural integrity should also be considered. Some concept criteria were established to evaluate the different concepts of hydrodynamics, and are presented in table 3.5.

Nr	**Name**	**Definition**	**Scoring**
20	Forward momentum	Reflect forces from aerofoil to generate net forward momentum	20
21	Pitch stability	The ability to maintain fluid flow over hydrofoils in seaway, to maintain forward momentum	20
22	Yaw stability	The ability to maintain a stable and predictable course heading for navigation purposes	15
23	Lift to drag ratio	Affects maximal velocity and angle to apparent wind	20
24	Cavitation and ventilation	Important aspects of robustness and redundancy regarding wear and tear	10
25	Flotsam	The ability to avoid entanglement of flotsam to avoid possible system failure	5
26	Cost	Research and development, production and maintenance cost	10
	Total		**100**

Table 3.5: Score chart for hydrodynamic concepts

3.2.1 Mass less hydrofoil

The concept of a mass less hydrofoil have foil forces dominating such that mass effects can be neglected. The application of a mass less hydrofoil system in the context of this thesis will be to reflect the forces from the aerofoil system to generated a net forward momentum, until steady state conditions are reached. The reflecting forces in consideration are leeway drift, vertical and horizontal lift, torque in pitch and roll, as well as yaw regarding directional stability for navigation purposes. Stability in pitch and heave will be important to prevent the system from becoming airborne and experience surface interactions, potentially resulting in system failure. The different possible designs can be a shunting vehicle, a tacking vehicle or a gybing vehicle. Both the gybing and tacking vehicle will have permanently defined leading and trailing edges, whereas the shunting design will not. A shunting proa design can possibly reduce weight by the reduction in foils needed to reflect leeway and lift forces from the aerofoil, but will possibly need an increased number of control surfaces to improve stability. This is due to the fact that the vehicle will discretely switch fore and aft during change of tacks, and the keel has to be symmetric in the structures longitudinal axis. Also worth mentioning is that yaw control can be done by moving the point of force transfer from the aerofoil fore and aft of the center of momentum, resulting in net torque in the desired direction of rotation for steering purposes. A tacking or gybing design will possibly need at least two center hydrofoils to reflect leeway and vertical forces from the aerofoil on both tacks. Both configurations may need active control of pitch. A J- or C-foil configuration of the center foils could be configured in such a way that they reflect the kite pull dynamically to increase stability. The high speed potential of this concept suggests a higher risk of loosing pitch stability in seaway and increase cavitation and ventilation. The foils should also be designed to minimize drag, avoid flotsam entanglement and to be able to generate lift reflecting the kite pull. There are some existing concepts that should be taken into consideration when developing the wind powered marine vehicle concept, and may reduce cost of research and development.

Nr	Scoring
20	20
21	15
22	15
23	20
24	7
25	4
26	8
Sum	**89**

Table 3.6: Score chart of mass less hydrofoil

Figure 3.8: Paravane: Ashford anchor. Image courtesy of Robert Biegler

3.2.2 Hull with hydrofoils

The application of a classical hull design may be considered for transportation and payload purposes where the design weight of payload or cargo is significant, and aerial suspension is deemed insufficient. Hereby a classical hull design is defined to be any geometrical bodies that provides a buoyancy force greater than the system gravity force. A hull may be of a classical displacement type, a planning design or hybrids. As in the mass less hydrofoil concept, the hull design should incorporate hydrofoils to reflect the leeway and forces from the aerofoil system, to ensure a net forward momentum. Important aspects for a hull design are minimization of wetted surface regarding drag, hull volume reflecting demanded buoyancy when system is at rest and during surface impacts, and longitudinal stability for navigation purposes. Also slamming effects at high speed travel in seaway should be considered, regarding the integrity of payload or cargo. The important aspects for the hydrofoils in this system will be similar as described in section 3.2.1. When considering the implementation of a hull in the overall system, one idea might be to let the hull be lifted out of the water by the aerofoil system forces to reduce and ultimately remove wetted surface induced drag.

Nr	**Scoring**
20	18
21	17
22	15
23	15
24	7
25	4
26	5
Sum	**81**

Table 3.7: Score chart of hull with hydrofoils

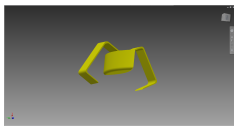

Figure 3.9: Sketch of hull with hydrofoils for tacking configuration

After the hull is foilborne the control system needs to stabilize the flight in such a way that the hull remains foilborne, without letting the system escape the surface, possibly demanding water suspended control surfaces. An airborne vehicle can potentially result in a system failure. When the hull is foilborne the system might be able to transit into a state similar to the mass less hydrofoil system still at market inspiring speed. Due to the fact that such a design potentially will be specialized regarding payload or cargo aspects, research and development is needed and may increase cost compared to a mass less hydrofoil design.

3.3 Total physical system aspects

A concept of aerofoil system and hydrofoil system ultimately has to be connected in a complete vehicle system. This section aims to highlight some important aspects regarding the physical properties of a wind powered marine vehicle that are not already mentioned.

The aerofoil system can be connected to the hydrofoil system and controlled by a bridle system, such as traditional kite surfing systems used for leisure purposes, to avoid torque transfer to the vehicle. Kite surfers control their kite by altering the length of the outermost tethers in the bridle system connected to the sides of the kite, resulting in a twist of the kite about the pitch (or yaw) axis, generating a change of yaw angle. They are usually able to control pitch angle directly by altering (all) control tethers at the same time. This concept of control demands actuators near the point of connection to the vehicle, and an analysis of forces and response frequency relative to total line force is suggested. Given the unstable flight dynamics of a kite, the energy cost of a control system may be substantially. In the absence of strong and conductive cables connecting the aerofoil and hydrofoil, a large actuator as well as energy storage and harvesting system must be carried in the air. This configuration will increase the volume of the aerofoil and possibly the aerodynamic forces, which again demands a larger actuator. If the main mass carried is water suspended, larger actuation forces can be tolerated.

The implementation of an aerofoil based on the concept of tensairity should consider the introduction of control surfaces, based on the resulting stiffness of the foil. If the foil stiffness becomes relatively large in comparison to a soft fabric kite, control by tether deflection resulting in twist about the pitch axis may not be optimal or even possible.

3.3.1 Bridle system

Bridles are hereby defined to be two or more lines or cables spreading a pull force in the bridle's longitudinal direction. Important aspects to be considered regarding the design of the bridle system should be wear and tear, such as corrosion of metals, UV-damaging of polymers, snap loads, extreme loads, maximum load capacity,fracture mechanics, ventilation in water and air, ringing from vortex shedding in water and air, lightning damage and influence on life at sea. Polymers are frequently used in sailing and kite surfing due to their low weight to strength ratio, but will be disposed to

UV-damage and fracture mechanics, where breaking of individual fibres and friction damage are important aspects. The bridles robustness is one of the most crucial factors for the overall system redundancy, as one can imagine the resulting system failure in the case of a broken bridle. If the communication between the aerofoil electronics and the hydrofoil electronics is wired, it will most certainly have to run along the bridle system and the redundancy of the overall system is even more reliant on the bridle system. Aerodynamic drag on the tether should be considered as an important factor regarding the kite dynamics.

3.3.2 Hinge

A hinge is hereby defined to be a part of a stationary frame that allows swinging of the attached part relative to the frame. The transfer of forces from the aerofoil to the hydrofoil system will be trough a hinge, to ensure zero torque transfer. Some important aspects of a hinge in the overall physical system are friction due to bridle interaction, maximum load capacity, corrosion of metals, snap loads, flotsam entanglement, lightning damage and fracture mechanics.

3.4 Cost

Total cost expectations should be estimated and compared to market expectations and its propensity to invest when evaluating the feasibility of different concepts. Suggested markets are oil and gas, oceanographic studies, fishing industry, maritime industry, aquaculture, crime spotting and leisure. These different markets span a variety of monetary resources, which will affect the course of a concept development. Some important cost factors are materials, research and development, production and eventually marketing.

3.5 Chosen concept of study

This section aims to describe the chosen concept of study in the proceeding sections of this thesis. The choice is based on the previous sections, as well as discussions, expert opinions and the authors personal references.

3.5.1 Aerofoil concept

The choice of aerofoil concept regarding propulsion fell on an soft fabric multi-panel kite of the parawing type. This kind of kite has slower dynamics compared to a stunt kite used in kite surfing due to its lower lift-to-drag-ratio, suggesting more forgiving response regarding a control system design. The multi-panel design provides a relative large kite volume that is optimal regarding LTA design. The soft fabric structure suggests a low storage volume. The non-rigid structure however may introduce significant higher-order effects, such as aeroelasticity and deformation due to differences in external and internal fluid pressure.

The parawing in consideration is controlled through a control bar, attached to the kites sides in such a way that dynamic control of local yaw and pitch is possible. This may be an advantage compared to kites where roll angle is dynamically control, while the pitch angle is more or less static regarding control response. An important aspect of consideration is loss of control when to aggressive control is applied in yaw, as it was observed that the tether lines twists instead of the kite responding to the control input.

3.5.2 Hydrofoil concept

The choice of hydrofoil concept regarding overall system design fell on a paravane designed by Robert Biegler. The choice fell on this design due to the fact that Biegler has been developing this kind of design for some time, as well as the potential high speed capabilities. The cost of research and development was virtually negligible. The design was somewhat unconventional and exciting regarding the authors personal reference.

According to Biegler, the long canard of prototype II seen in figure 3.11 is split into a separate canard and a ventral fin. Then the canard can be set to provide lift when contouring the surface, while the ventral fin is set at neutral, so that it does not drive the hull up out of the water. To gybe it may be enough to set the canard at neutral and make the ventral fin roll and turn the paravane, or perhaps it will need both. The idea behind using

Figure 3.10: Tow test of 1st paravane design iteration

servo rudders to control canard and ventral fin is both to reduce the power needed and that the effective lever arm between canard and servo rudder increases as the paravane pitches down, giving more lift to the canard. The elevator/rudder has a long lever arm so that it has effective control against the lever arm between the point where the kite line attaches and the centre of lift and drag. The kite line attaches to about the middle of the spine. The structure above the water surface, would be able to carry a few solar cells and position lights. Position lights could also be placed on each wing tip, and the set above the water switched on, if it is permitted for lights to be invisible for the few seconds of a gybe, when both sets are submerged. The line on the wing shows the bend, including that it is towed out. The paravane can be connected by tethers, one to transfer the main constraint force, one for steering the local yaw angle for navigation purposes, and one for steering the pitch angle for diving and gybing operations.

The paravane can be understood as a structure of foils where net momentum at the force transfer point is an important design factor. Biegler's design incorporates a wave breaker, as seen in figure 3.10, at the structure foremost point in the longitudinal axis, in order to avoid diving in seaway. Further the foil structure has a transverse control surface in front of the center of momentum to provide control input in pitch. In the longitudinal axis there is a spine designed for structural integrity regarding net momentum about the transverse axis, as well as a foil designed for stability in yaw and

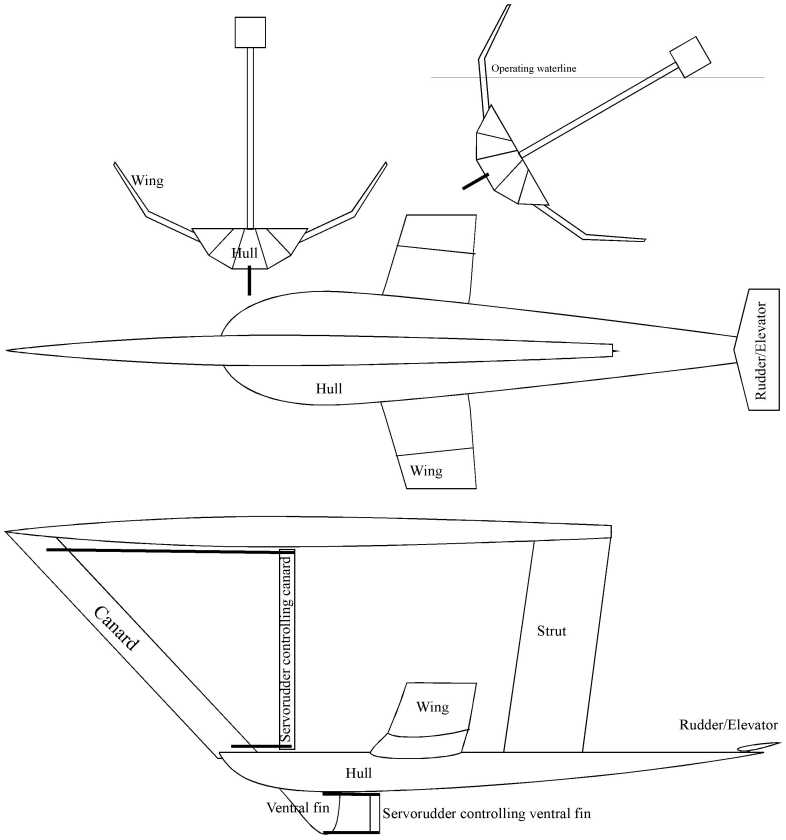

Figure 3.11: Gybing paravane: Image courtesy of Robert Biegler

sway. The aft foils consist of a set angle transverse foil as well as a rudder. Displaced in the transverial axis from the center point of momentum, there is a double L-shape foil in the vertical axis, designed to counter leeway pull similar to a keel on a conventional sailboat. The L-shape design should be able to reflect the vertical as well as the transverse pull even at significant roll angles. The double L-shape design is due to the discrete switching of system properties during gybing operations.

The overall design is intended to reflect the transverse and vertical pull at the point of force transfer, while minimizing drag in the longitudinal direction, as well as following the sea surface in order to stay submerged. The paravane can be controlled in pitch and yaw. During gybing operations, the paravane is controlled in pitch and yaw, such that it rolls $\approx 180^\circ$ about its longitudinal axis and switches dynamics, such that the L-shape keel design is able to reflect the vertical and transverse pull from the new tack while sailing.

3.5.3 Total system

The idea is to connect the paravane and the kite with actuators at the center of force transfer on the paravane. The further progress of the will be to investigate strategies in control system design for such a configuration. This thesis will be focusing on the dymamics and control of the kite system, modelled with a fixed origin. The goal will be to identify important aspects of control system design. The thesis will remain highly conceptual, considering the choice of concept.

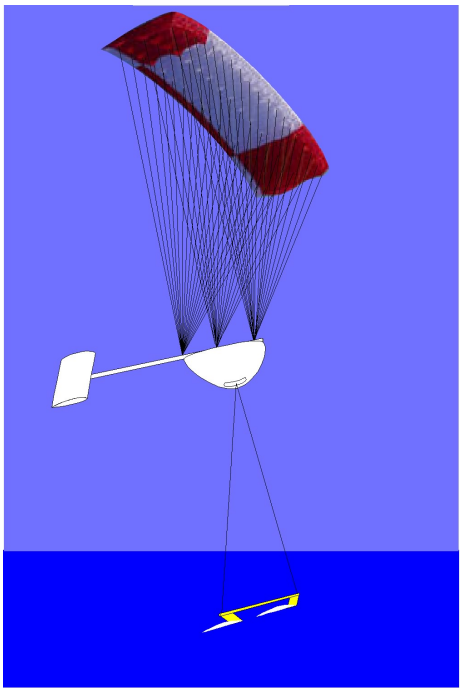

Figure 3.12: Conceptual illustration of parawing and paravane connected with wind rudder. Image courtesy of Robert Biegler

Chapter 4

Background and Mathematical Modelling

This section aims to introduce the reader to basic sailing mechanics and establish a mathematical model for the dynamics of a multi panel soft fabric parawing kite in order to further investigate important aspects of the design of a control system for a kite that can be applied in a wind powered marine vehicle concept. The topics covered are an introduction to sailing and foil dynamics and a mathematical model of the dynamics of a parawing kite.

4.1 Introducton to sailing

Sailing is hereby defined to be exploitation of wind power by active control of areo- and hydrofoils in order to generate a net forward momentum of a marine vehicle. Sailing can roughly be divided into traction based sailing and aerodynamic lift based sailing. In traction based sailing the idea is to utilize the aerofoil friction, and the impermeability of the wing, to pull the vehicle in the direction of the ambient wind velocity. Lift based sailing is further explained in this thesis and will remain the main focus regarding sail theory. This section ultimately aims to provide the reader with a basic understanding of sailing.

4.1.1 Wind velocity terms

True wind is defined to be the wind velocity vector in an inertial reference frame, such as the NED frame. **Apparent wind** is defined to be the wind velocity vector sum of true wind and body velocity, or trivially explained as the wind velocity experienced at the body in motion. For a high speed sailing vessel the sail configuration can be divided in relation to three different sectors of angle to the apparent wind; close hauled sailing, reaching and broad reaching. Sailing close-hauled is defined to be sailing with an heading angle $< 90°$, reaching at $\approx 90°$ and running $> 90°$ to the ambient wind, according to [19]. These sectors are chosen as they are generally known do define different areas of important loads. When sailing close hauled, the leeway drift and torque in roll are classically important loads, while pitch and roll torque is important while broad reaching. The reader should take note that the position in these zones vary dynamically for a high-speed sailing vessel, as the apparent wind shifts forward as the vehicle velocity increases. For high-speed sailing vehicles, the heading angle to the apparent wind will be the deciding factor.

4.1.2 Changing tack: tacking, gibing and shunting

The resulting force vector of any lift generating aerofoil need to have an angle of attack to the incoming wind in order to generate lift. When the angle of attack becomes large enough, the foil will **stall**. According to [14], the resulting force vector of a foil is governed by

$$\mathbf{F} = L\mathbf{u} + D\mathbf{l}, \quad \mathbf{u} \cdot \mathbf{l} = 0 \tag{4.1}$$

According to [2] when the angle of attack becomes small enough, a phenomena occurs that defines the no sail zone. This zone will be reflect about a symmetry axis parallel to true wind. The **tack** of a sail is defined to be the position of the sail regarding the symmetry axis facing true wind, divided into port and starboard tack. **Tacking** in general is defined to be the manoeuvre where the vehicle changes tack. Tacking by crossing the true wind bow first is called coming about or tacking, whilst changing tack stern to windward is called gybing. Shunting is defined to be the manoeuvre of changing tack on a proa, where stern and bow of the vessel is switched. The three different manoeuvres are illustrated in figure 4.1.

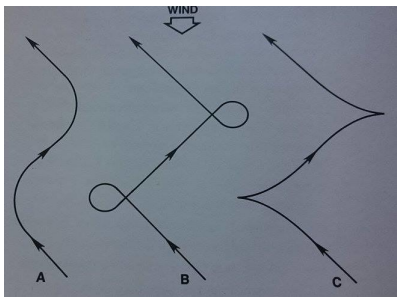

A Coming about

B Gybing

C Shunting

Figure 4.1: Different trajectories for change of tack.Taken from [2]

4.1.3 Sailing efficiency

How efficiently a vehicle is able to sail usually considers how well the vehicle sails in different angles to true wind. Note that sailing directly into the wind is impossible as discussed in section 4.1.2, and powered propulsion has to be incorporated. At large angles of attack, the aerofoil may stall and thus generating drag only. The lift-to-drag-ratio provides the drag angle that is the theoretical highest point to windward the vessel is able to sail. According to [6] this angle can be roughly defined to be a sum of aero- and hydrodynamic drag angle:

$$\alpha_s = \chi_h + \chi_a \tag{4.2}$$

where the drag angle is defined to be

$$\tan \chi_i = (L/D)^{-1} \tag{4.3}$$

where L/D is the lift-to-drag ratio. The maximal theoretical vehicle velocities at different heading angles to true wind ϕ can be calculated according to [2] by equation 4.2 and

$$V_b = \frac{\sin \phi - \alpha_s}{\sin \alpha_s} \tag{4.4}$$

This equation assumes constant angle of attack, constant L/D-ratio of aerofoil and hydrofoils, mass-less configuration, force sum transfer of forces between aerofoil and hydrofoils, zero leeway drift, and that the vehicle velocity V_b perfectly reflects the apparent wind. These assumptions may not reflect real world experience, but gives an initial perspective of the vehicles velocity potential. When the lift and drag force coefficients are varying with angle of attack, there will be a point at small angles of attack where lift equals drag. There will also be a region with declining lift at large angles of attack,

with lift eventually reaching zero, as well as the lift-to-drag-ratio. This will eventually define the closest angle to apparent wind the vehicle is able to sail in a real world situation, as well as performance throughout the wind directional window. A polar plot of maximum theoretical velocity vs angle to true wind ϕ at true wind speed $W = 10\ [ms^{-1}]$ is presented for a mass less configuration in figure 4.2 with parameters declared in table 4.1 at constant lift and drag coefficients.

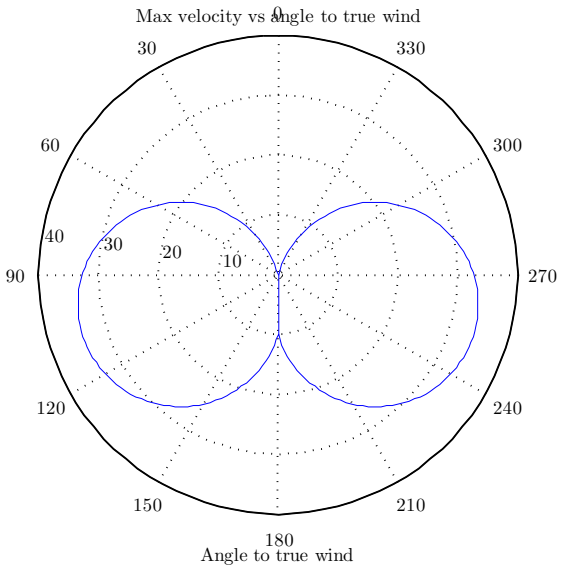

Figure 4.2: Polar plot of velocity potential vs heading angle to wind

The maximum theoretical velocity of such a configuration is computed to be 34.16 $[ms^{-1}]$ at and angle to incoming wind $\phi = 107.56°$.

Name	**Value**
L/D_h	10
L/D_a	5
W	10 $[ms^{-1}]$

Table 4.1: Parameters

4.2 Introduction to foil dynamics

This section aims to provide the reader with a basic understanding of rigid structure foil dynamics, which is an essential background for this thesis.

According to [20], a foil need an incoming fluid flow velocity U and circulation around the foil in order to generate lift. The lift and drag force magnitude $L,\ D$ in quasi-static modelling is defined as:

$$L = C_L \frac{1}{2} \rho U^2 S \tag{4.5}$$

$$D = C_D \frac{1}{2} \rho U^2 S \tag{4.6}$$

where $C_L,\ C_D$ is the lift and drag coefficients, ρ is the density of the fluid and S is the planform area,or area of the foil. The foil area is defined to be the projected area of the foil in the direction of the lift force of zero angle of attack.

α is the angle of attack, or the angle between the foil center line and incoming fluid flow as seen in figure 4.3. In practice the lift to drag ratio varies by angle of attack until the foil stalls. By assuming relatively small angle of attack with small or no change, constant lift to drag ratio may be assumed for a streamlined foil, such as the NACA-foil. F is the net force from the foil, which is a sum of the lift and drag force vectors.

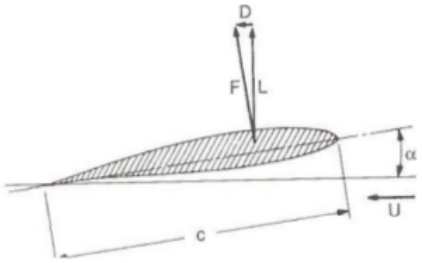

Figure 4.3: Foil definitions. Image taken from [20]

Foil theory is based on the following boundary conditions:

The kinematic boundary condition no fuild particle can penetrate the surface of the foil

The Kutta condition the flow must leave tangentially from the trailing edge, i.e. the foil must not be stalling

The far-field condition at a point at infinity distance from the foil, the fluid velocity equals the undisturbed fluid velocity U

The lift force vector is defined to be perpendicular to the incoming fluid flow vector. The drag force vector is defined to be parallel to the incoming fluid flow vector. The thrust force T of a foil is relevant in sailing, and is defined to be the the component of the lift and drag force along the α direction as seen in figure 4.4. As the angle of attack increases, the thrust force increases accordingly until the foil stalls.

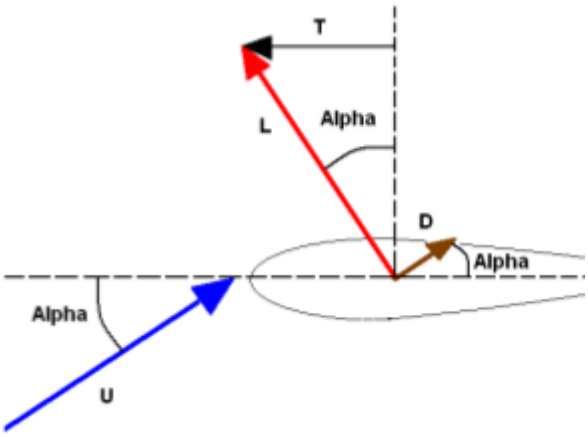

Figure 4.4: figure
Thrust force of foil. Image taken from [20]

4.3 Mathematical model of kite dynamics

In this section the dynamics of a multi panel, low aspect ratio, soft fabric kite are studied in detail. In order to carry out analytic and numerical analysis the kite model is simplified to a rigid wing with constant angle of attack, resulting in constant lift to drag ratio and associated coefficients. In a real world application, this relates to a set pitch angle on the kite and assuming the accelerations of the kite will be instantaneous compared to the slower dynamics of a connected hydrodynamic system according to [8]. This assumption implies that higher order aerodynamics, such as transient dynamics, aeroelasticity and vortex shedding are neglected. The kite used within this section is attached along both edges parallel to the kites local roll axis, through tether lines to a control bar also parallel to the roll axis when the yaw and pitch angles relatively between the control bar and the kite are zero. This implies that the control bar and the kite experience the same angular motions, and that the concept assumes direct control of yaw and pitch angle of the kite through manipulation of the orientation of the control bar. This assumption may not be true in a real world application.

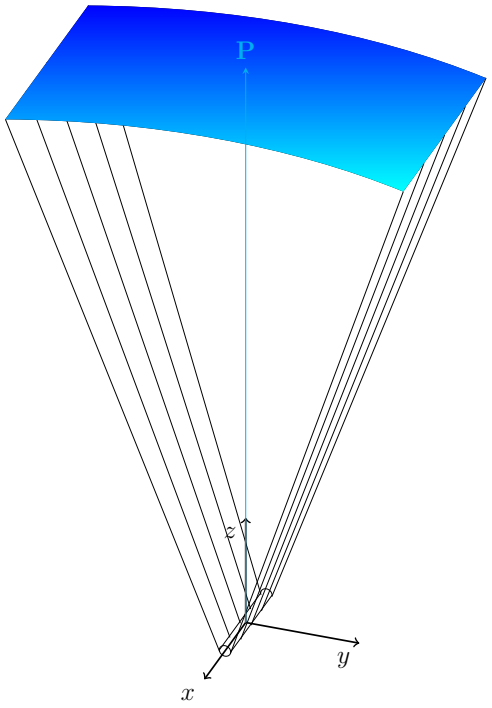

Figure 4.5: Soft fabric multi panel parawing kite model

4.3.1 Kite coordinate system

In order to carry out both an analytical and a numerical analysis of the kite system, the equation of motion and a local coordinate system describing the kites motion, has to be established. This section follows the nomenclature of [21]. As the kite is constrained by a tether with constant length l to the control bar, a spherical coordinate system is convenient to describe its flight dynamics. The position vector $\mathbf{p} \in \mathbb{R}^3$ in cartesian coordinates with its origin at the pivot center of the control bar as seen from the kite pilot, with the ambient wind $\mathbf{W} \in \mathbb{R}^3$ as positive in the x-direction, is defined as:

$$\mathbf{p} = \begin{pmatrix} x \\ y \\ z \end{pmatrix} = l\,\mathbf{e}_r \tag{4.7}$$

where $\mathbf{e}_r$ is the unit vector parallel to the tether described by spherical coordinates:

$$\mathbf{e}_r \in \mathbb{R}^3 = \begin{pmatrix} \sin\theta\cos\phi \\ \sin\theta\sin\phi \\ \cos\theta \end{pmatrix} \tag{4.8}$$

where θ is the spherical elevation angle and ϕ is the spherical azimuth angle. Let us introduce a local right handed coordinate system with the three basis vectors $\mathbf{e}_r$,

$$\mathbf{e}_\theta \in \mathbb{R}^3 = \begin{pmatrix} \cos\theta\cos\phi \\ \cos\theta\sin\phi \\ -\sin\theta \end{pmatrix} \tag{4.9}$$

and

$$\mathbf{e}_\phi \in \mathbb{R}^3 = \begin{pmatrix} -\sin\phi \\ \cos\phi \\ 0 \end{pmatrix} \tag{4.10}$$

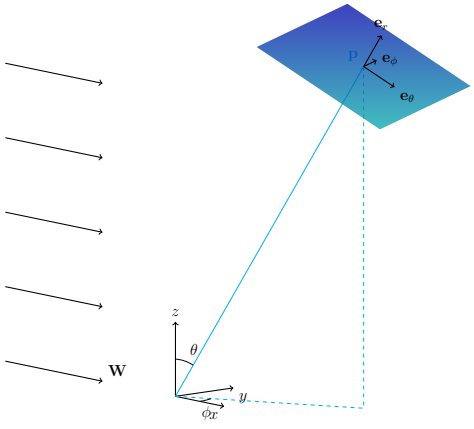

Figure 4.6: Local basis vectors

4.3.2 Equation of motion

The system equation of motion becomes:

$$\ddot{\mathbf{p}} = \frac{d^2\mathbf{p}}{dt^2} = \frac{\mathbf{F}}{m} \tag{4.11}$$

where $\mathbf{F} \in \mathbb{R}^3$ is the force vector containing the resultant forces acting on the kite in cartesian coordinates, and m is the mass of the kite system. In order to compute the velocity and accelerations of the kite, the time derivatives have to be established according to [21] with velocity

$$\dot{\mathbf{p}} = r\mathbf{e}_\theta\dot{\theta} + r\sin(\theta)\mathbf{e}_\phi\dot{\phi} + \mathbf{e}_r\dot{r} \tag{4.12}$$

and acceleration:

$$\begin{aligned}\ddot{\mathbf{p}} = {} & \mathbf{e}_\theta\big(r\ddot{\theta} - r\sin(\theta)\cos(\theta)\dot{\phi}^2 + 2\dot{r}\dot{\theta}\big) \\ & + \mathbf{e}_\phi\big(r\sin(\theta)\ddot{\phi} + 2r\cos(\phi)\dot{\phi}\dot{\theta} + 2\sin(\theta)\dot{r}\dot{\phi}\big) \\ & + \mathbf{e}_r\big(\ddot{r} - r\dot{\theta}^2 - r\sin^2(\theta)\dot{\phi}^2\big)\end{aligned} \tag{4.13}$$

By introducing the constant tether length $r = l_t \Rightarrow \dot{r} = \ddot{r} = 0$, (4.12) is simplified to

$$\dot{\mathbf{p}} = l_t\mathbf{e}_\theta\dot{\theta} + l_t\sin(\theta)\mathbf{e}_\phi\dot{\phi} \tag{4.14}$$

and (4.13) is simplified to:

$$\begin{aligned}\ddot{\mathbf{p}} = {} & \mathbf{e}_\theta\big(l_t\ddot{\theta} - l_t\sin(\theta)\cos(\theta)\dot{\phi}^2\big) \\ & + \mathbf{e}_\phi\big(l_t\sin(\theta)\ddot{\phi} + 2l_t\cos(\phi)\dot{\phi}\dot{\theta}\big) \\ & - \mathbf{e}_r\big(+ l_t\dot{\theta}^2 + l_t\sin^2(\theta)\dot{\phi}^2\big)\end{aligned} \tag{4.15}$$

If we now introduce components from the force vector $\mathbf{F}$ by the same scheme as for the local coordinates for the kite the projection of the total force in the respective axes can be represented as follows:

$$F_\theta = \mathbf{F}\cdot\mathbf{e}_\theta, \quad F_\phi = \mathbf{F}\cdot\mathbf{e}_\phi, \quad \text{and} \quad F_r = \mathbf{F}\cdot\mathbf{e}_r \tag{4.16}$$

the equation of motion can be established and solved for $\ddot{\theta}$ and $\ddot{\phi}$ such that:

$$\ddot{\theta} = \frac{F_\theta}{l_t m} + \sin(\theta)\cos(\theta)\dot{\phi}^2 \tag{4.17}$$

$$\ddot{\phi} = \frac{F_\phi}{l_t m} - 2\cot(\theta)\dot{\phi}\dot{\theta} \tag{4.18}$$

According to [21] the force component in the tether direction F_r, as defined by equation (4.16), will become redundant, as the force in the tether direction will be augmented by a constraint force contribution F_c, so that F_r in (4.13) is automatically satisfied when the augmented force $F_r' = F_r - F_c$ replaces F_r. The constraint force becomes:

$$F_c = F_r + ml_t(\dot{\theta}^2 + \sin^2\theta\,\dot{\phi}^2) \tag{4.19}$$

4.3.3 Kite orientation and aerodynamic forces

In this section the goal is to build a foundation of system vectors describing the resulting aerodynamic loads in the system as well as applying the control inputs, and their relations through the different coordinate systems. The kite is modelled as a point mass particle and it is assumed that the kites leading edge is always pulled towards the apparent wind vector $\mathbf{W}_e$. Only steady state aerodynamic forces at a constant angle of attack are considered. These assumptions greatly simplifies the computational cost and complexity in building a simulation environment.

The ambient wind $\mathbf{W}$, is modelled as a uniformly distributed field in the (y, z)-plane with magnitude in x-direction only, as seen in figure 4.5. This implies that the kite coordinate system is always rotated such that the x-axis is always parallel to the ambient wind vector $\mathbf{W}$. The kite will see the apparent wind vector $\mathbf{W}_e$ as a difference in the ambient wind and the kites velocity:

$$\mathbf{W}_e = \mathbf{W} - \dot{\mathbf{p}}, \quad \mathbf{e}_{We} = \frac{\mathbf{W}_e}{\|\mathbf{W}_e\|_2} \tag{4.20}$$

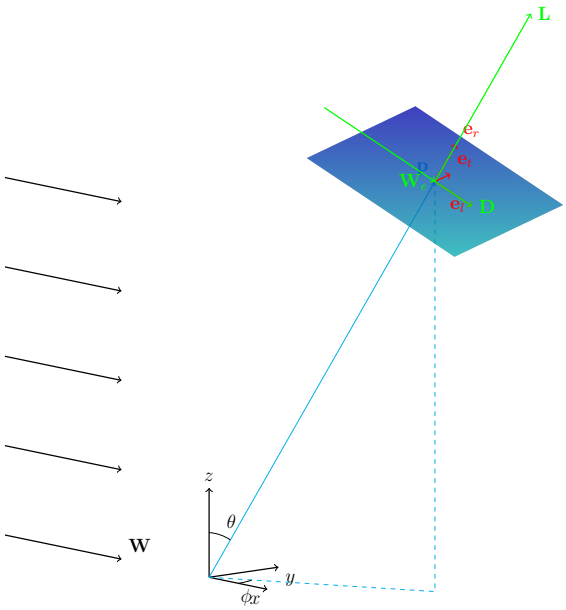

Figure 4.7: Resulting aerodynamic loads hand help vectors

By definition, the aerodynamic drag vector $\mathbf{D}$, is parallel to the apparent wind vector $\mathbf{W}_e$, before rotations are applied. The aerodynamic lift is always orthogonal to the drag vector. A new local coordinate system at $\mathbf{p}$ is defined by unit vectors $\mathbf{e}_l, \mathbf{e}_t$ and $\mathbf{e}_\psi$, as seen in figure 4.7, in order to project the aerodynamic force components. The kites longitudinal (roll) axis $\mathbf{e}_l$ is defined as:

$$\mathbf{e}_l = \frac{\mathbf{W}_e}{\|\mathbf{W}_e\|_2} \tag{4.21}$$

the kites transverse axis $\mathbf{e}_t$ is defined as:

$$\mathbf{e}_t = \frac{\mathbf{e}_l \times \mathbf{e}_r}{\|\mathbf{e}_l \times \mathbf{e}_r\|_2} = \frac{\mathbf{W}_e \times \mathbf{e}_r}{\|\mathbf{W}_e \times \mathbf{e}_r\|_2} \tag{4.22}$$

and the kites vertical axis $\mathbf{e}_\psi$ is defined as:

$$\mathbf{e}_\psi = \mathbf{e}_t \times \mathbf{e}_l = \frac{(\mathbf{e}_l \times \mathbf{e}_r) \times \mathbf{e}_l}{\|\mathbf{e}_l \times \mathbf{e}_r\|_2} = \frac{(\mathbf{W}_e \times \mathbf{e}_r) \times \mathbf{W}_e}{\|\mathbf{W}_e\|_2 \|\mathbf{W}_e \times \mathbf{e}_r\|_2} \tag{4.23}$$

where the fact that $\|\mathbf{e}_t \times \mathbf{e}_l\|_2 = 1$ due to orthogonality is applied. In order for $\mathbf{e}_t, \mathbf{e}_\psi$ to well defined, the following constraint on the system dynamics occurs:

$$\|\mathbf{W}_e \times \mathbf{e}_r\|_2 \neq 0 \tag{4.24}$$

that is when the apparent wind vector is parallel to the position vector of the kite, i.e. when the position vector is parallel to the kite x-axis, which is when $\theta = \phi = 0$. Before rotations by the control input, the aerodynamic drag is parallel to $\mathbf{e}_l$ and the aerodynamic lift is parallel to $\mathbf{e}_\psi$. The control input is defined as rotation ψ_c about the kites local yaw axis $\mathbf{e}_\psi$, and rotation φ_c about the kites local pitch axis. As seen in figure 4.8, the control input φ can be defined as:

$$\sin(\varphi_c) = \frac{\Delta l_t}{l_k} = \mathbf{e}_l^* \cdot \mathbf{e}_r, \quad \cos(\varphi_c) = \sqrt{\frac{l_k^2 - \Delta l_t^2}{l_k^2}} \tag{4.25}$$

where $\Delta l_t \in [-l_c, l_c]$,where l_c is the length of the control bar, Δl_t is the length difference that occurs in the tether lines at the fore and aft points of the control bar, when compared to the neutral position (when zero control is applied) in the control bars local pitch direction.

Note that the sign of Δl_t defines the direction of rotation in pitch, and can be defined arbitrary. l_k is the length of the kite and $\mathbf{e}_l*$ is the kites longitudinal axis after rotation φ_c is applied, such that φ_c defines the rotation angle between vectors $\mathbf{e}_l^*$ and $\mathbf{e}_r$. The control input ψ_c defines the rotation of the kite about its local yaw axis $\mathbf{e}_\psi$ such that:

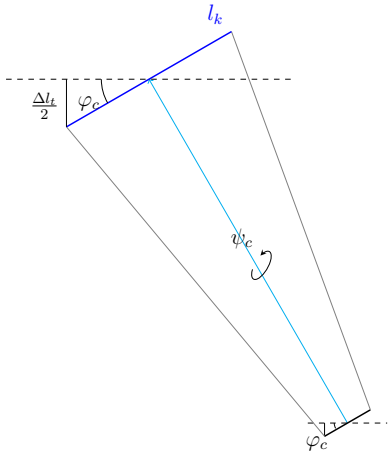

Figure 4.8: Control input ψ_c, φ_c

$$\cos(\psi_c) = \mathbf{e}_l \cdot \mathbf{e}_l^* = \sqrt{\frac{l_c^2 - 4l_{rc}^2}{l_c^2}}, \quad l_r \in [-l_c/2, l_c/2] \tag{4.26}$$

where l_{rc} is the reel out length of the control bar in the yaw-direciton.

$$\cos(\psi_c - 90°) = \cos(90 - \psi_c) = \sin(\psi_c) = \mathbf{e}_l \cdot \mathbf{e}_t^* = \frac{2l_{rc}}{l_c} \tag{4.27}$$

where $\mathbf{e}_t$ is the kites local transverse (pitch) axis after control input is applied. Note that it is assumed that the tether lines are always fully loaded by a pulling force. This may not be true in a real world application, specially when aggressive yaw control is applied in yaw, $\Delta\psi_c$. This phenomena can be described as the kite dynamics are slower than the control input, and

the result is a twist of the tether lines about $\mathbf{p}$. This phenomena is further described in section 7. The drag force magnitude is expressed as:

$$F_D = \frac{1}{2}\rho_a A_k C_D \|\mathbf{W}_e\|^2 \tag{4.28}$$

and the lift force magnitude is expressed as:

$$F_L = \frac{1}{2}\rho_a A_k C_L \|\mathbf{W}_e\|^2 \tag{4.29}$$

where ρ_a is the air density, A_k is the area of the kite, C_D is the kites constant drag force coefficient, C_L is the kites constant lift force coefficient. The projections of the drag and lift vectors onto $\mathbf{e}_l, \mathbf{e}_t, \mathbf{e}_\psi$ after control input can now be defined as:

$$\mathbf{D} = F_D(\cos\varphi_c \cos\psi_c \mathbf{e}_l + \cos\varphi_c \sin\psi_c \mathbf{e}_t + \sin\varphi_c \mathbf{e}_\psi) \tag{4.30}$$

and

$$\mathbf{L} = F_L(-\sin\varphi_c \cos\psi_c \mathbf{e}_l - \sin\varphi_c \sin\psi_c \mathbf{e}_t + \cos\varphi_c \mathbf{e}_\psi) \tag{4.31}$$

note that by inserting the relation $F_L/F_D = E = const$ and orthogonality, the following constraint has to be satisfied:

$$\frac{\mathbf{D}}{\|\mathbf{D}\|_2} \cdot \frac{\mathbf{L}}{\|\mathbf{L}\|_2} = 0 \tag{4.32}$$

Further the control input rotations in relation to $\mathbf{e}_l, \mathbf{e}_t, \mathbf{e}_\psi$ needs to be introduced. ψ_c rotates the system about $\mathbf{e}_\psi$ and φ_c rotates the system about $\mathbf{e}_t$. The relations to the main system coordinates needs to be established as well. The projection of $\mathbf{e}_l, \mathbf{e}_t, \mathbf{e}_\psi$ onto $\mathbf{e}_r, \mathbf{e}_\theta, \mathbf{e}_\phi$ are of interest. The projection of $\mathbf{e}_l$ onto $\mathbf{e}_r, \mathbf{e}_\theta, \mathbf{e}_\phi$ can be defined as:

$$\begin{gathered}(\mathbf{e}_l \cdot \mathbf{e}_r)\mathbf{e}_r = \frac{\mathbf{W}_e \cdot \mathbf{e}_r}{\|\mathbf{W}_e\|_2}\mathbf{e}_r, \quad (\mathbf{e}_l \cdot \mathbf{e}_\theta)\mathbf{e}_\theta = \frac{\mathbf{W}_e \cdot \mathbf{e}_\theta}{\|\mathbf{W}_e\|_2}\mathbf{e}_\theta \\ (\mathbf{e}_l \cdot \mathbf{e}_\phi)\mathbf{e}_\phi = \frac{\mathbf{W}_e \cdot \mathbf{e}_\phi}{\|\mathbf{W}_e\|_2}\mathbf{e}_\phi\end{gathered} \tag{4.33}$$

The projection of $\mathbf{e}_t$ onto $\mathbf{e}_r, \mathbf{e}_\theta, \mathbf{e}_\phi$ can be defines as:

$$\begin{aligned}&(\mathbf{e}_t \cdot \mathbf{e}_r)\mathbf{e}_r = (\mathbf{e}_l \times \mathbf{e}_r) \cdot \mathbf{e}_r = (\mathbf{e}_r \times \mathbf{e}_r) \cdot \mathbf{e}_l = 0, \\ &(\mathbf{e}_t \cdot \mathbf{e}_\theta)\mathbf{e}_\theta = [(\mathbf{e}_l \times \mathbf{e}_r) \cdot \mathbf{e}_\theta]\mathbf{e}_\theta = [(\mathbf{e}_\theta \times \mathbf{e}_r) \cdot \mathbf{e}_l]\mathbf{e}_\theta = -(\mathbf{e}_\phi \cdot \mathbf{e}_l)\mathbf{e}_\theta \\ &(\mathbf{e}_t \cdot \mathbf{e}_\phi)\mathbf{e}_\phi = [(\mathbf{e}_l \times \mathbf{e}_r) \cdot \mathbf{e}_\phi]\mathbf{e}_\phi = [(\mathbf{e}_\phi \times \mathbf{e}_r) \cdot \mathbf{e}_l]\mathbf{e}_\phi = (\mathbf{e}_\theta \cdot \mathbf{e}_l)\mathbf{e}_\phi\end{aligned} \tag{4.34}$$

where orthogonality in $\mathbf{e}_r, \mathbf{e}_\theta, \mathbf{e}_\phi$ is used. The projection of $\mathbf{e}_\psi$ onto $\mathbf{e}_r, \mathbf{e}_\theta, \mathbf{e}_\phi$ can be defines as:

$$\begin{aligned}(\mathbf{e}_\psi \cdot \mathbf{e}_r) &= -\|\mathbf{e}_l \times \mathbf{e}_r\|_2 \mathbf{e}_r, \quad \mathbf{e}_\psi \perp \mathbf{e}_l \\ (\mathbf{e}_\psi \cdot \mathbf{e}_\theta)\mathbf{e}_\theta &= ([(\mathbf{e}_l \times \mathbf{e}_r) \times \mathbf{e}_l] \cdot \mathbf{e}_\theta)\mathbf{e}_\theta = \Big(\frac{(\mathbf{W}_e \times \mathbf{e}_r) \times \mathbf{W}_e)}{\|\mathbf{W}_e\|_2^2} \cdot \mathbf{e}_\theta\Big)\mathbf{e}_\theta \\ (\mathbf{e}_\psi \cdot \mathbf{e}_\phi)\mathbf{e}_\phi &= \Big(\frac{(\mathbf{W}_e \times \mathbf{e}_r) \times \mathbf{W}_e)}{\|\mathbf{W}_e\|_2^2} \cdot \mathbf{e}_\phi\Big)\mathbf{e}_\phi\end{aligned} \tag{4.35}$$

Singularities in the force components can occur when the magnitude of the apparent wind is zero, which means that there is zero aerodynamic forces and the system fails. Now the lift and drag force components can be expressed according to (4.16):

$$\begin{aligned}D_\theta &= F_D\big[\cos(\varphi_c)\cos(\psi_c)(\mathbf{e}_l \cdot \mathbf{e}_\theta) + \cos(\varphi_c)\sin(\psi_c)(\mathbf{e}_t \cdot \mathbf{e}_\theta) + \sin(\varphi_c)(\mathbf{e}_\psi \cdot \mathbf{e}_\theta)\big] \\ &= F_D\Big[\cos(\varphi_c)\cos(\psi_c)\frac{\mathbf{W}_e \cdot \mathbf{e}_\theta}{\|\mathbf{W}_e\|_2} - \cos(\varphi_c)\sin(\psi_c)\frac{\mathbf{e}_\phi \cdot \mathbf{W}_e}{\|\mathbf{W}_e\|_2} \\ &+ \sin(\varphi_c)\Big(\frac{(\mathbf{W}_e \times \mathbf{e}_r) \times \mathbf{W}_e)}{\|\mathbf{W}_e\|_2^2} \cdot \mathbf{e}_\theta\Big)\Big]\end{aligned} \tag{4.36}$$

and

$$\begin{aligned}D_\phi &= F_D\big[\cos(\varphi_c)\cos(\psi_c)(\mathbf{e}_l \cdot \mathbf{e}_\phi) + \cos(\varphi_c)\sin(\psi_c)(\mathbf{e}_t \cdot \mathbf{e}_\phi) + \sin(\varphi_c)(\mathbf{e}_\psi \cdot \mathbf{e}_\phi)\big] \\ &= F_D\Big[\cos(\varphi_c)\cos(\psi_c)\frac{\mathbf{W}_e \cdot \mathbf{e}_\phi}{\|\mathbf{W}_e\|_2} + \cos(\varphi_c)\sin(\psi_c)\frac{\mathbf{W}_e \cdot \mathbf{e}_\theta}{\|\mathbf{W}_e\|_2} \\ &+ \sin(\varphi_c)\Big(\frac{(\mathbf{W}_e \times \mathbf{e}_r) \times \mathbf{W}_e)}{\|\mathbf{W}_e\|_2^2} \cdot \mathbf{e}_\phi\Big)\Big]\end{aligned} \tag{4.37}$$

and

$$\begin{aligned}D_r &= F_D\big[\cos(\varphi_c)\cos(\psi_c)(\mathbf{e}_l \cdot \mathbf{e}_r) + \cos(\varphi_c)\sin(\psi_c)(\mathbf{e}_t \cdot \mathbf{e}_r) + \sin(\varphi_c)(\mathbf{e}_\psi \cdot \mathbf{e}_r)\big] \\ &= F_D\Big[\cos(\varphi_c)\cos(\psi_c)\frac{\mathbf{W}_e \cdot \mathbf{e}_r}{\|\mathbf{W}_e\|_2} - \sin(\varphi_c)\frac{\|\mathbf{W}_e \times \mathbf{e}_r\|_2}{\|\mathbf{W}_e\|_2}\Big]\end{aligned} \tag{4.38}$$

and

$$\begin{aligned}L_\theta &= F_L[-\sin(\varphi_c)\cos(\psi_c)(\mathbf{e}_l \cdot \mathbf{e}_\theta) - \sin(\varphi_c)\sin(\psi_c)(\mathbf{e}_t \cdot \mathbf{e}_\theta) + \cos(\varphi_c)(\mathbf{e}_\psi \cdot \mathbf{e}_\theta)] \\ &= F_L\Big[-\sin(\varphi_c)\cos(\psi_c)\frac{\mathbf{W}_e \cdot \mathbf{e}_\theta}{\|\mathbf{W}_e\|_2} + \sin(\varphi_c)\sin(\psi_c)\frac{\mathbf{e}_\phi \cdot \mathbf{W}_e}{\|\mathbf{W}_e\|_2} \\ &+ \cos(\varphi_c)\Big(\frac{(\mathbf{W}_e \times \mathbf{e}_r) \times \mathbf{W}_e)}{\|\mathbf{W}_e\|_2^2} \cdot \mathbf{e}_\theta\Big)\Big]\end{aligned} \tag{4.39}$$

and

$$\begin{aligned} L_\phi &= F_L[-\sin(\varphi_c)\cos(\psi_c)(\mathbf{e}_l \cdot \mathbf{e}_\phi) - \sin(\varphi_c)\sin(\psi_c)(\mathbf{e}_t \cdot \mathbf{e}_\phi) + \cos(\varphi_c)(\mathbf{e}_\psi \cdot \mathbf{e}_\phi)] \\ &= F_L\Big[-\sin(\varphi_c)\cos(\psi_c)\frac{\mathbf{W}_e \cdot \mathbf{e}_\phi}{\|\mathbf{W}_e\|_2} - \sin(\varphi_c)\sin(\psi_c)\frac{\mathbf{W}_e \cdot \mathbf{e}_\theta}{\|\mathbf{W}_e\|_2} \\ &+ \cos(\varphi_c)\Big(\frac{(\mathbf{W}_e \times \mathbf{e}_r) \times \mathbf{W}_e)}{\|\mathbf{W}_e\|_2^2} \cdot \mathbf{e}_\phi\Big)\Big] \end{aligned} \tag{4.40}$$

and

$$\begin{aligned} L_r &= F_L[-\sin(\varphi_c)\cos(\psi_c)(\mathbf{e}_l \cdot \mathbf{e}_r) - \sin(\varphi_c)\sin(\psi_c)(\mathbf{e}_t \cdot \mathbf{e}_r) + \cos(\varphi_c)(\mathbf{e}_\psi \cdot \mathbf{e}_r)] \\ &= F_L\Big[-\sin(\varphi_c)\cos(\psi_c)\frac{\mathbf{W}_e \cdot \mathbf{e}_r}{\|\mathbf{W}_e\|_2} - \cos(\varphi_c)\frac{\|\mathbf{W}_e \times \mathbf{e}_r\|_2}{\|\mathbf{W}_e\|_2}\Big] \end{aligned} \tag{4.41}$$

4.3.4 Aerodynamic drag on tether

This section follows [22] in order to establish the aerodynamic drag force on the tether. The tether lines are modelled by a single line parallel to $\mathbf{p}$. The normal reaction coefficient $C_\perp$, is set to account for the total drag on the tether lines. Further, it is assumed that the tether lines are always loaded and by pull only. Higher order aerodynamics on the tether lines are neglected. Let the projection of the apparent wind onto the tangential plane spanned by the basis unit vectors $\mathbf{e}_\theta$ and $\mathbf{e}_\phi$ be defined as:

$$\mathbf{W}_e^p = \mathbf{W}_e - (\mathbf{e}_r \cdot \mathbf{W}_e)\mathbf{e}_r \tag{4.42}$$

such that the aerodynamic drag on the tether can approximated as:

$$\mathbf{D}_t = \frac{1}{8}\rho_a d_t C_\perp l_t \|\mathbf{W}_e^p\| \mathbf{W}_e^p \tag{4.43}$$

where d_t is the tether diameter, l_t is the tether length. Lets define $F_{Dt} = \frac{1}{8}\rho_a d C_\perp l \|\mathbf{W}_e^p\|$. Then the tether drag expressed according to (4.16) becomes:

$$D_{t,\theta} = F_{D,t}(\mathbf{W}_e \cdot \mathbf{e}_\theta) \tag{4.44}$$

and

$$D_{t,\phi} = F_{D,t}(\mathbf{W}_e \cdot \mathbf{e}_\phi) \tag{4.45}$$

where the orthogonality $\mathbf{e}_\theta \perp \mathbf{e}_r$ and $\mathbf{e}_\phi \perp \mathbf{e}_r$ has been used. Note that $\mathbf{W}_e^p \perp \mathbf{e}_r \Rightarrow D_{t,r} = 0$.

4.4 Sum of forces and system state definition

This section aims to build a decomposition of the force resultant on the kite defined by (4.16), in order to establish the open-loop system.

The resulting force in cartesian coordinates is defined as:

$$\mathbf{F} = \mathbf{L} + \mathbf{D} + \mathbf{D}_t + \mathbf{M}_g \tag{4.46}$$

where the gravity force is defined as:

$$\mathbf{M}_g = (0, 0, -mg)^T = M_\theta \mathbf{e}_\theta + M_\phi \mathbf{e}_\phi + M_r \mathbf{e}_r \tag{4.47}$$

The components according to (4.16) becomes:

$$F_\theta = L_\theta + D_\theta + D_{t,\theta} + M_\theta \tag{4.48}$$

,

$$F_\phi = L_\phi + D_\phi + D_{t,\phi} + M_\phi \tag{4.49}$$

and

$$F_r = L_r + D_r + D_{t,r} + M_r \tag{4.50}$$

where

$$M_\theta = \sin(\theta) mg, \quad M_\phi = 0 \quad \text{and} \quad M_r = -\cos(\theta) mg \tag{4.51}$$

where m is the system mass and g is the acceleration of gravity. Note that the system mass should take account for the mass experienced by a fully inflated kite, such that $m = m_0 + \Delta\rho V$, $\Delta\rho = \rho_i - \rho_a$, where ρ_i is the inflation gas density. In this mass model, the added buoyancy of a kite with LTA capabilities can be easily included. Now to obtain the relevant force components in (4.16) to solve (4.17), equations (4.39), (4.36), (4.44) and (4.51) is inserted in equation (4.48):

$$\begin{aligned} F_\theta = & \left[F_D \cos(\varphi_c)\cos(\psi_c) - F_L \sin(\varphi_c)\cos(\psi_c)\right] \frac{\mathbf{W}_e \cdot \mathbf{e}_\theta}{\|\mathbf{W}_e\|_2} \\ & + \left[F_D \cos(\varphi_c)\sin(\psi_c) - F_L \sin(\varphi_c)\sin(\psi_c)\right] \frac{\mathbf{e}_\phi \cdot \mathbf{W}_e}{\|\mathbf{W}_e\|_2} \\ & + \left[F_D \sin(\varphi_c) + F_L \cos(\varphi_c)\right] \frac{[(\mathbf{W}_e \times \mathbf{e}_r) \times \mathbf{W}_e] \cdot \mathbf{e}_\theta}{\|\mathbf{W}_e\|_2^2} \\ & + F_{D,t}(\mathbf{W}_e \cdot \mathbf{e}_\theta) + \sin(\theta) mg \end{aligned} \tag{4.52}$$

Now to solve (4.18), equations (4.40), (4.37), (4.45) and (4.51) is inserted in equation (4.49):

$$\begin{aligned} F_\phi = &\left[F_D\cos(\varphi_c)\cos(\psi_c) - F_L\sin(\varphi_c)\cos(\psi_c)\right]\frac{\mathbf{W}_e\cdot\mathbf{e}_\phi}{\|\mathbf{W}_e\|_2} \\ &+ \left[F_D\cos(\varphi_c)\sin(\psi_c) - F_L\sin(\varphi_c)\sin(\psi_c)\right]\frac{\mathbf{e}_\theta\cdot\mathbf{W}_e}{\|\mathbf{W}_e\|_2} \\ &+ \left[F_D\sin(\varphi_c) + F_L\cos(\varphi_c)\right]\frac{[(\mathbf{W}_e\times\mathbf{e}_r)\times\mathbf{W}_e]\cdot\mathbf{e}_\phi}{\|\mathbf{W}_e\|_2^2} \\ &+ F_{D,t}(\mathbf{W}_e\cdot\mathbf{e}_\phi) \end{aligned} \tag{4.53}$$

4.4.1 Tether tension

This section aims to provide a definition of the tether tension, which can be useful to identify extreme loads, and aid the design of the tether lines.

As discussed in sectoin 4.3.2 and summarized in (4.19), the tether tension becomes:

$$F_c = F_r + l_t\dot{\theta}^2 + l_t\sin^2(\theta)\dot{\phi}^2 - \cos(\theta)mg \tag{4.54}$$

where F_r is obtained by inserting equations (4.38), (4.41) and (4.51) into (4.50):

$$\begin{aligned} F_r = &\left[F_D\cos(\varphi_c)\cos(\psi_c) - F_L\sin(\varphi_c)\cos(\psi_c)\right]\frac{\mathbf{W}_e\cdot\mathbf{e}_r}{\|\mathbf{W}_e\|_2} \\ &- \left[F_D\sin(\varphi_c) + F_L\cos(\varphi_c)\right]\frac{\|\mathbf{W}_e\times\mathbf{e}_r\|_2}{\|\mathbf{W}_e\|_2} \end{aligned} \tag{4.55}$$

4.4.2 System state representation

Let us define the system state as $x = (\theta, \dot{\theta}, \phi, \dot{\phi})^T$ and the control input $u = (\psi_c, \varphi_c)^T$. The system can be summarized as:

$$\dot{x} = f(x, u) \tag{4.56}$$

where

$$f((\theta,\dot{\theta},\phi,\dot{\phi})^T,\psi_c,\varphi_c) = \begin{pmatrix} \dot{\theta} \\ \frac{F_\theta(\theta,\dot{\theta},\phi,\dot{\phi},\psi_c,\varphi_c)}{l_t m} + \sin(\theta)\frac{g}{l_t} + \sin(\theta)\cos(\theta)\dot{\phi}^2 \\ \dot{\phi} \\ \frac{F_\phi(\theta,\dot{\theta},\phi,\dot{\phi},\psi_c,\varphi_c)}{l_t m} - 2\cot(\theta)\dot{\phi}\dot{\theta} \end{pmatrix} \tag{4.57}$$

Note that the gravitation term of F_θ in (4.52) is explicitly stated in the system state representation in (4.57).

4.4.3 Fossen notation

This section aims to represent the kite process plant in standard Fossen notation, following the nomenclature of [23].

Let $\dot{\epsilon} \in \mathbb{R}^2 = \omega = (\dot{\theta}, \dot{\phi})^T$ be the angular velocities in from the spherical representation defined in section 4.3, and $\dot{\mathbf{p}} \in \mathbb{R}^3$ be the kites velocity vector in cartesian coordinates. $F_c \in \mathbb{R}$ is the tether constraint force which is useful to study important system loads, as well as generated thrust in an propulsion application and an optimization study.

$$\begin{aligned} \dot{\mathbf{p}} &= l_t J(\epsilon)\omega \\ M\dot{\omega} + D(\epsilon)\omega + g(\epsilon) &= \tau_t + \tau_c \\ F_c - l_t \omega^T V(\epsilon)\omega - g_r(\epsilon) &= F_r \end{aligned} \tag{4.58}$$

Where the rotation matrix from sphercial to cartesian coordinates is defined as:

$$J(\epsilon) \in \mathbb{R}^{3\times 2} = \begin{bmatrix} \mathbf{e}_\theta & \sin(\theta)\mathbf{e}_\phi \end{bmatrix} \tag{4.59}$$

where the unit vectors $\mathbf{e}_\theta, \mathbf{e}_\phi$ are defined under section 4.3. The non-linear damping matrix is defined as:

$$D(\epsilon) \in \mathbb{R}^{2\times 2} = \frac{m}{l_t} \begin{bmatrix} 0 & \sin(\theta)\cos(\theta)\dot{\phi} \\ -\cot(\theta) & -\cot(\theta) \end{bmatrix} \tag{4.60}$$

The mass matrix is defined as:

$$M = \begin{bmatrix} m & 0 \\ 0 & m \end{bmatrix} \tag{4.61}$$

and the gravitation matrix is defined as:

$$g(\epsilon) \in \mathbb{R}^2 = \frac{mg}{l_t}(\sin(\theta), 0)^T \tag{4.62}$$

The aerodynamic drag force on the tether is defined as:

$$\tau_t \in \mathbb{R}^2 = F_{D,t} \begin{bmatrix} \mathbf{W}_e \cdot \mathbf{e}_\theta \\ \mathbf{W}_e \cdot \mathbf{e}_\phi \end{bmatrix} = F_{D,t} \begin{bmatrix} \xi_1 \\ \xi_2 \end{bmatrix} \|\mathbf{W}_e\|_2 \tag{4.63}$$

and the control input force vector representation is defined as:

$$\tau_c = \chi^T R_{\psi_c}^T R_{\varphi_c}^T f^T \tag{4.64}$$

where the control input is defined in the rotation matrices:

$$R_{\varphi_c} \in \mathbb{R}^{3\times3} = \begin{bmatrix} c\varphi_c & 0 & s\varphi_c \\ 0 & 1 & 0 \\ -s\varphi_c & 0 & c\varphi_c \end{bmatrix}, \quad R_{\psi_c} \in \mathbb{R}^{3\times3} = \begin{bmatrix} c\psi_c & s\psi_c & 0 \\ -s\psi_c & c\psi_c & 0 \\ 0 & 0 & 1 \end{bmatrix} \tag{4.65}$$

where ψ_c rotates the aerodynamic force resultant about $\mathbf{e}_t$ and ψ_c rotates the aerodynamic force resultant about $\mathbf{e}_\psi$, where the unit vectors $\mathbf{e}_t, \mathbf{e}_\psi$ are defined in equations (4.22) and (4.23). The mapping of the aerodynamic force components onto $\mathbf{e}_{\theta,\,\phi}$ from the kites local coordinate system $\mathbf{e}_l, \mathbf{e}_t, \mathbf{e}_\psi$ is defined in matrix χ:

$$\chi \in \mathbb{R}^{3\times2} = \begin{bmatrix} \xi_1 & \xi_2 \\ \xi_2 & \xi_1 \\ \xi_3 & \xi_4 \end{bmatrix} \tag{4.66}$$

where ξ_i defines the cosine of the rotation angles in the respective mappins, such that:

$$\begin{aligned} \xi_1 &= \mathbf{e}_l \cdot \mathbf{e}_\theta, \quad \xi_2 = \mathbf{e}_l \cdot \mathbf{e}_\phi, \\ \xi_3 &= \mathbf{e}_\psi \cdot \mathbf{e}_\theta, \quad \xi_4 = \mathbf{e}_\psi \cdot \mathbf{e}_\phi \end{aligned} \tag{4.67}$$

where orthogonality is used. The aerodynamic force component vector is defined as:

$$f \in \mathbb{R}^{1\times3} = \begin{bmatrix} F_D & 0 & F_L \end{bmatrix} = F_D \begin{bmatrix} 1 & 0 & E \end{bmatrix} \tag{4.68}$$

where the relation $F_L/F_D = E$ has been used. A similar representation for the tether constraint force is defined as:

$$F_r \in \mathbb{R} = \chi_r^T R_{\psi_c}^T R_{\varphi_c}^T f^T \tag{4.69}$$

where the mapping of the the aerodynamic tether drag force components onto $\mathbf{e}_\theta, \mathbf{e}_\phi$ from the kites local coordinate system is defined as:

$$\chi_r \in \mathbb{R}^3 = \begin{bmatrix} \xi_{r1} \\ 0 \\ \xi_{r2} \end{bmatrix} \tag{4.70}$$

where

$$\xi_{r1} = \frac{\mathbf{W}_e \cdot \mathbf{e}_r}{\|\mathbf{W}_e\|_2}, \quad \xi_{r2} = -\frac{\|\mathbf{W}_e \times \mathbf{e}_r}{\|\mathbf{W}_e\|_2} \tag{4.71}$$

and further

$$V(\epsilon) \in \mathbb{R}^{2\times2} = \begin{bmatrix} 1 & 0 \\ 0 & \sin^2(\theta) \end{bmatrix} \tag{4.72}$$

and the gravitation component is defined as:

$$g_r(\epsilon) \in \mathbb{R} = -\cos(\theta) mg \tag{4.73}$$

Chapter 5

Kite control plant model strategies

This section aims to study different approaches in designing a control plant model for the multi panel parawing kite. Suggestions for appropriate goals for an ideal controller, a controllability analysis for a linearized open loop system, an attempt in establishing a feedback linearization controller as well as a short note on state estimation is presented.

5.1 Objectives for kite control system

This section aims to define a set of goals to be fulfilled by an ideal control plant design.

For sailing in a specific direction in the wind window the tuning goal can be to maximize thrust for a specific heading in the horizontal space, in for instance an inertial frame. The idea is to divide the wind window in different sectors and design an optimal controller for each sector. The sectors can be defined as closed hauled sailing, reaching and broad reaching. There will also be a need for a controller goal for the transition between these sectors as well as for the gybing operation. These controllers should consider the effective wind speed and resulting extreme loads, specially the vertical load, as it might result in an airborne system. Different controllers can for instance be designed based on the ambient wind velocity, ranging from low to moderate wind and extreme wind conditions. Thus, a study to identify the maximum wind speed, and the minimum wind speed defined by the limitations on the applied physical controller should be carried out, and is beyond the scope of this thesis.

A common goal for all sectors should be that the kite has to stay clear of the water ($\theta = 90°$). A hard path constraint function is therefore given, according to [21]:

$$h(x,u) = (75° - \theta) \in [0, 75°], \phi \in (-\pi/2 + \Delta\phi, \pi/2 - \Delta\phi) \tag{5.1}$$

where $\Delta\phi$ is some allowance based on the kites drag angle in order to constrain the kite from flying past the minimum theoretical drag angle. The resulting towing force from the kite in the xy-plane can be defined as $\mathbf{F}_t$. This force can be defined as the projection of the tether constraint force $\mathbf{F}_c$ in the x, y-plane in the system defined in section 4.3, and can be defined as:

$$\|\mathbf{F}_t\|_2 = F_c \left\| \begin{matrix} \sin\theta\cos\phi \\ \sin\theta\sin\phi \\ 0 \end{matrix} \right\|_2 = F_c|\sin\theta| \tag{5.2}$$

with corresponding components in x and y directions:

$$F_{t,x} = F_c|\sin\theta|\cos\phi, \quad F_{t,y} = F_c|\sin\theta|\sin\phi \tag{5.3}$$

where $\phi \in [\phi_0 - \Delta\phi, \phi_0 + \Delta\phi]$, where ϕ_0 is the desired heading in the wind window (reaching etc), and $\Delta\phi$ is the maximum allowance of deviation from this trajectory. Note that this representation will be optimized for speed at a given sailing zone, not heading. In an heading analysis, the rotation regarding angle between desired heading and ambient wind direction should be included, and can be represented as:

$$\max(\|\mathbf{F}_t(x,u)\|_2)|_{\phi=\phi_i} = \max(F_c(\theta, \psi_c, \varphi_c)|\sin\theta|\big|_{\phi=\phi_i} \tag{5.4}$$

where ϕ_i represents the desired direction of the maximized pull force in the local kite system representation, taking into consideration that the heading in an inertial frame is the top goal, such that ϕ_i counters the rotation between the ambient wind and desired heading upon changes in the direction of the ambient wind. Another constraint that should be fulfilled is to minimize the vertical force, in order to keep the vehicle from being pulled out of water:

$$\min(|F_z(\theta, \phi, \psi_c, \varphi_c)|) = \min(|F_c(\theta, \phi, \phi, \psi_c, \varphi_c)|\cos(\theta)) \tag{5.5}$$

The state definition can be rewritten as $\dot{x} = f(x,u)$, where

$$f(x,u) = \begin{pmatrix} \dot{\theta} \\ \frac{F_\theta}{l_t m} + \sin(\theta)\frac{g}{l_t} + \sin(\theta)\cos(\theta)\dot{\phi}^2 \\ \dot{\phi} \\ \frac{F_\phi}{l_t m} - \cot(\theta)\dot{\phi}\dot{\theta} \\ \|F_t\| \\ |F_z| \end{pmatrix} \tag{5.6}$$

To take advantage of the relative wind speed and the associated increase in net generated thrust, kite surfers fly their kites in a sinusoidal manner upwind. Downwind they maximize the net generated thrust by sailing the kite in a lying 8-loop manner. For either, the looping path can be characterised by a non-dimensional unknown period T that is relative to the ambient wind velocity, according to [21].

Periodic boundary conditions on these looping patterns can be expressed in a generalized way as:

$$r(x(0), x(T)) = \begin{pmatrix} \phi(T) - \phi(0) \\ \theta(T) - \theta(0) \\ \dot{\phi}(T) - \dot{\phi}(0) \\ \dot{\theta}(T) - \dot{\theta}(0) \\ \psi_c(T) - \psi_c(0) \\ \varphi_c(T) - \varphi_c(0) \\ \dot{\phi}(0) \\ \frac{1}{T}\int_0^T \|F_t\| dt(0) \\ \lim \frac{1}{T}\int_0^T |F_z| dt - e_{Fz} \end{pmatrix} = \mathbf{0}_{9\times 1} \tag{5.7}$$

where e_{Fz} is the error allowed on the minimization of F_z, and $\dot{\phi}$ is introduced in order to remove the indefiniteness due to symmetry of periodic flying patterns with regards to phase shifts, according to [11]. The constraints on the controller is defined to be:

$$|u| \leq u_{max} \tag{5.8}$$

The summary of the optimal control problem can now be expressed as:

$$\begin{aligned} &\text{maximize } \bar{F}_t(x(t), u(t), T) \\ &\text{minimize } \frac{1}{T}\int_0^T |F_z(x(t), u(t), T)| dt \\ &\text{subject to :} \\ &\forall\, t \in [0, T]: \quad \dot{x} = f(x(t), u(t)) \\ &\forall\, t \in [0, T]: \quad |u| \leq u_{max} \\ &\forall\, t \in [0, T]: \quad h(x(t), u(t)) \in [0, 75^\circ] \\ &\qquad 0 = r(x(0), x(T)) \end{aligned} \tag{5.9}$$

As suggested by Sørensen, this is a typical moving horizon problem to be solved using model predictive control (MPC) theory and nonlinear programming (NLP) algorithms, which is beyond the scope of this thesis.

5.2 Controllability of linearized open loop system

This section aims to investigate the controllability of the unforced open loop kite system at some chosen arbitrary points. The idea is to build a foundation to aid the process of designing a control system for the parawing kite.

The generalized jacobian matrices A, B of the system $\dot{x} = f(x, u)$ from equation (4.57) was computed in MATLAB using the script *main2.m*, seen in appendix B, using the Syms toolbox and can be summarized as:

$$A = \begin{bmatrix} 0 & 1 & 0 & 0 \\ f_1 & f_3 & f_5 & f_7 \\ 0 & 0 & 0 & 1 \\ f_2 & f_4 & f_6 & f_8 \end{bmatrix}_{4\times 4}, \quad B = \begin{bmatrix} 0 & 0 \\ g_1 & g_4 \\ 0 & 0 \\ g_2 & g_4 \end{bmatrix}_{4\times 2} \tag{5.10}$$

where $f_i = f_i(x, u), i = 1 \dots 8$, and $g_j = g_j(x, u), j = 1 \dots 4$. A controllability check was performed at data points: $((\dot{\theta}, \phi) = (0, 0), (-\pi, 0), (\pi, 0), (\pi, \pi), \theta \in [0, \pi/2], \phi \in [-\pi/2, \pi/2])$. The controllability matrix, and the associated jacobians A, B of the linearized system was evaluated at each point, according to [24]:

$$\mathcal{C} = \begin{bmatrix} B & AB & A^2B & A^3B \end{bmatrix}_{n\times(kn)}, n = 4, k = 2 \tag{5.11}$$

and the number of uncontrollable states was stored in a matrix $C_{TB} \in \mathbb{R}^{N\times N}$:

$$C_{TB,i,j} = n - \text{rank}(\mathcal{C}), n = 4, i = j = 1 \dots N \tag{5.12}$$

for $N \times N$ data points, defined by the resolution of θ and ϕ.
A contrallbility check was performed for a kite with parameters presented in table 5.1 for a $N = 50$ resolution on the data points. The results are plotted in figure 5.1 for each data point as defined, in the original kite system defined ins section 4.3. The system was fully controllable (green) for all data points in figure 5.1 a). For the remaining figures, 5.1 b)-d), the linearized system was fully controllable for all states except a region around $\theta = \phi = 0$ where

Parameter	Value	Unit
l_t	7.5	$[m]$
m	1.80	$[kg]$
ρ_a	1.23	$[kgm^{-3}]$
C_L	1.5	$[-]$
C_D	0.5	$[-]$
$C_\perp$	1.2	$[-]$
A_k	10	$[m^2]$
d_t	0.0.1	$[m]$
W	5	$[ms^{-1}]$

Table 5.1: Kite parameters

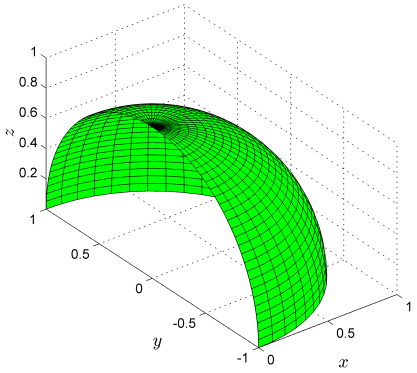

Figure 5.1 a): $\dot{\theta} = 0, \dot{\phi} = 0$

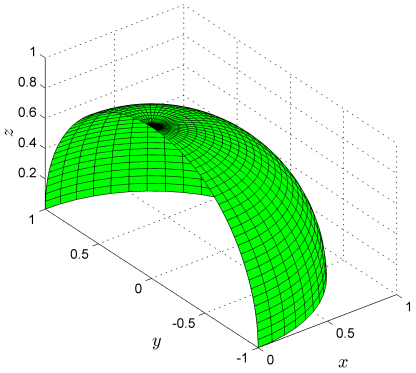

Figure 5.1 b): $\dot{\theta} = -\pi, \dot{\phi} = 0$

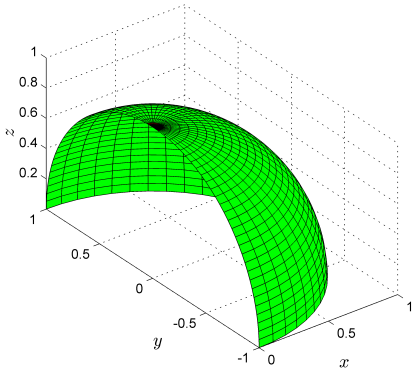

Figure 5.1 c): $\dot{\theta} = \pi, \dot{\phi} = 0$

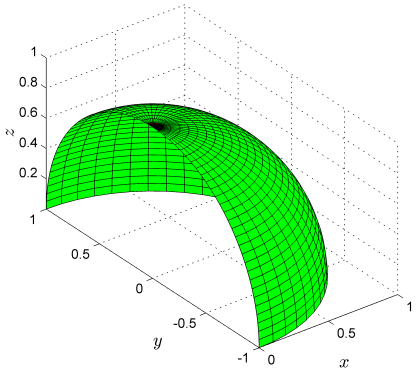

Figure 5.1 d): $\dot{\theta} = \pi, \dot{\phi} = \pi$

Figure 5.1: Controllability checks

controllability check was undefined (red) due to singularities for all ϕ-angles. These results does not completely conform with observed behaviour of kites, as they tend to generate less lift than drag and gravity pull as the angle between the kites longitudinal axis and the uniform ambient wind field goes to zero, with associated loss of control would be expected.

5.3 Feedback linearization of the kite system

This section aims to propose initial steps in the design of a controller based on feedback linearization based on the kite dynamics established in previous sections.

5.3.1 Taylor expansion around small control angles approach

The control input sine terms can be substituted in equations (4.52) and (4.53) by the linear definitions in equations (4.26) and 4.25. A feedback linearization controller can then be designed based on the system established in equaton (4.57) using Taylor expansion series around zero control input regarding the cosine terms as defined in (4.26) and (4.25), where the expansion

$$\sqrt{\frac{a^2 - b^2}{a^2}} \approx 1 + O(a^2) \tag{5.13}$$

can be used, where a, b are real. The F_θ can be approximated as:

$$\begin{aligned} F_\theta \approx \bar{F}_\theta = F_D\Big[1 - 3\frac{\Delta l_t}{l_t}\Big]\xi_1 + F_D\Big[\frac{2l_r}{l_c} - 3\frac{\Delta l_t}{l_t}\frac{2l_r}{l_c}\Big]\xi_2 \\ + F_D\Big[\frac{\Delta l_t}{l_t} + 3\Big]\xi_3 + F_{D,t}\xi_1\|\mathbf{W}_e\|_2 \end{aligned} \tag{5.14}$$

and F_ϕ can be approximated as:

$$\begin{aligned} F_\phi \approx \bar{F}_\phi = F_D\Big[1 - 3\frac{\Delta l_t}{l_t}\Big]\xi_2 + F_D\Big[\frac{2l_r}{l_c} - 3\frac{\Delta l_t}{l_t}\frac{2l_r}{l_c}\Big]\xi_1 \\ + F_D\Big[\frac{\Delta l_t}{l_t} + 3\Big]\xi_3 + F_{D,t}\xi_2\|\mathbf{W}_e\|_2 \end{aligned} \tag{5.15}$$

such that a feedback linearizing controller could be found. The control inputs are coupled. As stated in [21], errors accumulate quickly, and such a controller may not be feasible regarding the unstable dynamics of kites. The small gain theorem should be applied, and under compensating the control input could be wise, according to Sørensen. A PID-controller could be implemented on the state error dynamics, and a stability analysis should be performed on the closed loop system and compared to PID-control on the state error dynamics only. Solving the coupled control input is not trivial, and further linearizing of this control design is beyond the scope of this thesis.

5.3.2 Thrust allocation approach

In this section the aim is to study the approach of feedback linearization of the system represented by the Fossen standard notation in equation (4.58). It involves solving equation (4.58) for $M\dot{\omega} = 0$ such that:

$$\tau_{c0} = D(\epsilon)\omega + g(\epsilon) - \tau_t \tag{5.16}$$

A control input can then be applied as τ_{c1} based on constrained control allocation algorithms, similar to those for azimuth thrusters, as presented in [23] section 12.3.4 as suggested by Skjetne, such that $\tau_c = \tau_{c0} + \tau_{c1}$. Then the resulting demanded generalized control input τ_c can be used to find the demanded control input in equation (4.64) such that:

$$\tau_c = \Gamma R_1 R_2 f, \quad \tau_c = \Gamma v, \quad v = \Gamma^+ \tau_c, \quad v = R_1 R_2 f \tag{5.17}$$

where $R_1 = R_{\psi_c}^T$ and $R_2 = R_{\varphi_c}^T$. A constraint on the validity of such a controller will be if there exist a generalized inverse Γ^+. As $\Gamma \in \mathbb{R}^{2\times 3} = \chi^T$ is broad with rank 2. Assuming Γ is full row rank, the generalized inverse can be computed as:

$$\Gamma^+ = \Gamma^T(\Gamma\Gamma^T)^{-1} = \chi(\chi^T\chi)^{-1} \tag{5.18}$$

such that the existence of the generalized inverse Γ^+ relies on the singularity of $\chi^T\chi$ with eigenvalues:

$$\begin{aligned}
\lambda_1 &= -\Big(\frac{16\xi_1^2\xi_2^2 + 16\xi_1\xi_2\xi_3\xi_4 + \xi_3^4 + 2\xi_3^2\xi_4^2 + \xi_4^4}{2}\Big)^{\frac{1}{2}} + \xi_1^2 + \xi_2^2 + \frac{\xi_3^2}{2} + \frac{\xi_4^2}{2} \\
\lambda_2 &= \Big(\frac{16\xi_1^2\xi_2^2 + 16\xi_1\xi_2\xi_3\xi_4 + \xi_3^4 + 2\xi_3^2\xi_4^2 + \xi_4^4}{2}\Big)^{\frac{1}{2}} + \xi_1^2 + \xi_2^2 + \frac{\xi_3^2}{2} + \frac{\xi_4^2}{2}
\end{aligned} \tag{5.19}$$

where ξ_i's are defined in equation (4.67). For regions where the generalized inverse does not exist, the control input can be kept constant, according to Skjetne. The (generalized) inverse can be computed using singular value decomposition (SVD) for regions where Γ is not full row rank. The conditions of when Γ is full row rank is when there exists $(c_1, c_2, c_3) \in \mathbb{R}^3$ such that $(\xi_1, \xi_2, \xi_3) = (c_1\xi_2, c_2\xi_1, c_3\xi_4) \in \mathbb{R}^3$, where $c_1 \neq c_2 \neq c_3$. Then the only possibility of Γ is not full row rank is when

$$\mathbf{e}_l \cdot \mathbf{e}_\theta = \mathbf{e}_l \cdot \mathbf{e}_\phi = \pm\frac{1}{2} \;\Big|\; \mathbf{e}_\psi \cdot \mathbf{e}_\theta = \mathbf{e}_\psi \cdot \mathbf{e}_\phi = \pm\frac{1}{2} \tag{5.20}$$

Solving the system for the control inputs in the rotation matrices in (5.17) is not trivial, is beyond the scope of this thesis.

5.4 Control actuation, measurements and state estimation

This section aims to propose a setup of actuators and control surfaces for the wind powered marine vehicle concept of study, identify typical problems in obtaining essential state information in order to control the system defined in equation (4.57), and provide the reader with suggested solution strategies.

5.4.1 Control actuation

According to Wahl the most feasible approach for actuating the control angles suggested as control inputs in a control plant based on the kite dynamics presented in section 4.3 is linear servos, as they are able to match the demanded extreme calculated extreme loads as obtained in section 6. A typical inexpensive (1600-2000 NOK) linear servo operating on $12[V]$ DC electric power has $1500[N]$ rated load output, a $500[mm]$ stroke length and a piston speed of $10 - 45[mm/s]$ unloaded. Position servos are much more expensive regarding power output compared to linear servos, and would require a 3-phase power supply and probably a larger power supply and energy storage system, increasing the system mass. Regarding steering and gybing of the paravane, it can be actuated by using linear servos as well. Biegler suggested the use of wind and water suspended rudders such as those used in sailing for self steering purposes, in order to aid steering and possibly gain some inherent stability regarding the control system.

5.4.2 Measurments and state estimation

The system defined by equation (4.57) assumes that all states are known as well the ambient wind vector $\mathbf{W}$. This might be far from the case in a real world application. As discussed in [11] the apparent wind vector at the kite can be measured fairly easy using an anenometer. The position of the kite however, is somewhat more difficult to measure. According to T.I. Fossen, this is a typical attitude estimation problem, where the measurements from instruments such as gyroscopes, accelerometers and magnetometers can be combined with integrated inertial and satellite navigation systems in order to estimate the states involved in computing the kites position. According to [25], the accuracy of the method is dependent on the estimation of the bias on the body-fixed measurements, which is beyond the scope of this thesis.

Chapter 6

Simulation setup and results

In this section simulation results of the open loop system based on the kite dynamics described in section 4.3 in order to identify important system loads and provide an illustrative basis for discussing the validity of the mathematical model. MATLAB and Simulink was used as simulation tools, with the model file *KiteOpenLoop.slx* which is attached in the digital version of this thesis. The main MATLAB script running the simulations can be seen in appendix A.

6.1 Simulation setup

The main goal for the simulation was to investigate the validity of the kite dynamics by comparison to empiric data and identify important system loads. The kite is simulated with a stationary fixed origin, with the ambient wind modelled as a constant uniformly distributed field with a random walk process modelled as zero mean white noise with power density spectrum S_n at a frequency of $10[Hz]$, in order to simulate a real world situation. The simulations ran were with and without the random walk process for open and closed loop system with different initial conditions on the system states.

6.1.1 System block diagram and simulation parameters

In figure 6.1, the system is represented in a block diagram for a visualization of the simulation setup in Simulink. The model is based on equation (4.57). A PID-controller was applied on φ_c, ψ_c based on the error dynamics in θ, ϕ in the closed loop system. The parameters in the controller were chosen by trial and error as the smallest input that was able to reach the set point value

within a reasonable time limit.

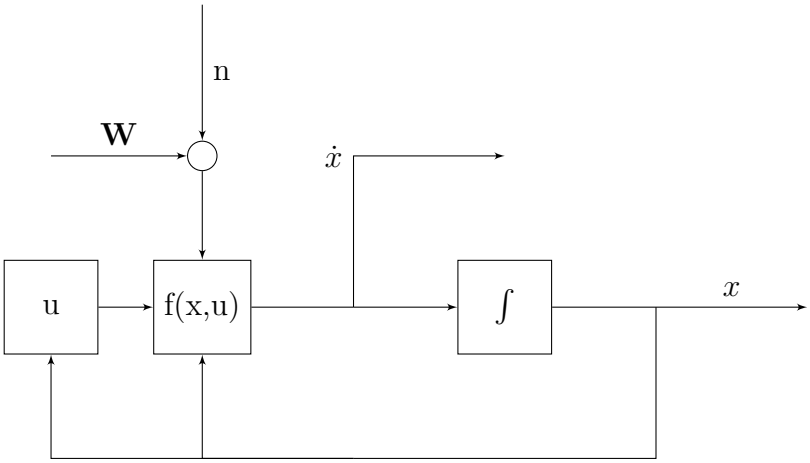

Figure 6.1: Block diagram representation of open loop kite system

The parameters used in the simulations is presented in tables 6.1 and 6.2. The states θ, ϕ where saturated by $\theta \in [\theta_{min}, \theta_{max}]$ and $\phi \in [\phi_{min}, \phi_{max}]$. For simulations 1 and 2 the control input was kept constant at zero, while for simulation 3 and 4, the control input on φ_c computed by the PID-algorithm was saturated by $\varphi_c \in [\varphi_{c,min}, \varphi_{c,max}]$, while the control input in ψ_c was kept constant at zero. For simulation 5, ψ_c was applied the same PID-controller as in simulation 3 and 4, independently of the controller φ_c. The main objective for simulation 1 and 2 was to investigate the behaviour of the open loop system with (simulation 2) and without (simulation 1) noise on the ambient wind velocity vector, as well as studying the tether constraint force.

The main objective for simulation 3 and 4 was to investigate the behaviour of the closed loop system with and without noise on the ambient wind vector, while investigating loads and control demand. According to Wahl, a typical linear servo delivering a force up to $1500[N]$, has a displacement rate in the region of $10 - 45[mms^{-1}$. In simulation 5, a dual PID controller was applied without noise. A guess on the demanded force from actuators applying control input in θ, ϕ was computed by:

$$\tau_\theta = 0.5\ddot{\theta} m_c l_c, \quad \tau_\phi = 0.5\ddot{\phi} m_c l_c \tag{6.1}$$

in order to get an initial perspective of the loads at the control bar. The existence of the generalized inverse of Γ in equation (5.18) was studied as discussed under section 5.3.2. Also the projections of the aerodynamic forces

from the kite local coordinate system described under section 4.3.3 onto the spherical coordinate system by ξ_i's in equation (4.66) was computed.

Name	Value	unit
ρ_a	1.23	$[kgm^{-3}]$
g	9.81	$[ms^{-2}$
C_L	1.5	$[-]$
C_D	0.5	$[-]$
$C_\perp$	1.2	$[-]$
m_k	1.80	$[kg]$
m_c	0.66	$[kg]$
A_k	10	$[m^2]$
l_t	7.5	$[m]$
l_c	1.0	$[m]$
d_t	0.01	$[m]$
θ_{max}	$\pi/2$	[rad]
θ_{min}	0	[rad]
ϕ_{max}	$\pi/2$	[rad]
ϕ_{min}	$-\pi/2$	[rad]
W	3	$[ms^{-1}]$
S_n	0.01	$[NA]$

Table 6.1: Simulation parameters

Simulation 1 & 2		
Name	**Value**	**unit**
T_{sim}	10	$[s]$
θ_0	$1.2\text{atan}(C_D/C_L)$	[rad]
$\dot{\theta}_0$	0	[rad/s]
ϕ_0	0	[rad]
$\dot{\phi}_0$	0	[rad/s]
Simulation 3, 4, 5		
T_{sim}	$10, 1.755, 10$	$[s]$
θ_0	60	[deg]
$\dot{\theta}_0$	0	[rad/s]
ϕ_0	$0, 0, -\pi/8$	[rad]
$\dot{\phi}_0$	0	[rad/s]
θ_{sp}	$\text{atan}(C_D/C_L)$	[rad]
ϕ_{sp}	0	[rad]
ψ_c	0	[rad]
$\varphi_{c,min}$	$-\pi/2$	[rad]
$\varphi_{c,max}$	$\pi/2$	[rad]
K_P	20	$[-]$
K_I	2	$[-]$
K_D	4	$[-]$

Table 6.2: Simulation specific parameters

6.2 Results

In this section the simulation results are presented in figures, and commented. In the end, the results are summarized and discussed to some extent. Red lines in the plots of θ, ϕ-states indicates system failure limits. The green lines in the plots of the θ, ϕ indicates the set point value for the PID-controller. The red lines in the plot of the projection angles ξ_i's indicates the critical value regarding the row rank of Γ. Tether constraint loads above 1000 [N] was chosen as an extreme load limit, as loads above this limit should be able to lift a human operator in a real world application. Fluctuations in the constraint force above 500 [N] over a period less than 1 [Hz] is suggested as a snap load.

6.2.1 Simulation 1: Open loop system

The simulation parameters are stated in tables 6.1 and 6.2. The results are plotted in figures 6.2 through 6.5.

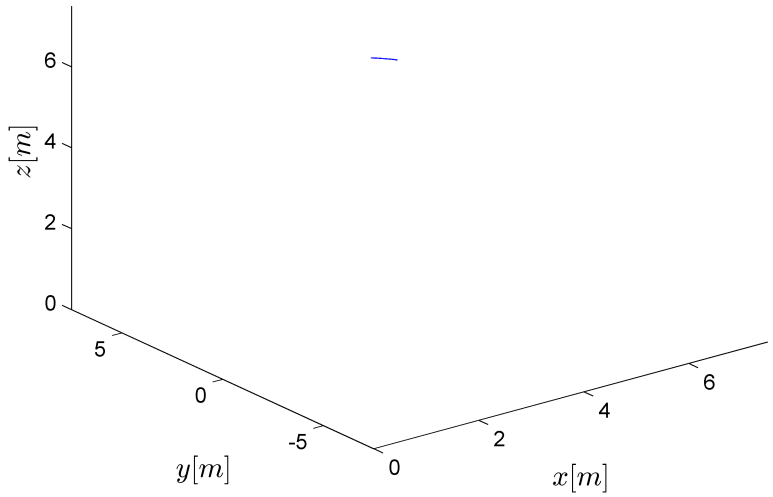

Figure 6.2: Kite 3D trajectory

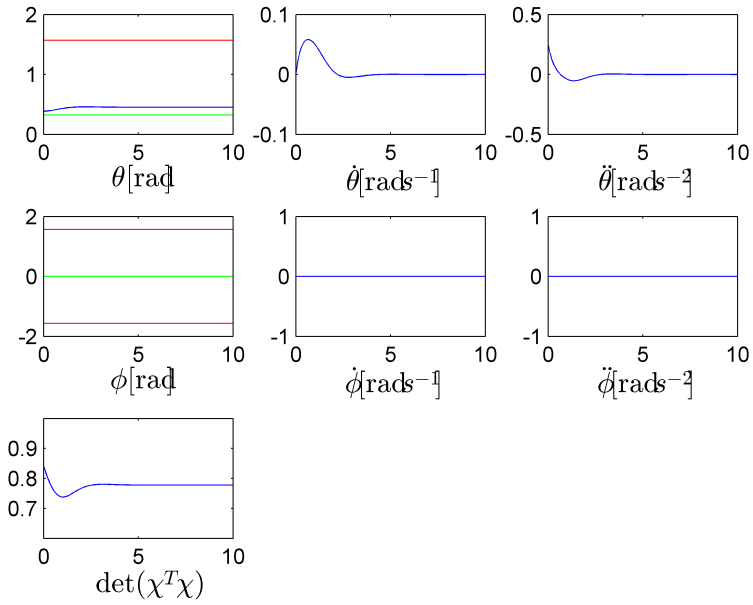

Figure 6.3: System states and det($\chi^T\chi$)

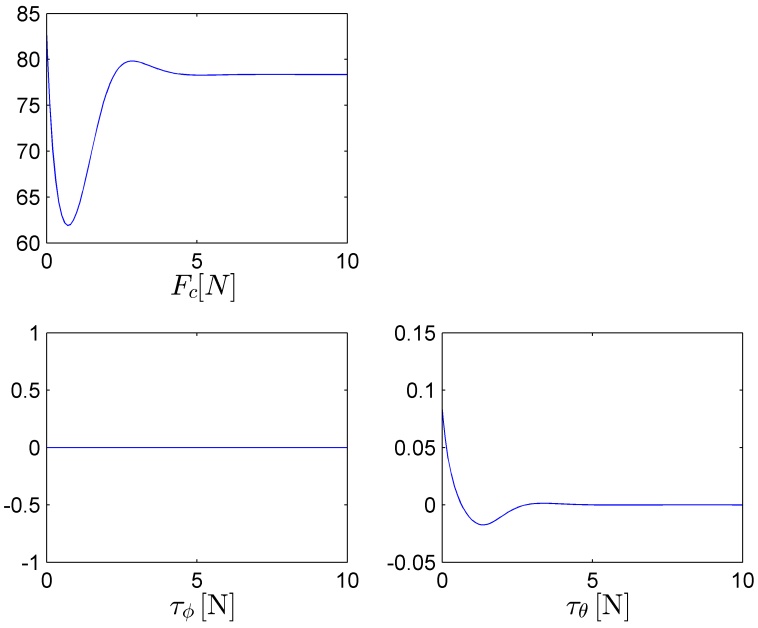

Figure 6.4: System loads

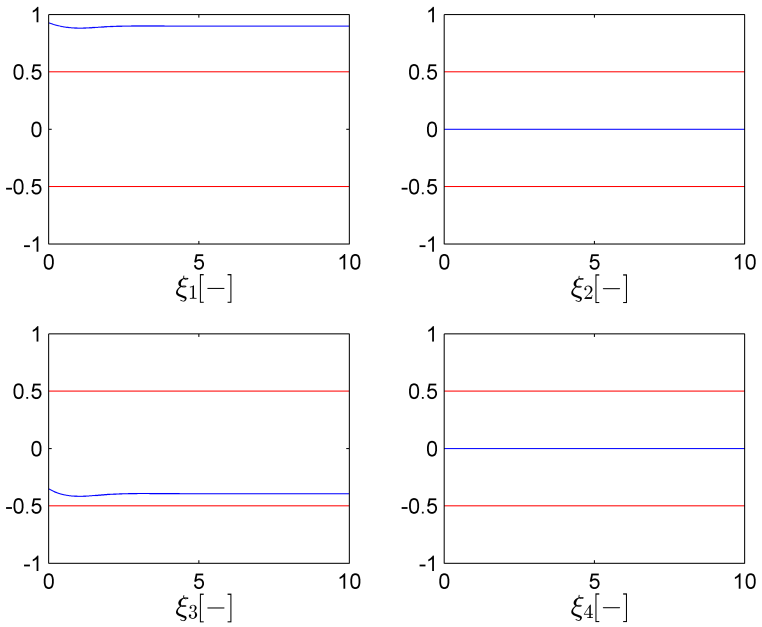

Figure 6.5: ξ_i-values: Row rank Γ

As seen in figure 6.2, for the open loop system without noise, the kite is initially positioned in the theoretical drag angle position and flies over to a position indicating a different computed drag angle where the system lies at rest. As seen in figure 6.3 it can be argued that the generalized inverse Γ^+ exists throughout the simulation. The tether constraint force is not to be considered an extreme load, nor a snap load. The theoretical actuator demand τ_θ, τ_ϕ is in range of suggested linear servos. Figure 6.5 suggests Γ in equation (4.66) is full row rank. The flight trajectory is similar to what one would expect in a real world situation where the wind is stable in direction and velocity.

6.2.2 Simulation 2: Open loop, random walk

The simulation parameters are stated in tables 6.1 and 6.2. The results are plotted in figures 6.6 through 6.9.

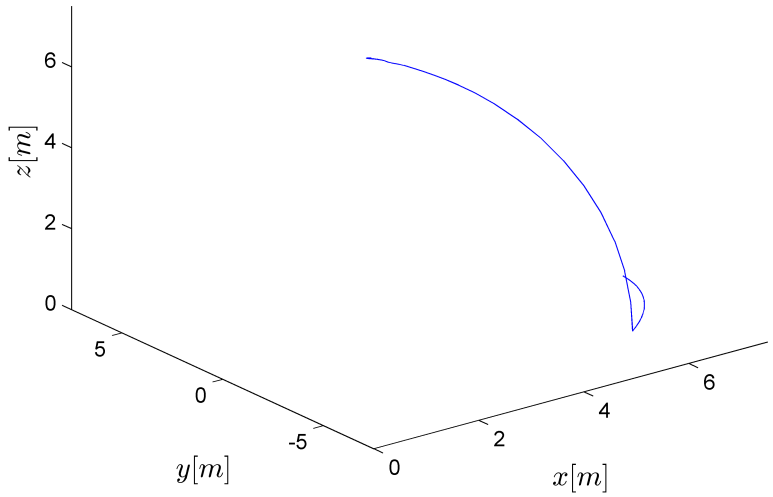

Figure 6.6: Kite 3D trajectory

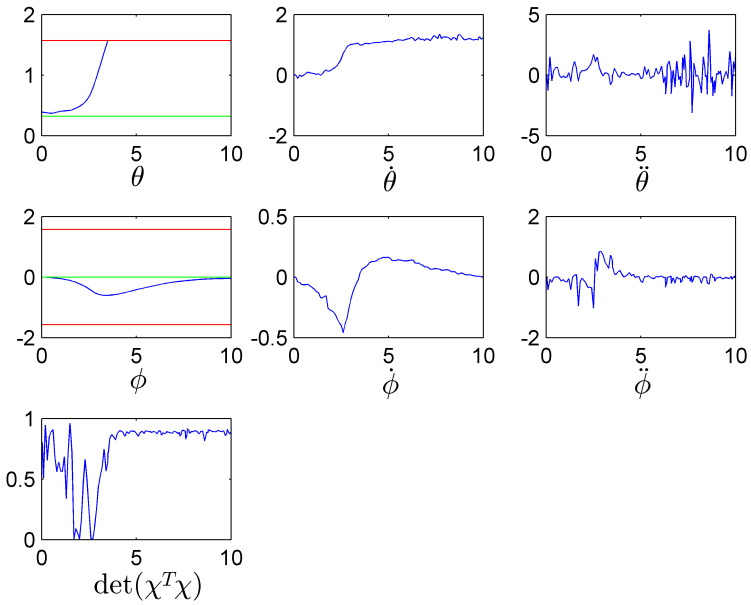

Figure 6.7: System states and $\det(\chi^T\chi)$

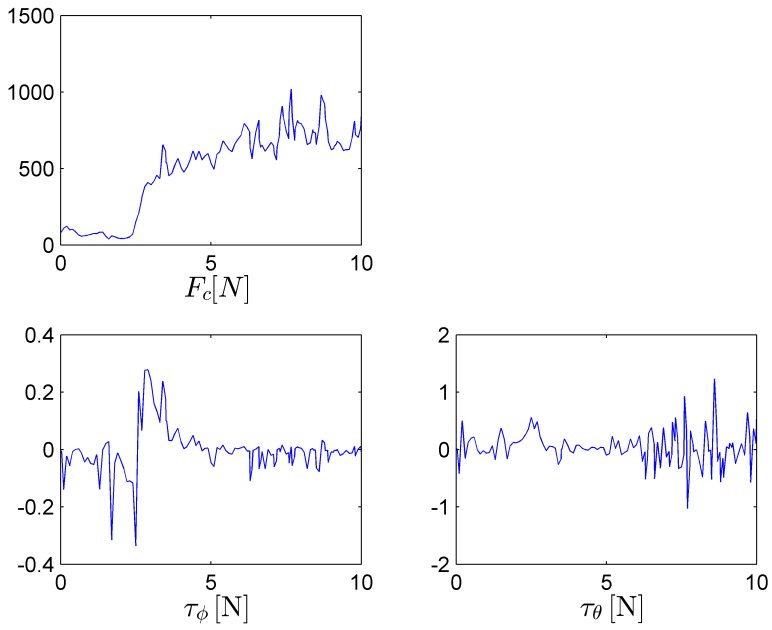

Figure 6.8: System loads

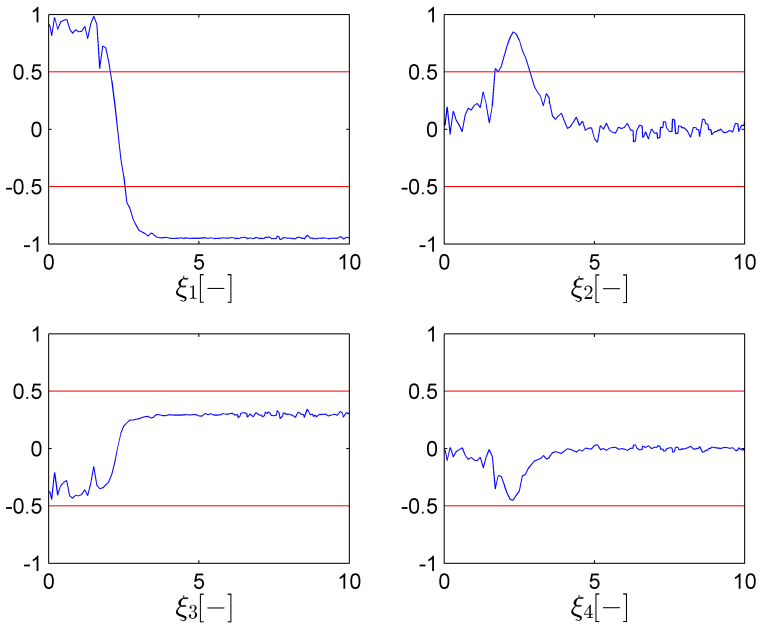

Figure 6.9: ξ_i-values: Row rank Γ

As seen in figure 6.6, the initial position of the kite is the same as in simulation 1. The simulation was run with a random walk process on the ambient wind vector. The kite crashes into the ground within 5 $[s]$ of simulation as it is disturbed from its resting position defined by the computed drag angle as discussed under simulation 1. Simulation results after the point of impact can be regarded as not physical. As seen in figure 6.7, $\det(\chi^T\chi)$ near to, or equal, zero within the first 5 $[s]$ of simulation, indicating that the thrust allocation approach would not be able to dynamically control the system in this region. The projection angles ξ_i's indicates that Γ in equation (5.20) is full row rank throughout the simulation. The loads are within range before the impact. The fluctuations in the constraint force may suggest a snap load situation. An interesting result is that the ϕ-state is influenced by the random walk process, if compared to simulation 1, and becomes non-zero before impact. This suggests a coupled system, as expected from the mathematical model. The response of the kite has high frequency ($< 1[Hz]$), close to the wind random walk process. The trajectory is spherical, which is expected.

6.2.3 Simulation 3: Closed loop system

The simulation parameters are stated in tables 6.1 and 6.2. The results are plotted in figures 6.10 through 6.13.

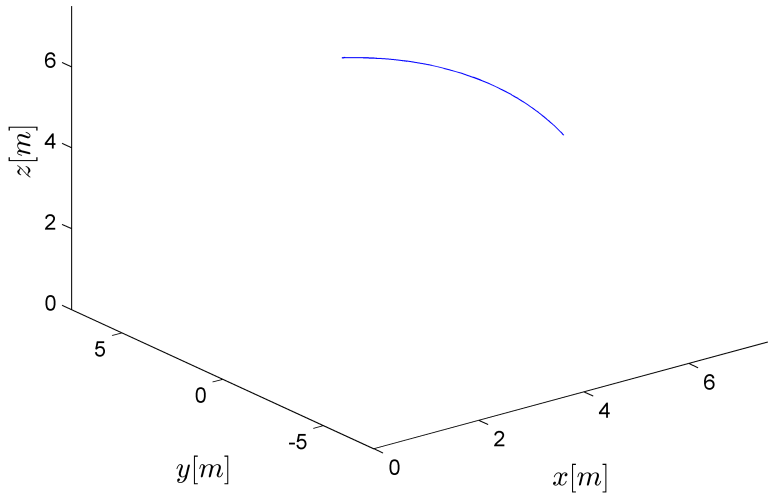

Figure 6.10: Kite 3D trajectory

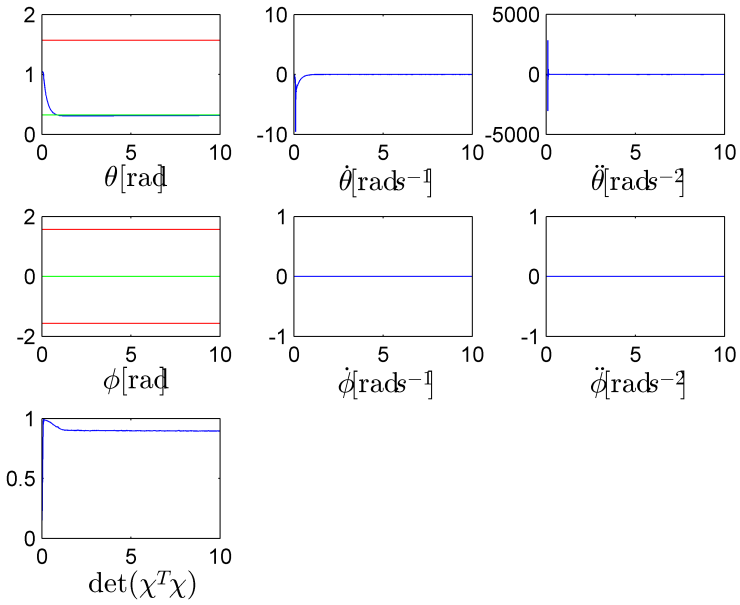

Figure 6.11: System states and det($\chi^T\chi$)

An attempt at controlling the elevation angle θ with a PID-algorithm was carried out without noise on the ambient wind vector. As seen in figure 6.10, the kite flies from its initial position to the set point elevation angle at the theoretical drag angle, and remains at rest. As seen in figure 6.11 the initial response in $\ddot{\theta}$ with associated loads seen in figure 6.12 is considered extreme as a result. The extreme load region suggest snap loads. However, this response may be considered of too high frequency to be physical, and suggests a singularity in the computations. det($\chi^T\chi$) is initially close to zero. Figure 6.13 indicates that Γ remains full row rank throughout the simulation. The theoretical computed controller demanded force and response frequency is too high to that of a typical linear servo.

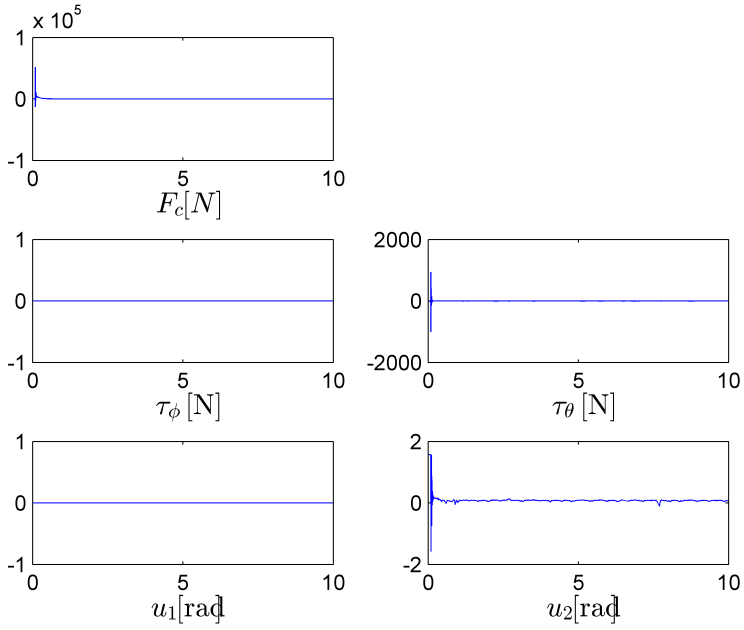

Figure 6.12: System loads

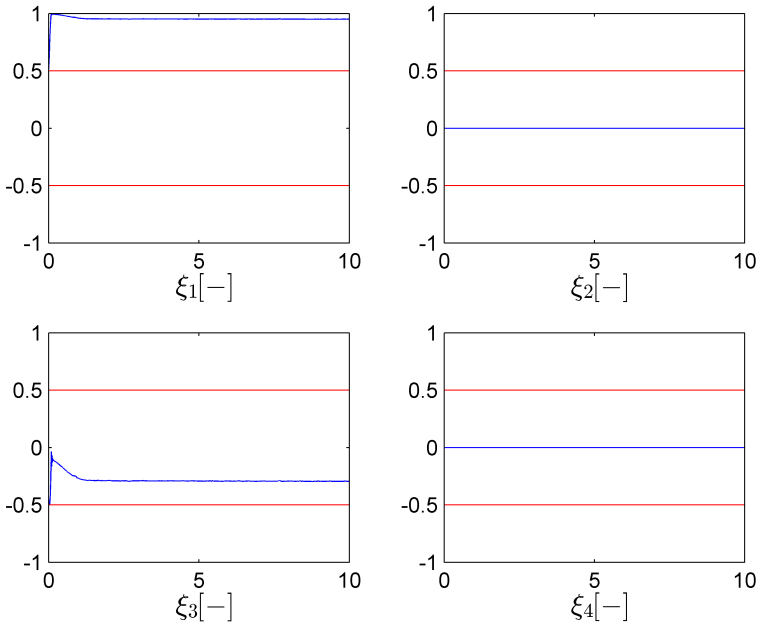

Figure 6.13: ξ_i-values: Row rank Γ

6.2.4 Simulation 4: Closed loop, random walk process

The simulation parameters are stated in tables 6.1 and 6.2. The results are plotted in figures 6.14 through 6.17.

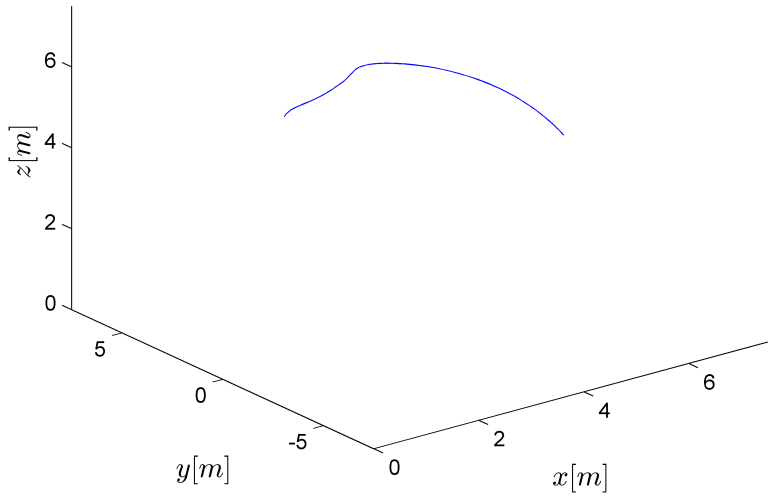

Figure 6.14: Kite 3D trajectory

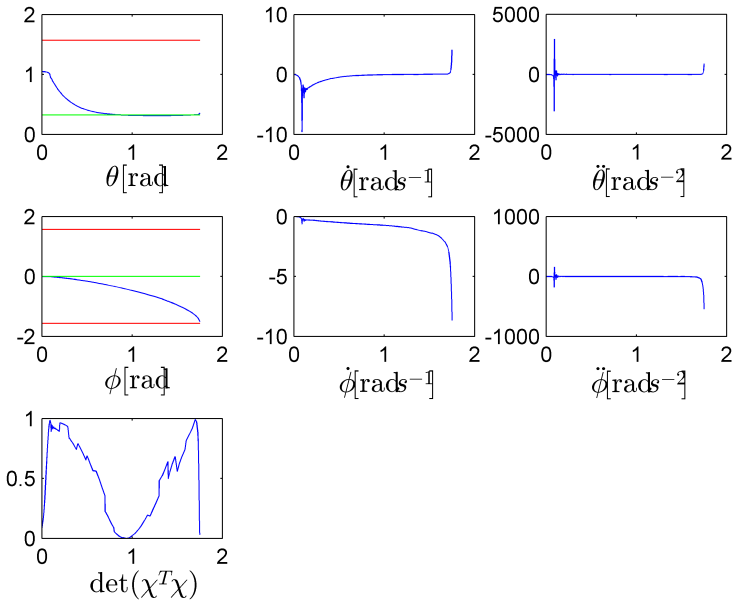

Figure 6.15: System states and det($\chi^T\chi$)

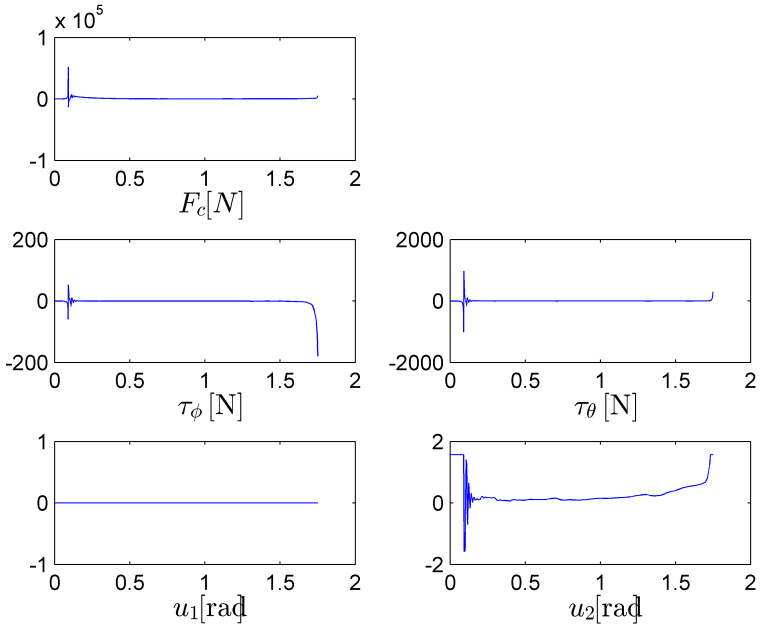

Figure 6.16: System loads

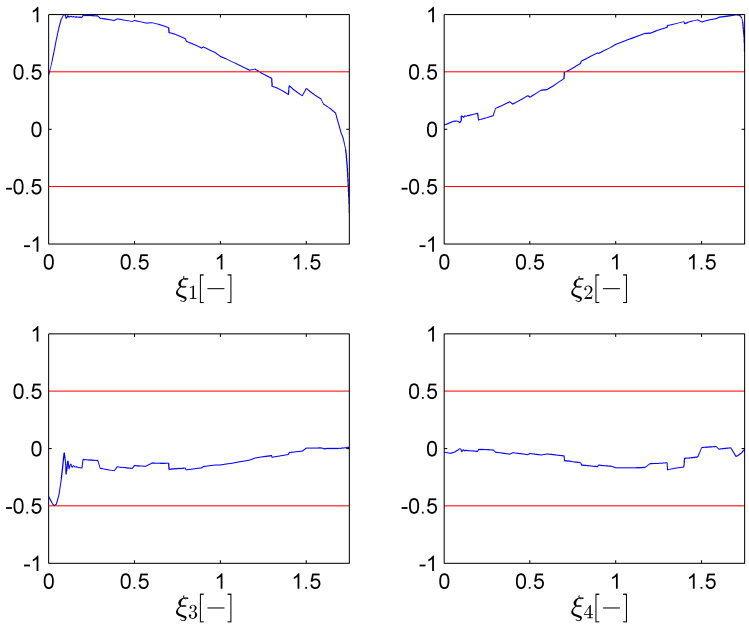

Figure 6.17: ξ_i-values: Row rank Γ

An attempt at controlling the elevation angle θ with a PID-algorithm was carried out with a random walk process on the ambient wind vector. The simulation was stopped after 1.755 $[s]$ due to a singularity in the θ state, as the kite flies past the drag angle towards $\theta = 0$ and the kite crashed. This result is similar to what one would expect in a real world situation. The noise on the wind vector results in exponentially growth of all states, and a controller that is unable to respond to changes in the system. $\det(\chi^T\chi)$ is close to, or equal to, zero around the 1 $[s]$ mark, as well as at the end of the simulation, as seen in figure 6.15. Figure 6.17 indicates that Γ remains full row rank throughout the simulation. As seen in figure 6.16, the control input u_2 is oscillating at a hihg frequency around the $0.1[s]$ mark, that a linear servo would not be able to exert. The singularity in the simulation results in loads growing infinitely at the end of the simulation. Load computations are considered not physical due to the singularity in the computation. Due to the singularity in the computation, the associated loads in the system are extreme and instantaneous.

6.2.5 Simulation 5: Closed loop system dual PID

The simulation parameters are similar as stated in tables 6.1 and 6.2 for simulation 3 and 4, except a PID-controller is applied on ψ_c with the same parameters as for φ_c, with initial value $\phi_0 = -\pi/8$. The results are plotted in figures 6.18 through 6.21.

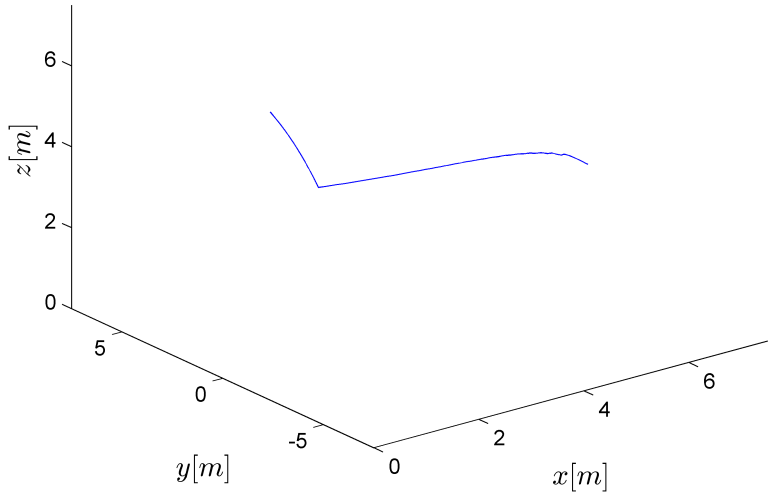

Figure 6.18: Kite 3D trajectory

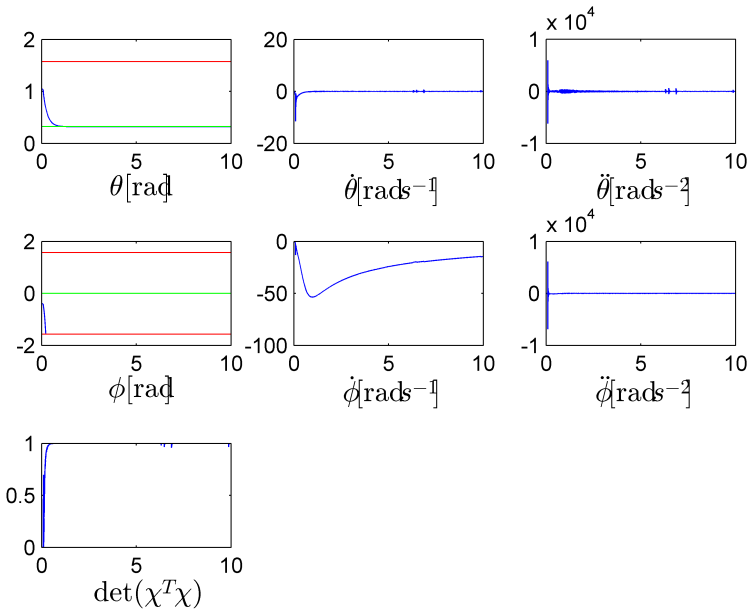

Figure 6.19: System states and $\det(\chi^T\chi)$

As seen in figure 6.18 the controller fails to reach the set point value of $\phi_{sp} = 0$ at full control demand u_1, as seen in figure 6.20 and the kite crashes. The kites trajectory is not spherical after impact, due to the way the path constraints on the states are applied (through saturation). The set point value in θ is overshot and the state reaches zero. The demanded control input is out of range for a typical linear servo. Figure 6.19 suggests there is a singularity in the state derivatives, or at least close to, in $\ddot{\theta}, \ddot{\phi}$ initially, with resulting extreme loads. $\det(\chi^T\chi)$ is close to, or equal to, zero initially. Figure 6.21 suggests that Γ remains full row rank throughout the simulation.

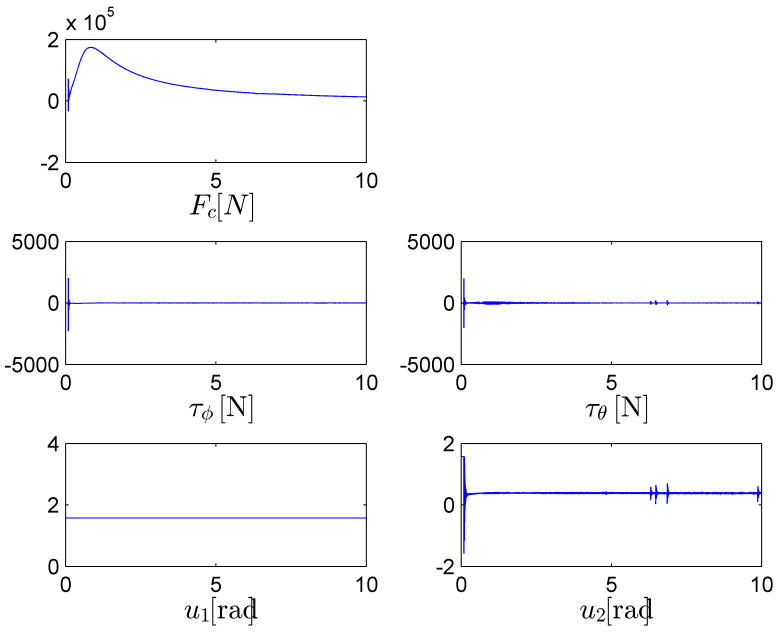

Figure 6.20: System loads

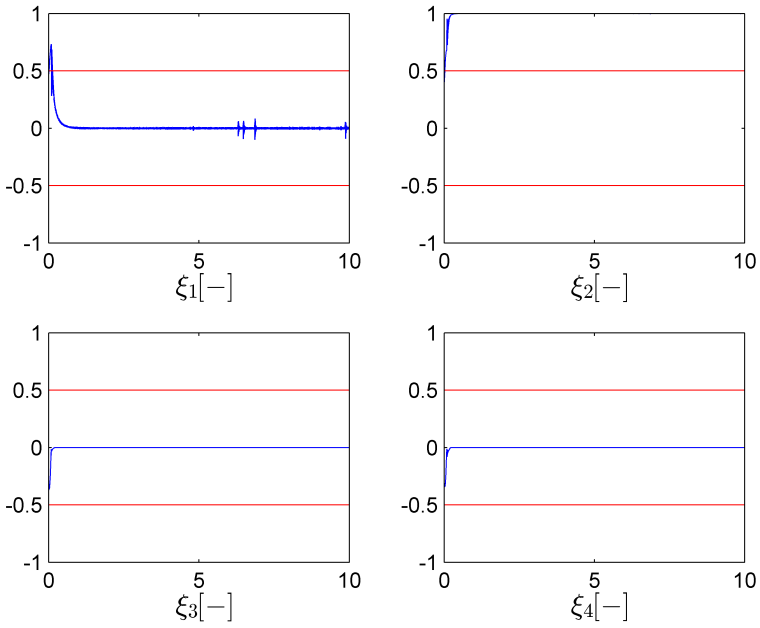

Figure 6.21: ξ_i-values: Row rank Γ

6.2.6 Summary of simulation results

The simulations confirms that small errors accumulates quickly, considering the error dynamics, as stated in [21]. PID-control on θ fails when a random walk process on the ambient wind is introduced, and the demanded control input is out of range of typical linear servos. PID-control applied on θ, ϕ independently fails to control the system. There are extreme loads in the simulation due to singularities in the computation. This phenomena is not considered physical and indicates inaccuracies in the mathematical model. However, the closed loop system with control input in φ was able to control the θ state without random walk process on the wind vector. The associated open loop system response indicates that the neutral position, defined by the drag angle is a marginally stable equilibrium point of the system. The simulation results can be summarized as:

- Not able to control states with PID when random walk process is included
- Singularities in the computations indicating inaccurate mathematical model
- Application of path constraints can be done in a different way
- Coupled dynamics in the system, as expected
- Spherical trajectory within path constraints

Chapter 7

Field Study

This section aims to describe and summarize the field study that was carried out in this thesis. Two tow tests were performed on two different iterations on Bieglers paravane design, as well as a flight test of the parawing kite. The main goal for the field study was to get an initial preference of the dynamics of both the paravane and the parawing kite. The field studies was recorded and are accessible at `https://vimeo.com/130117869` with password *Paraplyer4545*.

7.1 Paravane

Two tow tests were performed of Bieglers paravane design April 9^{th} and May 9^{th} 2015. The towing vessel used was Steinbiten III; a Hanse 370e sailboat. The objective of both tests were to get an initial preference of total drag on the paravane, constraint force capabilities, steering and performing change of tack operations. The structural integrity, seaway performance, pitch stability and directional stability was also investigated. The trials were captured on tape, using a GoPro Hero 3+ video camera. Still pictures from the video are presented in this section.

7.1.1 Sea trials April 9^{th}

The trials were carried out in seaway, with estimated significant wave height of $0.3 - 0.5[m]$. The observations during the trials suggests that to model the paravane as reflecting the horizontal transverse forces perfectly as long as the vehicle is sailing on course and adding a drag force in the longitudinal

direction locally on the paravane should be a reasonable assumption. Some inertial momentum should be added in regards to the yaw of the paravane, understood as turning moments about center of rotation in yaw. The effect of having a wing and rudder at some separation may have a greater effect than the rotational inertia of the mass, especially because the separation between wing and rudder may be increased to gain better control. The range of angles between kite line and paravane is largely restricted to anything between the resultant force going through the wing and the resultant force going through the rudder. In a previous design, that angle was small. Merely enlarging the rudder is unlikely to help. The submarine hull needs to be longer, and the rudder farther back. The rate at which yaw angle can change when the angle between kite line and paravane changes should be limited by how far wing and rudder are separated. If that behaves like a rotational inertia, it may be modelled as a greater mass distribution. The number may be the sum of a constant by representing mass distribution, and be proportional to the square of speed to represent the effect of flow over the foils.

The gybing operation looked highly non-linear and would be hard to model. It may be possible to model this operation as a discrete switching dynamic system: that it instantaneous mirrors the dynamics when it crosses the wind dead downwind, and shoots up onto the new tack, as we observed seen in figure 7.1. Either way, with the kite dead downwind, it would not exert any transverse force component, empirically speaking. The transverse force would be reduced because as the kite arcs up, the horizontal component of the force decreases. That is something that was not reproduced during the trials. It should make gybing easier. Until quantitative data is gathered, either from tests or from detailed modelling of a specific design, there is no justification from anything complicated.

Figure 7.1: Gybing of 1st paravane design iteration

A possible linearization of the paravane dynamics could be to constrain the rudder foil dynamics to linear lift-to-drag-proportions, but most preferably where the lift-to-drag-ratios are constant, thus varying only with the current velocity squared. This would simplify mathematical modelling regarding control system design. This would result in a conservative under estimate of the foil forces of the rudders, as long as they do not stall and have fluid flow to a certain velocity.

Proposed design changes for the paravane after these trials are:

- Extend the canard below the submarine hull, to provide greater torque around the roll axis when gybing.
- Lengthen the submarine hull to increase separation between wing and rudder (whether the vertical strut should also move aft, is not known at this point).
- Divide the rudder into two, so that when gybing the upper part of the rudder can be given a greater angle of attack, increasing the torque around the roll axis. (Should that two-part rudder have anhedral or dihedral angle, should it sweep back or sweep forward?)
- Find out whether the forward planning float (wave breaker) is necessary. Can the paravane be allowed to nosedive during a gybe? If not,

can the rudder take care of the problem?

The resistance to applied constraint force was tested by manually pulling the towing tether as hard as possible, and it was not possible to lift the paravane out of the water as long as the fluid at velocity over the foils. A force of approximately $50[kg]$ was applied. If funds could be found to build a prototype on which these factors could be rapidly adjusted, as in a few minutes without exposing anything that must not get wet, it should be possible to sort out a good design in roughly one year.

7.1.2 Sea trial May 9^{th}

The sea trials were carried out in a calm sea state. The trial objective was to investigate the gybe operation, steering performance and drag of the second iteration of Bieglers design, described in section 3.5.2. Steering and gybing performance was improved compared to the first sea trial, due to the altering in the design.

Figure 7.2: Gybing operation of 2^{nd} paravane design iteration

The canard below the submarine hull was extended to provide greater torque around the roll axis when gybing. The submarine hull was extended, the rudder was increased in size and its steering mechanics were improved, such that a greater angle of attack was made possible. The test was carried out without a forward float (wave breaker), and a test of pitch stability in seaway remains inconclusive, due to the calm sea state during the trial. Due to the

difference in sea state, an estimate of drag was inconclusive. The second paravene design iteration proved to be more controllable in a physical sense, compared to the first design iteration. The increased length of the submarine hull, as well as the canard provided greater torque around the roll axis, and these structures can have increased resistance to bending moment around the pitch axis to ensure structural integrity. The resistance to applied constraint force was tested by manually pulling the towing tether as hard as possible, and it was not possible to lift the paravane out of the water as long as the fluid at velocity over the foils. A force of approximately $50[kg]$ was applied.

7.2 Kite

A flight test was performed June $8^{[th}$ to investigate important loads, response on different control inputs, forced system failure and measurement of the ambient wind in order to compare the mathematical model to real data to some extent. The test setup consisted of measuring loads at the control bar using simple digital weights and an anenometer to capture the ambient wind velocity. The data was sampled using a GoPro Hero 3+ video camera. Still pictures from the test are presented in this section.

Figure 7.3: Aggressive control on elevation angle

The ambient wind velocity was highly unstable, estimated to be in the region $6 - 10[knots]$ with gusts up to $14[knots]$ with fluctuating heading.

The test consisted of launch, and trying to control the kite to reach its neutral position, defined by the drag angle. An attempt at measuring the forces at the control bar was carried out. The idea was to sample data from fish weights with the camera attached to the pilots head, but the unstable wind, with resulting extreme response of the kite made the data sampling unsuccessful. The ambient wind was measured, using an anenometer of the type WindMate.

As seen in figure 7.3, a force of $5[kg]$ was applied at some point in time on the end of the control bar in order to generate a turning moment in pitch on the kite, trying to simulate control input φ_c. The kite responded by flying towards the neutral position, defined by the drag angle.

Figure 7.4: Aggressive control in yaw

As seen in figure 7.4, when aggressive high frequency control was applied in yaw, simulating control input in ψ_c, the kite does not respond immediately and the result is a twist of the tether lines around the position vector $\mathbf{p}$ represented by the red center tether. As a result of the unstable wind conditions, the kite was difficult to control by a human operator, and data sampling proved to be inconclusive.

Chapter 8

Conclusion

In this thesis different concepts of wind power exploitation, as well as total system concepts for a wind powered marine vehicle have been studied. A concept of study was chosen, a mathematical model of the dynamics of a multi-panel soft fabric kite was developed and different approaches regarding control plant design has been presented. Field study of the kite and Bieglers paravane design was carried out. This part concludes the thesis and proposes further work.

8.1 Concluding remarks

Robert Bieglers paravane design was working as expected and looks promising in an wind powered marine vehicle application where sailing is the main source of propulsion. The first iteration of the paravane design was difficult to steer and gybe, which was improved in the second design iteration. Overall, the paravane showed a decent structural integrity with possibilities of improvement. The second iteration proved to be controllable and operational. Bieglers design could be part of a future of high speed sailing design.

The mathematical model of the kite proved to be accurate to some extent regarding the kite trajectory. The model resulted in some regions with singularities in the simulations. Based on the field study, and the control design, the validity of the mathematical model remains inconclusive. In the future, the implementation of the control inputs should be revised, as control of rotations only proved to be a non trivial control problem. Whether this is physical for a parawing kite or not, remains inconclusive. The tether constraint force on the kite during aggressive accelerations, as seen in the simulations and in the field study suggests a high power output

at relative low ambient wind velocities. This indicates possibilities for high speed sailing and states a challenge regarding the design of a control system.

A PID-controller on one state proved interestingly enough to be sufficient in the open loop case without the random walk process, but was unable to control the system when noise on the ambient wind was introduced. The simulations suggest that the simulated drag angle is a marginally stable equilibrium point of the system. A guess on the power output demand from a linear servo connected to the kite control bar may be greater than the available performance of a typical low budget linear servo. The demanded response frequency was too high for such an actuator in closed loop case including a random walk process. Regarding the thrust allocation approach for designing a control plant, the defining mapping matrix Γ does not have an generalized inverse at some points in the cases where the PID-controller fails. By setting the controller constant at these points, it may not be possible to stabilize the system. However, the controllability check for the linearized open loop system however argues that the system is fully controllable, except for a region close to $\theta = 0$. Simulations confirm singularities in the solution within this region. This corresponds to the observed dynamics of kite in a real world situation, where the wind would catch the opposite side of the kite, and it would not remain inflated, and loose its foil properties.

The chosen concept at an early state looks promising regarding velocity, and poses an exciting challenge for future work.

8.2 Further work suggestions

This section aims to propose further work regarding the wind powered marine vehicle.

8.2.1 Design of control system for kite

Based on the kite dynamics described in this thesis, MPC incorporating NLP algorithms may be the optimal controller regarding a wind powered marine vehicle designed for high speed sailing. Applying optimization theory on the kite dynamics should be considered in order to design a high performance controller. If online computational resources poses a challenge the thrust allocation method could be considered. However, this approach may not result in an optimal controller. Due to the fact that the control inputs are coupled and that errors accumulate quickly for a kite that is configured to

be controlled by pitch and yaw suggests that the approach of incorporating feedback linearization is not optimal. State estimation of the kite dynamics is a typical attitude estimation problem. The control system design should incorporate a parameter study in order to ensure a relation between demanded control input and available actuator properties.

8.2.2 Lagrangian mechanics approach in dynamics modelling

The kite dynamics could be modelled as a modified inverted pendulum using energy relations and Lagrangian mechanics with respect to non-linear control for underactuated systems. The fact that the control inputs in the mathematical model developed in this thesis only rotates and project the aerodynamic force components, may argue for this approach. According to [26], in such a model, the kinetic and potential energy representation are used in order to compute the Euler-Lagrange equations, and obtain the equations of motion. The passivity of the system should be investigated, and a controllability analysis on the linearized system should be performed. Further investigation of dynamic and static path constraints should be done in order to develop a stabilizing control law. As presented in section 5.1 the constraints on the motion of the system suggests this is a non-holonomic system.

8.2.3 Navigation: path planning and path following

The most important constraint on the trajectory of any sailing vehicle is that it can not sail directly into the direction of the ambient wind, and the minimum relative heading can be theoretically defined by the drag angle, as discussed in section 4.1.3. As seen in figure 4.2, sailing dead downwind is not an optimal trajectory for a high speed sailing vehicle, and should be considered a constraint on the path. A path planning algorithm should also take into consideration geographical constraints, as well as avoidance of marine traffic, extreme weather and wild life when setting up waypoints and computing the path between points of interest. Objectives for a path planning algorithm can be the shortest, fastest or safest path. Objectives such as minimizing energy cost from the control plant and maximizing energy harvesting in such configuration should also be considered.

As seen in figure 4.1, the trajectory during any of the three different manoeuvres of changing tack are circular to some extent. As stated in [27] section 8.4.1, the shortest path from one point to another, where the path has specified initial and terminal tangents and bounded curvature, consist of

a circular arch followed by a straight line, followed by another circular arch. Dubins path following algorithm can be suited for vehicles with circular turning motions, i.e. negligible side-slip, while implementing the vehicles minimum turn radius. According to [28], the path following algorithm can be further improved by combining Dubins path with clothoids to ensure continuity in curvature of the path. Computing the total length of such a path is not computational expensive.

The high vantage point of a kite incorporated in a wind powered marine vehicle should be exploited in a navigation system. A payload containing radar and AIS-system for marine traffic communication, inertial and satellite navigation systems can be air suspended to increase overall redundancy in operations.

A system based on hub parking can be incorporated, to expand the workspace of a wind powered marine vehicle. The vehicle can park to avoid extreme weather, for maintenance, altering of operational modes, charging on-board energy storage etc. The hub can be designed as buoys as well as a configuration involving a parent ship.

8.2.4 Further work regarding kite

One idea that can be considered in future work is controlling the kite indirectly, through a partially balanced rudder. The maximum load depends on the size of the rudder and the air flow speed. Depending on how well that rudder can be balanced, taking into account movements of the centre of effort, a lever arm could be designed to optimize added stability on kite control.

Another approach can be a model sized version with high speed in goal. Equipment is fairly inexpensive and testing can be performed indoors. However, developing model sized kites may be a challenge regarding scaling factors and modelling of material properties. High speed position servos are fairly inexpensive as long as the torque demand is below $1[Nm]$. However, indoors testing would provide reliable wind, such that the model kite does not drop, even without having the volume to carry enough helium to list its payload in such a configuration. That could be optimal for testing the concept, provided that different Reynolds numbers of a smaller kite do not put it into a different regime that affect extrapolation to a larger scale.

There are two more alternatives. One is to control the rudder, not through a servo while testing, but to lead control lines from the rudder to

the point where the kite is anchored. Control those by hand, but measure torque at the rudder. The other is to reduce the control loads by attaching the servo not directly to the rudder, but to a tailplane that controls the rudder. That is a concept utilized for flaps on aircrafts. See Figure 72d on page 117 of [29]. There is some discussion in the text, which might give an added factor on the control actuation needed. Or the rudder could be designed as an autoptére rudder.

An analysis on extreme loads on the tether lines can be carried out, by simulation and in a field study. An analysis by simulation should incorporate a detailed model of the kite tethers, considering tensile properties regarding extreme loads, and snap loads. The load analysis can also be setup to investigate velocity potential of a wind powered marine vehicle, structural integrity of the total system as well as actuator demand and design.

8.2.5 Further work on paravane design

Further development in the design of the paravane in the context of a high speed sailing vehicle would benefit from a detailed hydrodynamic analysis, where optimization of the design regarding drag, steering, pitch stability as well as reflecting the kite forces as previously discussed should be an objective. If resources were available, development of a prototype of the concept should make it possible to achieve a good design in roughly one year.

According to Biegler, different self-steering concepts from the sailing community can be applied in order to minimize the energy cost of a controller on the paravane. The autoptére rudder is supposed to require a smaller control input for a given effect. It might enable smaller servos to control the canard and the paravanes rudder, or the kites rudder or control bar, although a servo rudder on a long lever would reduce inputs even more. However, the control dynamics are supposed to be different. A servo rudder effectively gives the control surface a constant angle of attack. A wave making a boat luff up, would increase the angle of attack of a rudder that is fixed, and ideally self-steering should increase that angle even more. The description of the autoptére rudder in [30] claims that if the trim tab is just fixed, then the autoptére rudder will change its angle of attack in exactly that way.

Bibliography

[1] Johan Gregorius Hagedoorn. Ultimate sailing: Introducing the hapa. *Amateur Yacht Research Society*, 1993.

[2] Bernard Smith. *Sailloons and Fliptackers*. American Institute of Aeronautics and Astronautics, Inc., 1989.

[3] Corporation Exxon Mobile. The outlook for energy: A view to 2040. 2014.

[4] nettavis Dagens Næringsliv. Om 53 år og 4 måneder er verden tom for olje, 2014. URL `http://www.dn.no/nyheter/energi/2014/07/02/0648/Olje-og-gass/om-53-ar-og-4-maneder-er-verden-tom-for-olje`.

[5] Asgeir J. Sørensen. Robotics part 1: Introdcuction and underwater technology platforms. *TMR 4240 Marine Control Systems*, 2014.

[6] Amateur Yacht Research Society 122 AYRS122. Ultimate sailing iv: Progress with kite and hapa. *AYRS*, 1996.

[7] Amateur Yacht Research Society AYRS. Homepage, 2014. URL `http://www.ayrs.org/ayrs.htm`.

[8] M. Erhard and H. Strauch. Control of towing kites for seagoing vessels. *Control Systems Technology, IEEE Transactions on*, 21(5):1629–1640, Sept 2013. ISSN 1063-6536. doi: 10.1109/TCST.2012.2221093.

[9] Uwe Fechner, Rolf van der Vlugt, Edwin Schreuder, and Roland Schmehl. Dynamic model of a pumping kite power system. *Renewable Energy*, 83:705–716, 2015.

[10] US Saildrone Inc. Saildrone - revolutionizing ocen science, 2014. URL `http://www.saildrone.com/`.

[11] Boris Houska and Moritz Diehl. Optimal control of towing kites. In *Decision and Control, 2006 45th IEEE Conference on*, pages 2693–2697. IEEE, 2006.

[12] Limited Allsopp HeliKites. Helikite, 2014. URL `www.allsopp.co.uk`.

[13] J Kim and Chul Park. Wind power generation with a parawing on ships, a proposal. *Energy*, 35(3):1425–1432, 2010.

[14] George M Dadd, Dominic A Hudson, and RA Shenoi. Determination of kite forces using three-dimensional flight trajectories for ship propulsion. *Renewable Energy*, 36(10):2667–2678, 2011.

[15] Ocean Rodeo. Ocean rodeo razor 10m2, 2014. URL `http://www.sideshore.no/products/ocean-rodeo-razor10m2`.

[16] Joep CM Breuer and Rolf H Luchsinger. Inflatable kites using the concept of tensairity. *Aerospace Science and Technology*, 14(8):557–563, 2010.

[17] Luc Armant. l'aile d'eau: réflexion pour un voilier sans masse, 1999.

[18] energies Altaeros. The altaeros buoyant airborne turbine (bat), 2014. URL `http://www.altaerosenergies.com/`.

[19] JJ Isler and Peter Isler. *Sailing for dummies*. Wiley Publishing, Inc., 2006.

[20] Christian Thomas Borgen. Application of an active foil propeller on an offshore vessel, 2010.

[21] Moritz Mathias Diehl. *Real-Time Optimization for Large Scale Nonlinear Processes*. PhD thesis, Ruprecht-Karls-Universität Heidelberg, 2001.

[22] I Argatov and R Silvennoinen. Asymptotic modeling of unconstrained control of a tethered power kite moving along a given closed-loop spherical trajectory. *Journal of Engineering Mathematics*, 72(1):187–203, 2012.

[23] Thor I. Fossen. *Handbook of marine craft hydrodynamics and motion control*. John Wiley & sons Ltd., 2011.

[24] João P. Hespanha. *Linear Systems Theory*. 2009.

[25] Havard Fjaer Grip, Thor Fossen, Tor Arne Johansen, Ali Saberi, et al. Attitude estimation using biased gyro and vector measurements with time-varying reference vectors. *Automatic Control, IEEE Transactions on*, 57(5):1332–1338, 2012.

[26] Isabelle Fantion and Rogelio Lozano. *Non-linear Control for Underactuated Mechanical Systems*. 2002.

[27] Andreas Reason Dahl. Path planning and guidance for marine surface vessels, 2013.

[28] A. M. Lekkas. Introduction to path planning, properties of curves, dubins paths, clothoids. 2014.

[29] A. C. Kermode. *Flight Without Formulae*. 1988.

[30] Bill Belcher. Wind-vane self-steering: How to plan and make your own. 1982.

Appendix A

Parameters2.m

```
% Kite parameters used for the simulink model KiteModel.slx
clear; close;
% Simulation parameters

rsb = 0; %1e-10;    % Singularity bias for 1/tan in dhteta
T_sim = 10;%2.3;%4.34;          % Simulation time [s]
plotter = 1;    % plot trajectory or not?
plotTetherTension = 1;  % Plot the tether tension?
figflag = 1;
savefigs = 0;

%E = 3;  % L/D-ratio
CL = 1.5; % Lift coefficient
E = 3;
CD = CL/E;  % Drag coefficient
beta = atan2(CD,CL);    % L-D coefficient
cbeta = cos(beta);
sbeta = sin(beta);
M = 1.80;  % Mass of kite (included payload=0)
A = 10; % Area of kite
l_t = 7.5; % tether length


r_0 = [0 0 1 ]'.*l_t;% initial position of kite
theta_0 = 75*pi/180; %pi/3;%beta;      % initial position of kite in spherical
```

```
26 dtheta_0 = 0;          % initial velocity of kite in
       spherical
27 phi_0 = -pi/12;             % initial position of kite in
       spherical
28 dphi_0 = 0;            % initial velocity of kite in
       spherical
29 theta_max = pi/2;      % Saturation on elevation angle (
       hit ground)
30 theta_min = 0;         % Saturation on elevation angle (
       cant go against the wind)
31 phi_max = pi/2;
32 phi_min = -pi/2;
33 % Air Rudder parameters
34 Ear = 20;
35
36 % Tether properties
37 CT = 1.2;      % Normal reaction coefficient
38 d_t = 0.01;              % Diameter
39 m_tether = 0;
40
41 % Control bar properties
42 m_c = 0.66; % [kg]
43 l_c = 1.0;  % [m]
44
45 % PID controller values
46 x1_0 = beta;
47 x3_0 = 0;%pi/8;
48
49 % Abrevated parameters
50 Ge = CL/(CD + (l_t*d_t*CT)/(4*A));     % Effective glide
       ratio
51 kappa_g = 0;     % Geodesic curvature of trajectory
52
53 % Physical properties
54 rho_a = 1.23;     % density of air kg/m^3
55 g = 9.81;
56
57 % Ambient wind
58 W = [3 0 0]';       % NED ambient wind velocity
59 z_0 = 10;              % reference height dynamic wind
       formula.
```

```
60 alpha = 1/7;
61 noise_power = 0.0;     %0.01
62
63 set(0,'defaulttextinterpreter','latex');
64 if plotter
65     sim('Openloopkite2',T_sim)
66     figure(1)
67     plot3(posout.Data(:,1),posout.Data(:,2),posout.Data
       (:,3));
68     %title('Kite 3D trajectory');
69     axis([0 l_t -l_t l_t 0 l_t]);
70     xlabel('$x$');
71     ylabel('$y$');
72     zlabel('$z$');
73
74     % Save fig 2 file as bitmap 600 dpi resolution
75     if savefigs
76         fig2img( 600, 1 );
77     end
78
79     figure(2)
80     subplot(3,3,1)
81     plot(thetavec.Time,thetavec.Data(:,1),[thetavec.
       Time(1) thetavec.Time(end)],[pi/2 pi/2],'r',[
       thetavec.Time(1) thetavec.Time(end)],[0 0],'r',[
       thetavec.Time(1) thetavec.Time(end)],[x1_0 x1_0
       ],'g');
82     xlabel('$\theta$');
83     subplot(3,3,2)
84     plot(thetavec.Time,thetavec.Data(:,2));
85     xlabel('$\dot{\theta}$');
86     subplot(3,3,3)
87     plot(thetavec.Time,thetavec.Data(:,3));
88     xlabel('$\ddot{\theta}$');
89
90
91     subplot(3,3,4)
92     plot(phivec.Time,phivec.Data(:,1),[phivec.Time(1)
       phivec.Time(end)],[phi_min phi_min],'r',[phivec.
       Time(1) phivec.Time(end)],[phi_max phi_max],'r'
       ,[phivec.Time(1) phivec.Time(end)],[x3_0 x3_0],'
```

```
    g');
93      xlabel('$\phi$');
94      subplot(3,3,5)
95      plot(phivec.Time,phivec.Data(:,2));
96      xlabel('$\dot{ \phi }$');
97      subplot(3,3,6)
98      plot(phivec.Time,phivec.Data(:,3));
99      xlabel('$\ddot{ \phi }$');
100
101     subplot(3,3,7)
102     plot(detXtX.Time, detXtX.Data );
103     xlabel('det($\chi^T \chi$)');
104
105     % Save fig 2 file as bitmap 600 dpi resolution
106     if savefigs
107         fig2img( 600, 1 );
108     end
109
110     figure(3)
111     subplot(2,2,1)
112     plot(xis.Time,xis.Data(:,1),[xis.Time(1) xis.Time(
        end)],[0.5 0.5],'r',[xis.Time(1) xis.Time(end)
        ],[-0.5 -0.5],'r')
113     xlabel('$\xi_1$');
114     subplot(2,2,2)
115     plot(xis.Time,xis.Data(:,2),[xis.Time(1) xis.Time(
        end)],[0.5 0.5],'r',[xis.Time(1) xis.Time(end)
        ],[-0.5 -0.5],'r')
116     xlabel('$\xi_2$');
117     subplot(2,2,3)
118     plot(xis.Time,xis.Data(:,3),[xis.Time(1) xis.Time(
        end)],[0.5 0.5],'r',[xis.Time(1) xis.Time(end)
        ],[-0.5 -0.5],'r')
119     xlabel('$\xi_3$');
120     subplot(2,2,4)
121     plot(xis.Time,xis.Data(:,4),[xis.Time(1) xis.Time(
        end)],[0.5 0.5],'r',[xis.Time(1) xis.Time(end)
        ],[-0.5 -0.5],'r')
122     xlabel('$\xi_4$');
123
124     % Save fig 2 file as bitmap 600 dpi resolution
```

```
125     if savefigs
126         fig2img( 600, 1 );
127     end
128
129 end
130
131 if plotTetherTension
132
133     figure(4)
134     %sim('Openloopkite2',T_sim)
135     subplot(3,2,1)
136     plot(FcOUT.Time, -FcOUT.Data(:,1) );
137     %title('Tether Constraint Force' );
138     xlabel('$F_c [N]$');
139
140     subplot(3,2,4)
141     plot(thetavec.Time, thetavec.Data(:,3).*l_c*m_c*0.5
            );
142     xlabel('$\tau_\theta$ [N]');
143
144     subplot(3,2,3)
145     plot(phivec.Time,phivec.Data(:,3).*l_c*m_c*0.5 );
146     xlabel('$\tau_\phi$ [N]');
147
148     subplot(3,2,5)
149     plot(u1.Time, u1.Data );
150     xlabel( '$u_1(t)$');
151
152     subplot(3,2,6)
153     plot(u2.Time, u2.Data );
154     xlabel( '$u_2(t)$' );
155
156     % Save fig 2 file as bitmap 600 dpi resolution
157     if savefigs
158         fig2img( 600, 1 );
159     end
160 end
```

Appendix B

main2.m

```
clear;
N = 30; % Number of elements per input in
    controllability analysis
closetest = 0;


h = waitbar(0,'Initializing sym objects...');

syms x1 x2 x3 x4 u1 u2; %w
%syms l w m g rho_a CD CL Cnorm Ak dt;
syms f Fx1 Fx3 G a b c d H I FD FL psi1 psi2;

assume(x1 > 0 & x1 < pi/2 );
assume(x2,'real');
assume(x3 > -pi/2 & x3 < pi/2 );
assume(x4,'real');
assume(u1 > -pi & u1 < pi );
assume(u2,'real');

assume(f, 'real');
assume(Fx1, 'real');
assume(Fx3, 'real');
assume(G, 'real');
assume(a, 'real');
assume(b, 'real');
assume(c, 'real');
assume(d, 'real');
assume(H, 'real');
```

```
28 assume(I, 'real');
29 assume(FD, 'real');
30 assume(FL, 'real');
31 assume(psi1, 'real');
32 assume(psi2, 'real');
33
34 waitbar(1/10,h,'Simplifying first group...');
35
36 l = 7.5;% assume(l > 0 );
37 % assume(w > 0 );
38 m = 1.80;% mass of kite. Mass of ctrl-bar: 0.66;
39 g = 9.81;% assume(g > 0 );
40 rho_a = 1.23;% assume(rho_a > 0);
41 CL = 1.5;% assume(CD > 0 );
42 Ee = 3;%effective glide ratio
43 CD = CL/Ee;% assume(CL > 0 );
44 Cnorm = 1.2;% assume( Cnorm > 0 );
45 Ak = 10;% assume( Ak > 0 );
46 dt = 0.01;% assume( dt > 0 );
47 bias = eps;
48 w = 3;       % ambient wind speed [m/s] in x-direction
49
50 er = [sin(x1)*cos(x3);sin(x1)*sin(x3);cos(x1)];
51 etheta = [cos(x1)*cos(x3);cos(x1)*sin(x3);-sin(x1)];
52 ephi = [-sin(x3);cos(x3);0];
53
54 W = [w 0 0]';
55 p = l.*er;
56 dp = l.*etheta.*x2 + l*sin(x1).*ephi.*x4;
57 We = W - dp;
58 Wep = We - dot(er,We).*er;
59 simplify(Wep,'IgnoreAnalyticConstraints',true,'Steps'
      ,10);
60 el = We/norm(We);
61 et = cross(We,er)/norm(cross(We,er));
62 et = simplify(et,'IgnoreAnalyticConstraints',true,'
     Steps',10);
63 % epsi = cross(et,el);
64 % simplify(epsi,'IgnoreAnalyticConstraints',true,'Steps
      ',10);
```

```
65 epsi = cross(cross(We,er),We)/(norm(We)*norm(cross(We,
       er)));
66 simplify(epsi,'IgnoreAnalyticConstraints',true,'Steps'
       ,10);
67
68 waitbar(2/10,h,'Simplifying second group...');
69
70 FD = 0.5*rho_a*CD*Ak*dot(We,We);
71 FD = simplify(FD, 'Steps', 10, '
       IgnoreAnalyticConstraints',true);
72 FL = 0.5*rho_a*CL*Ak*dot(We,We);
73 FL = simplify(FL, 'Steps', 10, '
       IgnoreAnalyticConstraints',true);
74 Fdt = eval(1/8*rho_a*Cnorm*dt*l*norm(Wep));
75 Fdt = simplify(Fdt, 'Steps', 10);%, '
       IgnoreAnalyticConstraints',true)
76
77 waitbar(3/10,h,'Simplifying third group...');
78
79 psi1 = dot(We,etheta)/norm(We);
80 psi1 = simplify(psi1, 'Steps', 10, '
       IgnoreAnalyticConstraints',true);
81 psi2 = dot(ephi,We)/norm(We);
82 psi2 = simplify(psi2, 'Steps', 10, '
       IgnoreAnalyticConstraints',true);
83 psi3 = dot(cross(cross(We,er),We),etheta)/dot(We,We);
84 psi3 = simplify(psi3, 'Steps', 10, '
       IgnoreAnalyticConstraints',true);
85
86 waitbar(4/10,h,'Simplifying 4th group...');
87
88 psi4 = dot(We,ephi)/norm(We);
89 psi4 = simplify(psi4, 'Steps', 10,'
       IgnoreAnalyticConstraints',true);
90 psi5 = dot(etheta,We)/norm(We);
91 psi5 = simplify(psi5, 'Steps', 10,'
       IgnoreAnalyticConstraints',true);
92 psi6 = dot(cross(cross(We,er),We),ephi)/dot(We,We);
93 psi6 = simplify(psi6, 'Steps', 10,'
       IgnoreAnalyticConstraints',true);
94
```

```
95  waitbar(5/10,h,'Simplifying 5th group...');
96
97  psi7 = dot(We,etheta);
98  psi7 = simplify(psi7, 'Steps', 10,'
        IgnoreAnalyticConstraints',true);
99  psi8 = dot(We,ephi);
100 psi8 = simplify(psi8, 'Steps', 10,'
        IgnoreAnalyticConstraints',true);
101 % psi9 = dot(We,er)/norm(We);
102 % psi9 = simplify(psi9, 'Steps', 10,'
        IgnoreAnalyticConstraints',true);
103 % psi10 = norm(cross(We,er))/norm(We);
104 % psi10 = simplify(psi10, 'Steps', 10,'
        IgnoreAnalyticConstraints',true);
105 %
106 waitbar(6/10,h,'Simplifying 6th group...');
107
108 Fx1 = (FD*cos(u2)*cos(u1) - FL*sin(u2)*cos(u1))*psi1...
109     + (FD*cos(u2)*sin(u1) - FL*sin(u2)*sin(u1))*psi2...
110     + (FD*sin(u2) + FL*cos(u2))*psi3...
111     + Fdt*psi7;
112 Fx1 = simplify(Fx1,'Steps',10);
113 Fx3 = (FD*cos(u2)*cos(u1) - FL*sin(u2)*cos(u1))*psi4...
114     + (FD*cos(u2)*sin(u1) - FL*sin(u2)*sin(u1))*psi5...
115     + (FD*sin(u2) + FL*cos(u2))*psi6...
116     + Fdt*psi8;
117 Fx3 = simplify(Fx3,'Steps',10);
118
119
120 f = [x2;Fx1/(l*m) + sin(x1)*g/l + sin(x1)*cos(x1)*x4^2
      + u2; x4;Fx3/(l*m) - 2*cot(x1)*x2*x4];
121
122 waitbar(7/10,h,'Computing Jacobian matrices A and B...'
      );
123
124 A = jacobian( f, [x1 x2 x3 x4] );
125 B = jacobian( f, [u1 u2] );
126
127 waitbar(8/10,h,'Simplifying Jacobian...');
128
129 for i = 1:4
```

```
130         for j = [2 4]
131             A(i,j) = simplify(A(i,j), 'Steps', 2, '
                IgnoreAnalyticConstraints',true);
132         end
133     end
134
135
136
137     % fid = fopen( 'Ageneral2.dat','w');
138     % for i = 1:4
139     %     for j = 1:4
140     %         fprintf( fid, '%s\n', char(A(i,j)) );
141     %     end
142     % end
143     % fclose(fid);
144
145     % Controllability analysis at W = 5 m/s and u2 = 0
146     waitbar(9/10,h,'Substituting w and u2 as constants in
            jacobians...');
147     A = subs(A,u2,0);
148     B = subs(B,u2,0);
149     close(h)
150
151     CTB = zeros(N,N);
152
153     x_1 = linspace(0,pi/2,N);
154     x_2 = pi;
155     x_3 = linspace(-pi/2,pi/2,N);
156     x_4 = pi;
157     u_1 = 0;
158     %u_2 = 0;
159
160     h = waitbar(0,'Progress of controllability check...');
161     for i = 1:N
162         %disp([num2str(i),'/',num2str(N),' outer iterations
                in 2D (N^2)']);
163         if (i==1)
164             time0 = tic;
165         end
166         for j = 1:N
```

```
167             dumA = eval(subs(A,{x1,x2,x3,x4,u1},{x_1(i),x_2
                    ,x_3(j),x_4,u_1}));
168             dumB = eval(subs(B,{x1,x2,x3,x4,u1},{x_1(i),x_2
                    ,x_3(j),x_4,u_1}));
169
170             dumNan = isnan(dumA);
171             if (max(max(dumNan)))
172                 CTB(i,j) = -1;
173             else
174                 CTB(i,j) = length(dumA) - rank(ctrb(dumA,
                        dumB));
175             end
176         end
177
178         if(i>=2)
179             tfin = toc(time0);
180             ttotal = round((N/i)*tfin - tfin);
181             totalm = floor(ttotal/60);
182             totals = ttotal - totalm*60;
183             waitbar(i/N,h,['Progress of controllability
                    check... [ETA: ', num2str(totalm), 'm ',
                    num2str(totals),'s]']);
184         end
185
186
187 end
188 close(h);
189
190 % Graphical representation of controllability analysis
        results
191 x_12 = linspace(0,pi/2,N+1);
192 x_32 = linspace(-pi/2,pi/2,N+1);
193
194 zs = repmat(cos(x_12),N+1,1)';
195 for i = 1:(N+1)
196     for j = 1:(N+1)
197         xs(i,j) = sin(x_12(i))*cos(x_32(j));
198         ys(i,j) = sin(x_12(i))*sin(x_32(j));
199     end
200 end
201 set(0,'defaulttextinterpreter','none');
```

```
202 fig1 = figure(1)
203 surf(xs,ys,zs,CTB), axis equal
204 colormap([1 0 0;0 1 0 ])
205 xl1 = xlabel('$x$');set(xl1,'interpreter', 'latex');
206 yl1 = ylabel('$y$');set(yl1,'interpreter', 'latex');
207 zl1 = zlabel('$z$');set(zl1,'interpreter', 'latex');
208
209 %t1 = title('Controllability check for $\forall (x_1,
      x_3) $ at $x_2=x_4=\pi, u_1=u_2=0$ and $w = 5 [m/s]$
      '); set(t1,'interpreter', 'latex');
210 colorbar('YTickLabel',{'','Uncontrollable','','','','',
      '','','','','Fully controllable'})
211 fig2img( 600, 1 );
212
213 % Running controllability test in the close range near
      x1 = 0 and x1 = pi/2
214
215 if closetest
216     CTBc1 = zeros(N,N);
217     CTBc2 = zeros(N,N);
218
219     x_13 = linspace(x_1(1),x_1(2),N);
220     x_14 = linspace(x_1(end),x_1(end-1),N);
221
222     for i = 1:N
223         for j = 1:N
224             dumA1 = eval(subs(A,{x1,x2,x3,x4,u1},{x_13(
                  i),x_2,x_3(j),x_4,u_1}));
225             dumB1 = eval(subs(B,{x1,x2,x3,x4,u1},{x_13(
                  i),x_2,x_3(j),x_4,u_1}));
226
227             dumA2 = eval(subs(A,{x1,x2,x3,x4,u1},{x_14(
                  i),x_2,x_3(j),x_4,u_1}));
228             dumB2 = eval(subs(B,{x1,x2,x3,x4,u1},{x_14(
                  i),x_2,x_3(j),x_4,u_1}));
229
230             dumNanA1 = isnan(dumA1);
231             dumNanB1 = isnan(dumB1);
232
233             dumNanA2 = isnan(dumA2);
234             dumNanB2 = isnan(dumB2);
```

```
235
236                 if max(max(dumNanA1))
237                     CTBc1(i,j) = -1;
238                 else
239                     CTBc(i,j) = length(dumA1) - rank(ctrb(
                        dumA1,dumB1));
240                 end
241
242                 if max(max(dumNanA2))
243                     CTBc2(i,j) = -1;
244                 else
245                     CTBc2(i,j) = length(dumA2) - rank(ctrb(
                        dumA2,dumB2));
246                 end
247             end
248         end
249
250 end
```